POLITECNICO DI TORINO

MASTER OF SCIENCE IN BIOMEDICAL ENGINEERING

Extraction of Control Signal for Lower Limb Exoskeletons through Non-Negative Matrix Factorization and High-Density sEMG

Author:
Alberto Pala

Supervisor:
Prof. Marco GAZZONI
Advisor:
Prof. Dario FARINA

26 July 2018

Ai miei genitori.
Per l'amore,
Per il sostegno,
Per la fiducia.

Declaration of Authorship

I, Alberto Pala, declare that this thesis, titled Extraction of control signal for lower limb exoskeletons through Non-Negative Matrix Factorization and High-Density sEMG, and the work presented in it are my own. I confirm that:

- Where I have consulted the published work of others, this is always clearly attributed.

- Where I have quoted from the work of others, the source is always given. With the exception of such quotations, this thesis is entirely my own work.

- I have acknowledged all main sources of help.

- Where the thesis is based on work done by myself jointly with others, I have made clear exactly what was done by others and what I have contributed myself.

Signed:

_____

Date:

_____

"There is a driving force more powerful than steam, electricity and nuclear power: the will."

Albert Einstein

POLITECNICO DI TORINO

Abstract

Department of Electronics and Telecommunications (DET)

Master of Science

**Extraction of Control Signal for Lower Limb Exoskeletons through
Non-Negative Matrix Factorization and High-Density sEMG**

by Alberto Pala

Robotic devices such as exoskeletons are becoming ever more relevant for what concerns the rehabilitation process of injured people. In this context, the overcoming of the issues related to interaction human-device and the implementation of a EMG-based exoskeleton control strategy represent a great challenge. This study, starting from disadvantages of traditional supervised control method, proposes a semi-supervised approach in order to extract a proportional and simultaneous myoelectric control for a lower-limb rehabilitation exoskeleton. This allows, through the synergy model assumptions, to evaluate a control signal directly from EMG signals recorded on muscular surface. Five able-bodied subjects participated to this study, and the experimental setup consisted in two phases (Exp1 and Exp2): in the Exp1 all subjects performed movements of flexion-extension for knee and ankle joint separately. Exp2 instead asked them to couples the single movements in order to activate simultaneously two DOFs in a complete movement. For both phases signals from lower-limb have been detected by using high-density surface electromyography (HD sEMG). Specifically, electrodes grids of 8x4 and 8x8 channels have been employed. In addiction, during the Exp2, joint angles were recorded with two electrogoniometers. Data were factorized offline through a Non-negative factorization method. This linear factorization algorithm allows to extract information related to muscle synergies and activation signals. Different analysis were conducted in this study: in order to verify the assumptions of the theoretical synergy model, 15 channel sub-configurations (8 evaluated with 10mm interelectrode distance, 5 with 20mm) were selected from the total channels number of knee (196 single differential signals) and ankle (84 single differential signals) joint. The investigation showed that the proposed method is robust both with channels shift (in a transversal and longitudinal direction with respect to the muscle fiber) and with a channels dimensionality reduction and it is suitable for a control signal extraction. This confirmed that the EMG signals recorded from lower-limb muscles can be approximated as a linear instantaneous mixture of activation signals. In addiction, the proposed method has been validated comparing calculated control signals and recorded joint angles showing high R^2 values.

Initial Considerations

As reported from World Health Organization (WHO), since 2000 a growth related to the number of worldwide people over 60 years has occurred. Specifically, data from United Nations affirmed that in 2012 this category represented more or less 11.5% of the whole world population. This percentage is destined to reach 22% no lather than 2050. During this period, the number of people aged over 60 years will rise from 605 million to 2 billion. This category of people has not an equal distribution. For example, 54% of elderly people live in Asia. Specifically, Japan in 2012 registered more than 30% of 60 aged people. Europe instead shows a 22% [1][2].

In addiction, 10% of the worldwide population presents different disabilities. As reported from *"2013 China Statistical Yearbook of disabled people"*, their presence is about 37,95 millions. This value includes also the physically limb disabled for 16 millions roughly[2]. The consequences of this situation lead to increasingly frequent issues related to physiological functions of this people. Indeed, their daily living activities are nowadays compromised by the most common and known neurologic injuries as weaknesses of the skeletal muscles or spinal cord injuries or stroke[3]. The last one has a particular importance because it cause long-term disability. Stroke is defined as a death of nervous cells caused by lack of oxygen due to an interruption in blood flow or by a rupture of an artery and it can lead to dementia and depression[6]. Further, stroke survivors are affected especially in gait.

For all these reasons, rehabilitation techniques acquired a great importance to restore the functionality of injured patients. Nevertheless, employed methods are strongly related to therapist's experience. Consequently, it is difficult to couple repetitive training and with high-intensity. This is due to the fact that each treatment can result subjective and the effect is not ensured. From this perspective, robotics for rehabilitation allows to overcome the cited limits. Indeed, by using robots the physical capabilities of the therapist are not so relevant and it is possible to supervise the recorded data during each training, in order to evaluate the patient recovery status[4]. Moreover, for the rehabilitation purposes, wearable robots such exoskeletons are employed. Wearable robots are mechanical devices that have been projected to be worn by the subject and they are able to increase his strength or physical resistance and, in addiction, to assist him during the motor function recovery[1].

Thesis Aim

This work of thesis has been developed thanks to the cooperation between LISiN (Laboratory for Engineering of the Neuromuscular System, Turin) and department of Bioengineering at Imperial College of London. This project aims to produce a signal useful to control a lower limb exoskeleton (multi DOFs movements) using high density surface electromyography. Hence, electrical signals have been recorded from principal muscles of knee and ankle joint. More specifically, muscular activations have been acquired through electrodes grids. The contribution of this thesis is the use of a semi-supervised method as control strategy. Indeed, most the employed methods to perform a simultaneous and proportional control of more DOFs are supervised. This means that they need to acquire both EMG signals and kinematic in order to train the algorithm. A large amount of data implies more hardware and time required [22]. Hence, the proposed method needs only EMG signals. It is based on muscle synergy model [20], where it is assumed that a movement can be considered as a translation of low-dimensional commands into muscle activation patterns with high dimensionality through a translation matrix, or synergy matrix[22]. In addiction, the examined model sustains that muscle activation patterns recorded on surface are a linear instantaneous mixture of low-dimensional command signals[21], even if the volume conductor exerts a filtering effect that can annul the hypothesis of linearity, showing a convolutive behavior of the signal mixture [23]. Confirm this assumption would allow the extraction of a control signal without the influence of electrodes number or placement.

Previous researches applied a control strategy with a semi-supervised approach on forearm, in order to control a multi-DOFs upper limb prosthesis. In those cases, there was only wrist joint to control [22][29]. More specifically, in [22] the hypothesis of linearity has been proved. This thesis instead want to apply this approach to two different joint (knee and ankle), in order to extract two control signals. They will be sent to the exoskeleton with the aim to perform a complex movement. For this reason, this research investigated through different analysis to verify if it is possible to confirm the fundamental assumption for the studied joint. After that, the control signals were extracted.

Two experiment were performed. The first one aimed to estimate a synergy matrix that includes weights from both joint. For this reason, in this phase each subject performed simple flexo-extension movements activating only one joint at a time. The second instead was useful to the extraction of a control signal for each joint. EMG related to complete movements (coupling of knee and ankle activation) were

recorded. Thus, the synergy matrix estimated during the first experiment was used to extract control signals from EMG recorded in the second phase.

Data have been processed using a Non-negative matrix factorization algorithm in order to extract both synergies and activation signals (low-dimensionality commands). For each joint, from the total number of electrodes a progressive channels reduction was applied in order to create different channels subsets.

In addiction, for what concerns the first experiment a similarity investigation between channels subsets of different size has been conducted with the objective to verify the basic assumption of this model. The analysis has been applied both on extracted synergies and activation signals.

In the second experiment instead, a qualitative study about the goodness of resulted control signal of each joint was realized. In particular, each control (calculated by the proposed method) was compared with a joint angle signal acquired by using some electrogoniometers during the exercises of second experiment. This choice is due to the necessity to match the outcomes obtained from the algorithm (thus estimated) with the ground truth measure.

This work of thesis is organized as follows; Chapter 1 provides general information concerning surface electromyography and describes which muscles have been included in the study. In addiction, an overview of existing exoskeletons is described. Chapter 2 explains all experimental phase. First of all, the employed algorithm is explained and then each experiment is described singularly. Moreover, everything about data processing is stated. After that, Chapter 3 shows all results focusing on similarity analysis for first experiment and performance of extracted control for the second one. Further, outcomes from a statistical test are showed. Finally, Chapter 4 summaries all achieved results. In addiction, some future developments are proposed.

Contents

List of Figures

List of Tables

List of Abbreviations

MU   *Motor Unit*

IAP   *Intracellular Action Potential*

CV   *Conduction Velocity*

MUAP   *Motor Unit Action Potential*

BSS   *Blind Signal Separation*

MIMO   *Multiple-Input,Multiple-Output*

NMF   *Nonnegative Matrix Factorization*

DOF   *Degree of Freedom*

ADL   *Activities of Daily Living*

SENIAM   *Surface Electromyography for Non Invasive Assessment of Muscles*

EXP 1   *Experiment 1*

EXP 2   *Experiment 2*

SD   *Single Differential*

DD   *Double Differential*

IED   *Inter-Electrode Distance*

NDP   *Normalized Dot Product*

NCC   *Normalized Cross Correlation*

ANOVA   *Analysis Of Variance*

Chapter 1

Introduction

1.1 Physiology of Motor Control

The motor system in humans has to face with a wide number of stimulus, both internal and external. In particular, the skeletomotor system has a fundamental influence for what concerns the control of force and movements.

Figure 1.1 shows a scheme of the central motor system. It is organized in a top-down structure. Indeed, impulse for movement comes from different region such premotor cortex and supplementary motor area. Stimulus from these areas reach the primary motor cortex where it is possible inhibit or excite the neurons in this region. This step is very important because the outgoing impulses are able to influence motor neurons related to brain stam and spinal cord. In addiction, alfa (α)-motorneurons and the corticospinal tract are connected and this allows a cortical control of muscle activity. Looking at the right side of Figure 1.1 a fundamental motor unit (MU) is showed. It is composed by an α-motoneuron in the spinal cord, that constitutes the final point of all contributions resulting from descending and reflex input, and by all muscle fibers that it innervates.
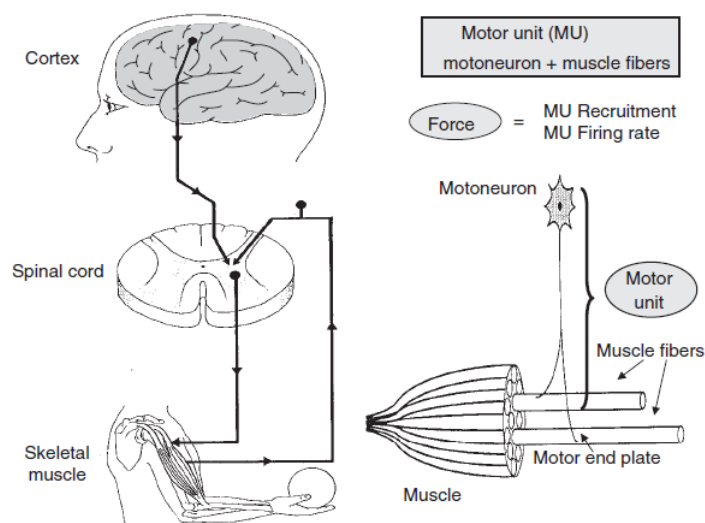
FIGURE 1.1: *Figure shows a framework of basic motor control mechanisms. All components are depicted[7].*

Withing a motor neuron, sites of synaptic innervation produce a current that causes the firing pattern of the motor unit. In this way, MU expresses its activity. Human muscles present an amount of MUs per muscle with high variability. In fact, a small muscle in a hand can show 100 MUs whereas a large muscle achieves 1000 or more MUs. There exists different types of motor units, but make a classification based on physiological properties results very difficult. For this reason, muscle fibers have been classified with histochemical criteria: there are type 1 muscle fiber with elevated value of ATPase and low level related to SDH (succinic dehydrogenase, that influences the aerobic energy production). As opposite, type 2 fibers presents the reverse enzymatic behavior [7].

1.2 Electromyographic Signal

The electromyographic (EMG) signal is the result of depolarization process performed from the outer fiber muscle membrane, also called sarcolemma. This action lead to the existence of an electric potential field which represents the EMG signal. Usually, in order to detect him it is necessary employ intramuscular or surface electrodes. They are positioned more or less distant from the signal sources. In addiction, a very important factor for the signal acquisition is represented by the tissue in the middle between source and electrode. It is also called volume conductor and its properties play a crucial role for the characteristics of detected signals. In particular, the tissue acts as low-pass filter (both spatial and temporal) and it modifies the potential distribution.

For what concerns the process in details, a motor neuron generates an action potential that reaches the neuromuscular junction. This implies that acetylcholine is released between the nerve termination and the muscle fiber membrane. The latter is turned on for the neurotransmitter effect and a potential gradient takes place within the fiber. This potential is expressed by an inward current density, corresponding to a depolarization zone. It spreads along the fibers and it goes from the neuromuscular junction where the phenomena starts, to the tendons. The generated potential is known as intracellular action potential (IAP).

The following Figure 1.2 describes how a motor unit generates a surface potential: it is possible observe that a motor neuron reaches three different fibers, creating a neuromuscular junction for all of them. When a potential is generated, within each fiber there is a depolarization zone that propagates in both direction towards tendons. In addiction, on the top of the figure is depicted the propagation velocity of the action potential. Because of the relation with signal conduction inside the fiber, it is called conduction velocity (CV). It is influenced from diameter of muscular fibers. Generally it is equal to 4 m/s within them. It must be noted that this relation holds true also within muscles with neuromuscular diseases. Finally, on the bottom (right side) of the figure a focus on the source is showed. It is modeled by a tripole with a positive charge in the middle and two negative charges on left and right side[8].
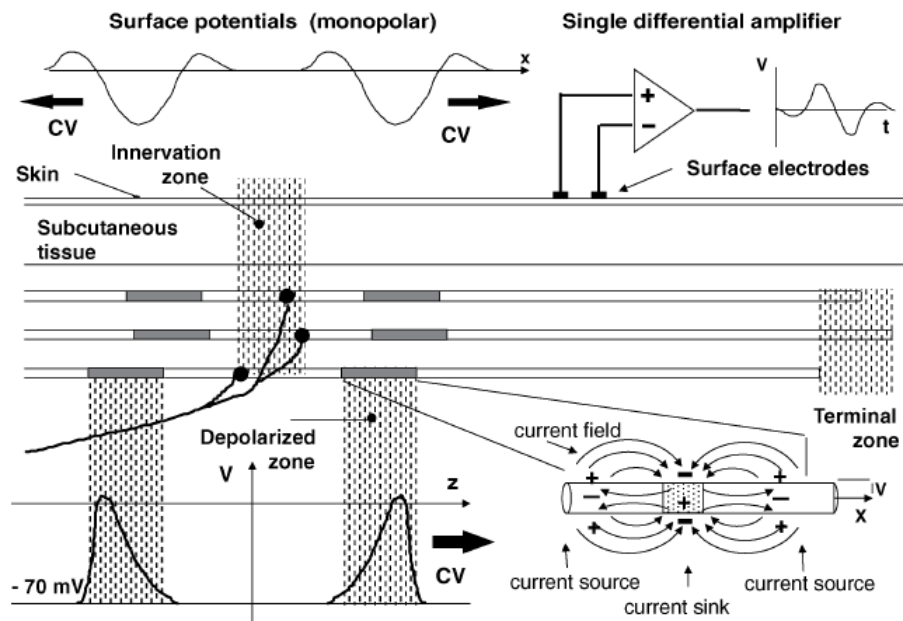
FIGURE 1.2: *Figure depicts the process of action potential propagation. In addiction a focus on the tripole that models the depolarization zone is showed[8].*

1.3 EMG Collection

The EMG detection can be realized using two different approaches, a intramuscular technique or an acquisition with electrodes placed on muscular surface. The first cited approach expects to insert the electrodes (usually needles) directly in the muscle. This allows to identify the potential near to the source. In addiction, the volume conductor effect in this case is minimal because there is no the same portion of interposed tissue between source and detector. These considerations lead to a good separability for the detected action potentials of MUs; in fact they can be distinct also with low/medium force levels. For what concerns the surface acquisition technique instead everything is different. Indeed, in this case the phenomena of volume conductor is relevant and the electrodes placement plays a key role and it can cause some issues. In order to attenuate the power line interference and the low-pass filtering effect related to interposed tissue, signals on surface are detected as linear combination of EMG derived from more electrodes. This causes a spatial filtering effect. EMG signals can be recorded as monopolar or bipolar fashion. First one includes EMG and a reference electrode that can be positioned far-away, the other consists in two electrodes at a limited distance. In addiction, they have to be positioned along the fiber direction. The following Figure 1.3 shows a comparison between intramuscular and surface detention as a function of distance from source and detector. It is evident that volume conductor plays a fundamental role; in fact deeper sources highlight small amplitude on surface if compared with the others[8].
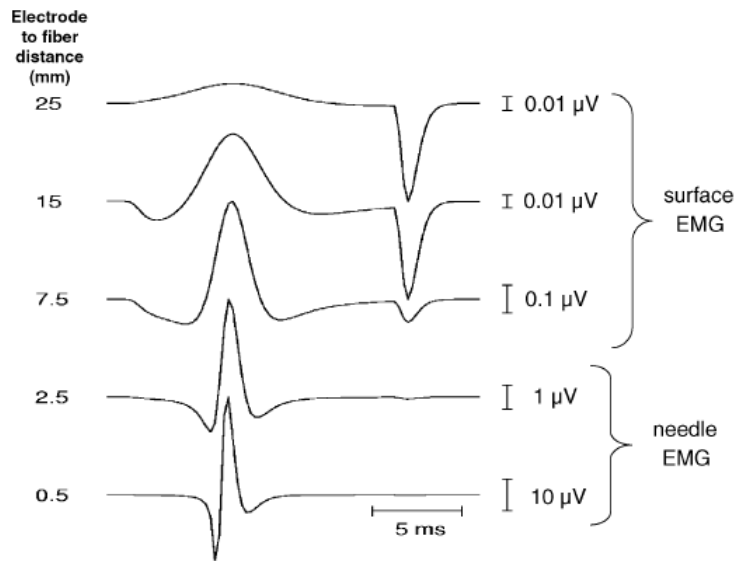
FIGURE 1.3: *Comparison between signals detected with surface or intramuscular EMG as a function of depth[8].*

1.4 Surface EMG

The most known method to acquire electromyographic signals from muscles surface (surface EMG or sEMG) is simply represented by a pair of electrodes positioned on the skin surface, above the interested area to detect. In addiction, a differential amplifier allows to represent the signal with an acquisition software. Properties of acquired EMG depend on the distance between electrodes (IED), placement and size[8].

As discussed before, the fundamental role of electrodes configuration and location for EMG acquisition is known for several years. In addiction, these factors are still a challenge and sometimes lead to different issues. There are three type of configurations with which realize EMG detection. The simplest one is the monopolar configuration, as cited before. A recording conducted with this modality, it allows to maintain all available information. However, it has the drawback that also common mode signals are preserved. An other type of detection is the bipolar o single differential (SD) configuration where noise is mitigated. In addiction, there is also a double differential (DD) configuration that is useful when it is necessary to evaluate the CV or limit the volume of acquisition or have a great selectivity. Beyond the discussed configuration, there is also a category of surface EMG related to a wide number of electrodes. In fact, since the electrical potentials describe EMG maps on muscular surface, it is possible use electrodes grids applied on the skin in order to appreciate a different representation. This type of recording is related to high-density surface EMG (HDsEMG). This depiction is very interesting; indeed acquiring these EMG potential maps from the same region in time, it is possible to see how the potential distribution changes in time. In order to show these maps in a better way, it is not employed the electrical potential but a specific EMG feature within them[8].

1.5 Motor Synergies

The human movement, also the simplest one, is the outcome related to the coordination of many muscles. For example, hundreds of activations are necessary to produce a locomotion. In any case, the aim is the activation of the α-motorneurons. In this view, the importance of motor control strategies is crucial for what concerns the mechanical effect produced with a muscle activation[8]. Motor control theories have been developed many years ago. One of these sustained that the generation of a movement would be too much costly for CNS if it would control singularly each muscle. For this reason, the control strategy of CNS should be based on a internal representation, related to low dimensional task-level, of the complex external environment. Consequently, these task-level command are converted in muscle activation patterns to perform a complex movement. Hence, CNS organizes its neuronal networks with modules, or synergy. It is defined as a "set of relative non-negative levels of muscle activation"[9]. Given a synergy, an action to change also a complex pattern can be traced back to the linear combination of a given number of basic patterns.
EMG detection represents a valid instrument to analyze the strategies used by CNS to coordinate a lot of muscles that activate together. For this reason, it is necessary to record simultaneously a large number of muscles, or at least those with a significant activation during the movement. This is due to the fact that a lack of information, because of a missing muscle, does not allow to discover the hidden organization of muscular patterns. Usually, in order to study motor synergies from sEMG, envelopes are evaluated because their trend is similar to the muscular activation. Moreover, synergies are studied by factorizing the recorded sEMG with the objective to discover both modules and activation signals.

There are two models useful to describe synergy. The first one is the *time-invariant synergy model*, expressed by the following equation:

$$\mathbf{m}(t) = \sum_{i=1}^{N} c_i(t)\mathbf{w}_i + e(t) \tag{1.1}$$

where the muscle pattern $\mathbf{m}(t)$ comes from synergies $\mathbf{w}_i$ and coefficients c_i that are combined in a linear way.
The second type is a *time-varying synergy model*, where

$$\mathbf{m}(t) = \sum_{i=1}^{N} c_i\mathbf{w}_i(t - t_i) + e(t) \tag{1.2}$$

In this case, the muscular activation is composed by combinations of the whole number of synergies that are time-dependent.
In this work of thesis only the time-invariant model, expressed in relation 1.1 will be used.

1.6   Neurophysiological Processes within EMG

On the fundamental concepts discussed for motor synergies, in this section a model for surface EMG is described in order to understand the CNS control strategy.
Figure 1.4 shows a model for surface EMG proposed in [21]. It indicates that the information useful to control a movement exists at the spinal level. In addiction, this control information is modeled as a group of *force functions*, varying in time. This functions include all activation levels for every DOFs. Hence, they have dimension that corresponds to the number of DOFs of the movement.
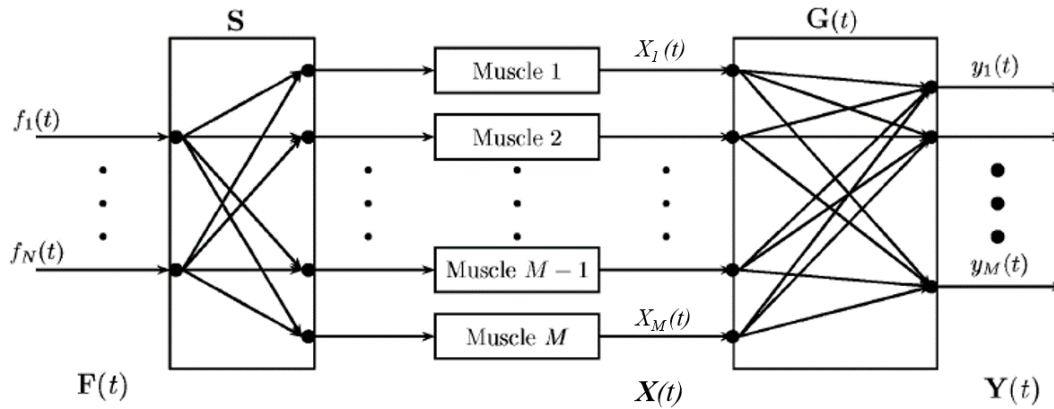
FIGURE 1.4: *Figure shows a schematic representation of the model for surface EMG. Image has been modified from [21].*

Considering a single joint, able to perform N DOFs, the force functions are expressed as

$$\mathbf{F}(t) = [f_1(t), f_2(t), ..., f_N(t)]^T \tag{1.3}$$

where f_n(t) indicates the force function for the *nth* DOF. Further, each force function has a maximum frequency f_f lower than 5 Hz and this is due to the physiological ability of neuromuscular system. At this point, if the movement of the considered joint includes M muscles, the equation

$$\mathbf{X}(t) = [x_1(t), x_2(t), ..., x_M(t)]^T \tag{1.4}$$

describes the activation function for every muscles. Specifically, x_m(t) is related to the *mth* muscle and it can be indicated as

$$x_m(t) = \sum_{n=1}^{N} (s_{mn} \cdot f_n(t)) \tag{1.5}$$

while in matrix form, it is possible simply express with

$$\mathbf{X}(t) = \mathbf{S} \cdot \mathbf{F}(t) \tag{1.6}$$

In the last 2 equations, $\mathbf{S}$ is a matrix with dimensions *M x N* where each element (in general s_{mn}) correlates the activation of a given DOF (indicated with subscript n)

performed by a given muscle (indicated with m)[21].

The investigation can be conducted for both intramuscular and surface EMG detection, but this work of thesis focuses only on acquisition from muscular surface. In case of sEMG, if it assumes that there is not effect of volume conduction filtering but the only attenuation depends on the distance between source and detector, the mixture can be considered linear instantaneous. Consequently, the activation $y_k(t)$ recorded on a muscle for the generic kth electrode is explained as

$$y_k(t) = \sum_{m=1}^{M} g_{km} \cdot x_m(t) = \sum_{n=1}^{N} (\sum_{m=1}^{M} g_{km} \cdot s_{mn}(t)) f_n(t) = \sum_{n=1}^{N} w_{kn} \cdot f_n(t) \qquad (1.7)$$

This relation explains the linearity between activation signals and the surface of detection. The factor g_{km} indicates the attenuation value that it is influenced only by the distance source-electrode. In addiction, w_{kn} is a weighting factor between the nth command signal and the kth electrode.

If the hypothesis regarding the volume conductor is not applicable, the signals mixture is convolutive and the contribution on muscular surface changes. In fact, the activation at the kth electrode is expressed as

$$z_k(t) = \sum_{m=1}^{M} \sum_{l=1}^{L} g_{km}(l) \cdot x_m(t-l) = \sum_{m=1}^{M} \sum_{l=1}^{L} g_{km}(l) \cdot \sum_{n=1}^{N} s_{mn} \cdot f_n(t-l) \qquad (1.8)$$

It is noticeable that in this case the filtering effect plays a fundamental role; in fact L represents the filter length. Thus, this case indicates that the mixture related to the kth electrode is not linear instantaneous but it is a noninstantaneous combination of activation signals.

In order to describe both cases in a compact fashion, matrix form for the linear instantaneous can be indicated as

$$Y(t) = G \cdot X(t) = G \cdot S \cdot F(t) = W \cdot F(t) \qquad (1.9)$$

where W is a matrix with K rows (channel recorded) and N columns (number of channels weighting vectors) and, in a study related to motor control, it can be interpreted as synergy matrix. Matrix form underlines the linear relation between EMG signals detected Y(t) and command signals F(t). In addiction, weights matrix W is not related with the synergies that CNS encodes. On the opposite, they are weighting factors that allow to activation signals to be transferred on surface. Moreover, the number of weighting vectors corresponds to the number of activation signals N.

Instead, if the mixture is convolutive, matrix form is expressed as

$$
\begin{aligned}
Z(t) &= G * X(t) \\
&= \sum_{l=0}^{L} G(l) \cdot X(t-l) \\
&= \sum_{l=0}^{L} G(l) \cdot S \cdot F(t-l) \\
&= \sum_{l=0}^{L} H(l) \cdot F(t-l) \\
&= [H(0)|H(1)|\ldots|H(L)|] \\
&\quad \cdot [F(t)|F(t-1)|\ldots|F(t-l)]^T
\end{aligned}
\tag{1.10}
$$

where the matrix [H(0) | H(1) | ... | H(L) |] now has dimensions of K $\times$ [N $\times$ (L+1)]. It is evident that the dimensionality of channel weighting vectors is larger than N. For this reason, the N command signals are not correlated. Further, the delayed versions can be partially correlated. Thus, it would be necessary to obtain a dimensionality wider than N in order to consider also the information related to partially correlated signals.

1.7 Muscular Joint Interested

This thesis focused on the control of a lower-limb exoskeleton. Thus the most important muscles related to knee and ankle joint were employed for EMG detection. In particular for both of them, movements of flexion-extension for knee and dorsi/plantar flexion for ankle have been realized.

1.7.1 Knee Joint

Muscles related to knee joint can be separated between extensors and flexors by a fundamental characteristic: those with a movement path anterior respect the knee joint axis (for example quadriceps femoris) are extensors, whereas those with a path posterior to knee axis are flexors. Extensors muscles in the knee originate on the femoral surface and they spread along the anterior-posterior thigh surface. The biggest muscle that encourages the extension of the knee is the *Quadriceps femoris*. It consists of wide muscles: *Vastus Lateralis* and *Vastus Medialis* and *Vastus Intermedius*. The first two muscles are superficial while the Vastus intermedius is in depth. These muscles originate along the femur bone and, all togheter, wrap the *Rectus Femoris*. This muscle comes from the anterior-inferior iliac spine; for this reason, it is involved both during knee extension and also in hip flexion. For what concerns the distal termination, all these muscles end onto the tibial tuberosity, through the tendon of

quadriceps. Figure 1.5 shows a global vision of knee joint; all interested muscles have been highlighted with a colored box.
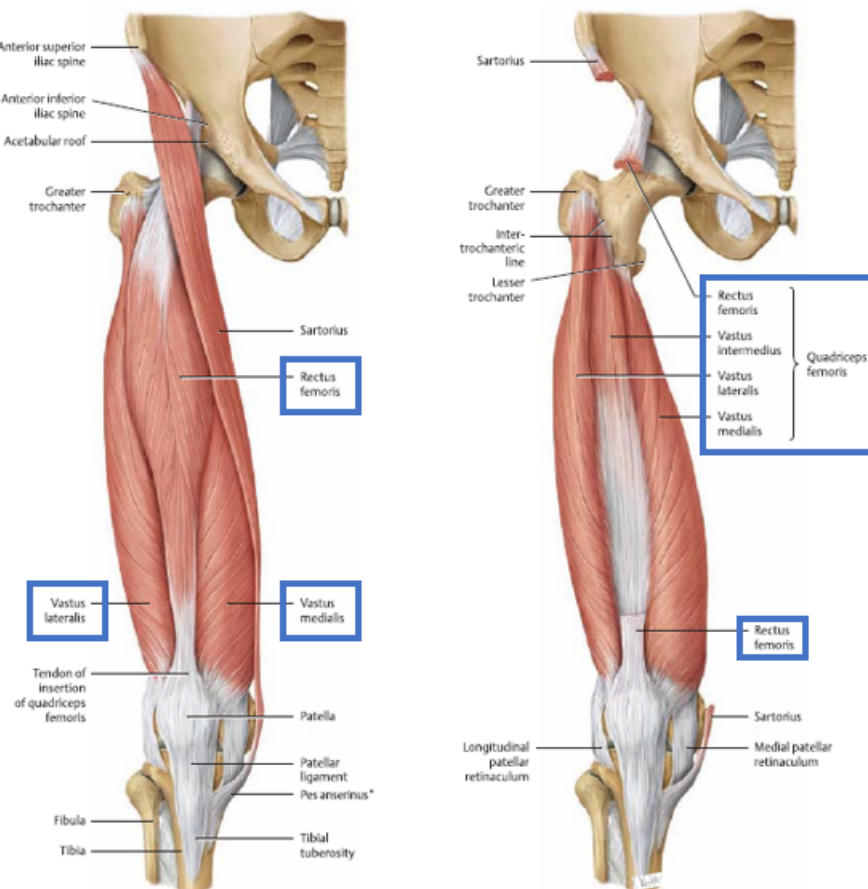
FIGURE 1.5: *Figure shows muscles related to anterior region of knee joint. Left-side: superficial view, Right-side: deep view [11].*

For what concerns flexors, knee joint shows *Biceps Femoris* (short and long head), *Semitendinosus*, *Semimembranosus* and *Sartorius*. In this thesis only first two cited muscles have been recorded. All these muscles originates on pelvis edge and then they insert on tibia and fibula. By contracting, they perform a flexion of the knee. The first three cited muscles are known also as "back thigh muscles". Because of their origin on pelvis and posterior respect to the acetabulum, their activation cause also an hip extension[10]. Flexors muscles are depicted in Figure 1.6.

1.7.2 Ankle Joint

Most of the muscles related to ankle joint are useful to produce a plantar flexion. This movement occurs during activities as gait and run. In this view, *Gastrocnemius* is a wide muscle split in medialis and lateralis. Their power is increased because of the presence of the *Soleus* in depth. Gastrocnemius origins from two tendons that are linked to both medial and lateral femur condyles, while it ends (together with soleus) on a common tendon (calcaneal tendon, most commonly known as Achilles tendon).
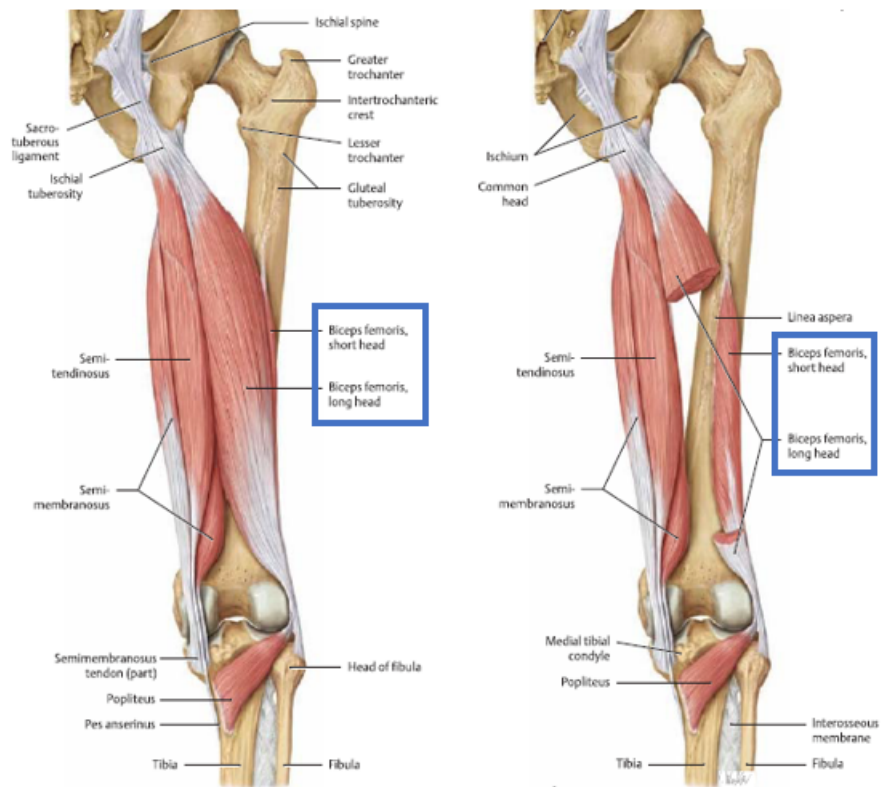
FIGURE 1.6: *Figure shows muscles related to back region of knee joint. Left-side: superficial view, Right-side: deep view* [11].
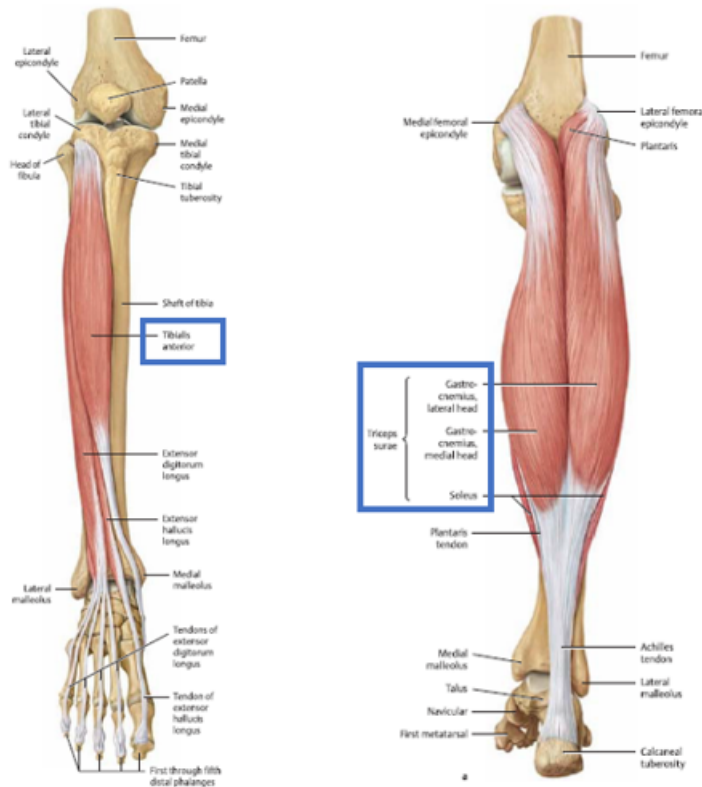
FIGURE 1.7: *Figure shows muscles related to ankle joint. Left-side: front view, Right-side: back view* [11].

In addiction, there are two muscles responsible for the plantar flexor; they are fibularis muscles and they are located in depth, under gastrocnemius and soleus. For what concerns the dorsi flexion of the ankle, the most representative muscle that provides this movement is the *Tibialis Anterior* that it is opposed to the gastrocnemius. For the ankle in this thesis have been recorded tibialis anterior and both gastrocnemius lateralis and medialis[10]. Figure 1.7 summaries all cited muscles.

1.8 Lower-Limb Exoskeletons

This section provides general information related to exoskeletons development in previous years with some examples. In addiction, a few considerations about EMG control-based exoskeletons are supplied. Finally, a brief description of the employed exoskeleton is provided.

1.8.1 Related Researches

Research oriented to the exoskeletons control in order to support human does not represent a new technology field; in fact, during '70s a group (guided by Vukobratovic) realized a model of rehabilitation exoskeleton. Results were not positives because of technological limits, like a reduced computer processor power and heavy actuators. In the years following many projects have been developed thanks to technological improvements. There are some fundamental factors to consider for an exoskeleton design; mobility of the operator is maybe the most important and the increasingly reduced size and weight facilitate this aim. Although the mechanical part has a great relevance, also the exoskeleton control strategy is an important challenge, in order to avoid a misinterpretation of the operator movements that can result in injuries[12]. Some examples of projects related to exoskeletons are described below.

Exoskeleton Walking Aid, Yugoslavia This device was projected around 1970 from Vukobratovic research group and it was conceived as wearable exoskeleton to help patients with locomotive deficits. A few versions were projected. In general, first version had actuators for only hip and knee joint while ankle was passive. It had an high encumbrance and heavy weight. In addiction, a complete paraplegic needed a support from two assistants to keep his balance. However, after many changes, main issues were a system constricted to indoor use because of the air supply (separated from exoskeleton) and large hardware required[12].

BLEEX, University of Berkeley, USA This project was conducted with the aim to design an exoskeleton for human strength augmentation. In fact, the main use was the application within outdoor environments where there is a need to transport heavy loads over large paths in a limited time. BLEEX included, for both legs, actuators of hip, knee and ankle joint in sagittal plane.

This exoskeleton is not provided of sensors that record biological signals of the operator. In addiction, neither interaction forces between human and devices are measured. Despite this, the device tries to minimize these interaction forces with a philosophy of "out of the way of the operator as quickly as possible".

Thus, the operator does not feel the load applied. For what concerns the control in case of unexpected forces on the person, no algorithms were implemented to manage the postural stability. For this reason, for this devices the response of the operator plays a key role, because he has to counterbalance an eventual imposed movement[12].

FIGURE 1.8: *BLEEX Exoskeleton design [13].*

HAL, University of Tsukuba, Japan   The Hybrid Assistive Leg (HAL) exoskeleton has been designed with the purpose of support elderly people and gait disordered people. With HAL, the process starts from the EMG signal detected from muscle of the operator. First prototype of HAL included four actuators localized at the hip and knee (both legs), while latest version introduced also actuators for both shoulder and elbow joint. For this exoskeleton, different control strategies have been realized. The first is a "phase sequence algorithm", employed for stepping-up motion. This control consists of five phases: switch among each of them happens only when joint angles and measured center of gravity respects some criteria. In addiction, within every phases there is a predefined path for all joint.
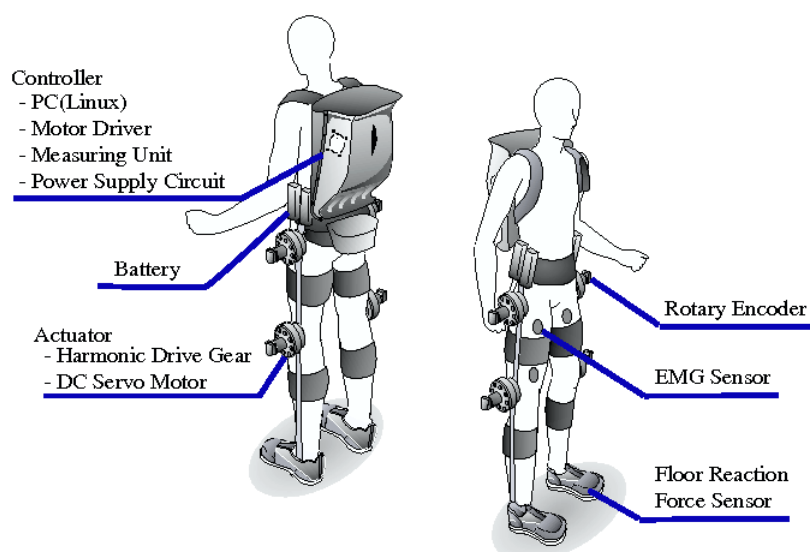
FIGURE 1.9: *HAL Exoskeleton design (first prototype) [14].*

With HAL exoskeleton, EMG signal is detected from the Rectus Femoris muscle in order to start the movement. At this point, the system wait for an increased muscular activation and select 300ms of signal in order to process it. Thanks to a linear relation obtained with a calibration performed at the beginning, EMG signal is converted into a hip angle. This angular value is used as reference for the position. Hence, after 300ms, the device on the basis of calculated angle decides which change of phase apply. For the remaining parts of the movement are used predefined trajectories. In addiction to control strategy for stepping-up, others controls have been improved in order to perform tasks as sitting-down or walking[12].

1.8.2 H2 EMG Controlled Exoskeleton

From all examples showed until now it is evident that a rehabilitation with lower-limb exoskeletons, controlled with information from biological signals, is hard to realize. However, these rehabilitation devices continue to be developed but they are affected of some issues. One of the most evident problems is that gait rehabilitation should be projected to ensure a repetitive training for longer therapy sessions. Unfortunately, patient has a passive role during the exercises, so he achieves some results initially but after a few weeks all advances stagnated. To solve this issue rehabilitation robotics have been improved in order to stimulate the patient with the possibility to change a fixed trajectory, providing feedbacks in different fashion (visual or force) and acting only when he requires assistance.

FIGURE 1.10: *H2 Exoskeleton design [5].*

Nevertheless, all these efforts did not lead to appreciable results. This is due to the fact that there is a substantial gap between the intention of user and the fixed device trajectories and there is a lack of concentration from user because of his passive role during the exercise. For all these reasons, a new concept of rehabilitation with robots has been proposed in the last few years. The novel approach would try to decode user's neural activity in order to evaluate his effective intention and, in the next step, apply a correct command to the robot actuators. This method aims to two outcomes; the first is to improve gait task of the patient, while the second is to stimulate and reinforce the interested cortical region during recovery tasks[15]. With these purposes, EMG signal can represent a solution to control a lower-limb exoskeleton. In this direction, a EMG-driven algorithm was presented in [16] in order to control the exoskeleton employed in this work of thesis. The H2 lower-limb exoskeleton showed in Figure 1.10 (Technaid S.L.,Spain) includes six DOFs organized for hip, knee and ankle joint. Each DOF includes a position sensor and a motor torque sensor[16]. For what concerns the mechanical side, H2 has been designed to rehabilitate adults with height between 1.50 m and 1.95 m. It can able to support a maximum body weight of 100 kg [5].

Chapter 2

Materials and Methods

2.1 Blind Source Separation Problem

In the science and engineering environment data analysis, data mining and signal processing earned an important role. As a matter of fact, the extraction of knowledge from raw dataset constitutes an important challenge. Sometimes the analyzed datasets hide complex phenomena as result of several inter-related factors and, for this reason, they have to be separated into components in order to discover their hidden internal structure.

Blind Source Separation (BSS) is a mathematical method that decompose the original data by a lower-dimensional approximation through matrix factorization or data decomposition. The optimal strategy depends on the different type of data to factorize. For example, a great number of analyzed data are partially or totally non-negative. Thus, in these cases, it needs to take in account the non-negativity constraint to extract positive information. This is crucial to ensure a correct physical meaning and proceed to a reasonable explanation, avoiding unpredictable outcomes.

BSS adopts a large number of unsupervised learning algorithm, which are used in a lot of applications from engineering to neuroscience. The aim of BSS is, starting from a structure of multi-dimensional data as input, to express the meaning of a physical source and the parameters forming part of a unknown mixing system.

Figure 2.1 shows an example of BSS problem; the system output

$$y(t) = [y_1(t), y_2(t), ..., y_I(t)]^T \qquad (2.1)$$

includes all the observation recorded from I sensors. All signals belong from a MIMO (multiple-input/multiple output) mixing and filtering system. The output signals are an overlapping (also called signals mixture) of J unknowns source signals

$$x(t) = [x_1(t), x_2(t), ..., y_J(t)]^T \qquad (2.2)$$

and noise expressed as

$$e(t) = [e_1(t), e_2(t), ..., e_I(t)]^T \qquad (2.3)$$

Because of the system composition, it is necessary to estimate the source signals *x(t)* from the output *y(t)*. Usually it is more useful identify the mixing system and
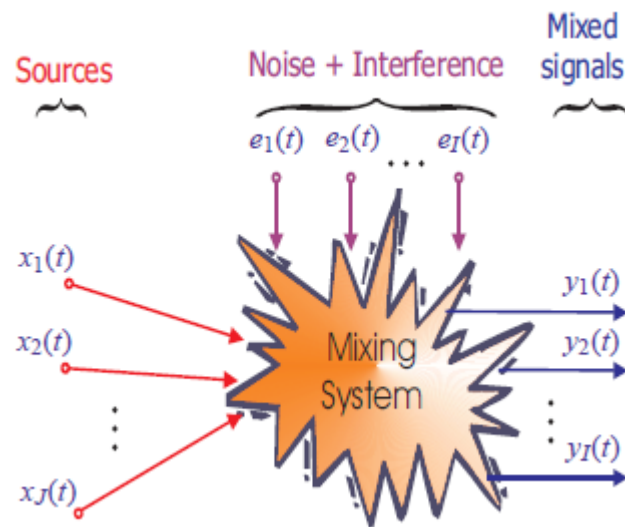
FIGURE 2.1: *General model illustrating blind source separation (BSS). The output y(t) is known and it is composed from the overlapping of unknown sources x(t) and interference e(t)[17].*

then to estimate the source signals with some *a priori* information but this appears very complicated since the mixing system is unknown. Furthermore, without *a priori* information about source signals the estimation is not unique. Anyway it is possible to assess them with indeterminacy or ambiguity because in mathematical terms these properties can be translated on source signals as arbitrary scaling and permutation. Fortunately, in a wide number of applications, the most relevant information about the source signals are included in the temporal waveforms or in the time-frequency patterns rather than in their amplitude or in the output order. Thus, since the waveform is preserved, source signals can be approximated from a mixture of signals without the knowledge of the mixing system. The BSS method that match with the non-negativity constraint required by muscular activation data is the Non-negative Matrix Factorization (NMF)[17].

2.2 Non Negative Matrix Factorization

In the previous paragraph basic concepts about Blind Source Separation have been analyzed. The complexity of studied phenomena requires to adopt models able to approximate the original data applying a lower dimensional representation. In addiction, it has been said that sometimes analyzed data are non-negative. Thus, this constraint has to be included also inside the low-rank data evaluated in order to prevent inappropriate conclusion. The non-negative factorization problem can be stated as:

"Giving a non-negative matrix $A \in R^{mxn}$ and a positive integer $k < min(m,n)$, find nonnegative matrices $W \in R^{mxk}$ and $H \in R^{kxn}$ to minimize the functional"

$$f(\mathbf{W}, \mathbf{H}) = \frac{1}{2}||\mathbf{A} - \mathbf{WH}||_F^2 \tag{2.4}$$

The product **WH** is an approximation of the input matrix **A** with rank k. A crucial point for a correct factorization of the input matrix is the k parameter choice; usually it is chosen in order to obtain $k \ll min(m,n)$[18]. Thus the NMF is able to decompose an input matrix A such that

$$\mathbf{A} \approx \mathbf{WH} \tag{2.5}$$

For the purpose of this thesis the input is a *mxn* matrix where *m* is the number of EMG channel recorded and *n* is the number of samples in the dataset. In addiction, the dimension *k* in the product WH represents the number of synergies chosen. The meaning of the (2.5) is simple: it can be written column by column as

$$a \approx Wh \tag{2.6}$$

where *a* and *h* are the columns of matrices A and H and it is noted that each vector of data *a* is approximated with a linear combination of the columns of matrix W, weighted by the components of h. Hence the matrix W can be identified as container for the optimized coefficients that allow to approximate the data in A [19].
The relation expressed in (2.4) represents a non-trivial minimization process due to two reasons: the first one is the non-convexity of **f(W,H)** in both W and H and this can lead to local minima phenomena. Moreover, as expressed previously, the NMF solution is not unique and this is easily proved by considering the product **WDD⁻¹H** for a general non-negative and invertible matrix **D** where its inverse **D⁻¹** remains non-negative.

2.2.1 Numerical Approach for NMF

The NMF algorithm needs the random initialization of W and H matrices with non-negative values before the iteration starts [18]. This step is crucial because the initial conditions, particularly in a multivariate context, influence the solution and convergence provided by the algorithm. Indeed, poor matrices initializations can lead both to a slow convergence and wrong solutions. A wide number of studies suggested different approaches for NMF initialization, for example based on a spherical k-means clustering or based on SVD (Singular Value Decomposition). In this thesis project the following multi-start random initialization has been proposed:

- A parameter R useful to fix the number of initialization procedure has been chosen. Typically, it is between 10 and 20 times.

- For each cycle, W and H matrices have been initialized with random number and they are used to perform an NMF algorithm run with Alternating Least

Square (ALS). At the end of the optimization in each cycle, estimated matrices $\mathbf{W^{(r)}}$ and $\mathbf{H^{(r)}}$ have been saved.

- At the end of all R cycles, the W and H matrices chosen for the next phase of the NMF algorithm namely $\mathbf{W^{(r_{min})}}$ and $\mathbf{H^{(r_{min})}}$ correspond to the cycle with the lowest cost function among the R trials [17][18].

For what concerns the classes of NMF algorithms, there are three fundamental categories to cite: multiplicative update algorithm, gradient descent algorithm and alternating least square algorithm. This work of thesis focuses the attention only on the last one.

2.2.2 ALS Algorithm

The alternating least squares algorithm is based on a sequence of least square step. This type of non-negative matrix factorization take advantage of the non total convexity of the relation (2.4). Indeed, the optimization problem is only convex in either W or H. Due to this reason, if one matrix is known, the other one can be easily calculated with a least squares computation. Principal steps of the ALS algorithm can be appreciated in Figure 2.2; the procedure perform at the beginning a least square computation to solve matrix H and then set to 0 all negative elements. After that, the procedure is repeated for W matrix. The ALS shows a lot of advantages: it is very fast and it reaches convergence in a limited time. This means that it need to work less despite the other NMF implementation. In addition, it has an important benefit if compared with the multiplicative algorithm. As a matter of fact during multiplicative update procedure, if an element of W or H acquires a null value it is not possible to change it. This means that when the algorithm starts walking towards a fixed point, even if a bad fixed point, it can't correct the wrong path. The ALS algorithm instead doesn't suffer of this problem and it is able, during the iterative process, to run away from a wrong path [18].

BASIC ALS ALGORITHM FOR NMF

$\mathbf{W} = \text{rand}(m, k);$ % initialize $\mathbf{W}$ as random dense matrix or use another
            initialization from Langville et al. (2006)
for $i = 1$: maxiter
(LS)   Solve for $\mathbf{H}$ in matrix equation $\mathbf{W^T W H} = \mathbf{W^T A}$.
(NONNEG) Set all negative elements in $\mathbf{H}$ to 0.
(LS)   Solve for $\mathbf{W}$ in matrix equation $\mathbf{H H^T W^T} = \mathbf{H A^T}$.
(NONNEG) Set all negative elements in $\mathbf{W}$ to 0.
end

FIGURE 2.2: *Principal steps of the Non-negative matrix factorization based on Alternating Least Squares algorithm[17].*

2.2.3 DOF-wise NMF Approach

In Chapter 1 the theory of CNS control strategy has been illustrated. In addiction, it has been said that if the mixture of signals recorded on the muscular surface can be approximated as a linear instantaneous combination of the activation signals, their extraction is attributed to an instantaneous linear BSS problem that can be solved applying a non-negative matrix factorization. In this work of thesis, the input matrix decomposition aims to extract information with a physiological meaning but, as seen previously, NMF produces solutions that are not unique both in amplitude and order. In order to perform a clear control to an exoskeleton for rehabilitation, data extracted have to be meaningful. It is necessary, as in the myoelectric control, to know which degree of freedom (DOF) is operative (indeterminacy in order) and quantify its activation (indeterminacy in amplitude). To satisfy these requirements, the following DOF-wise approach has been proposed [21].

Starting from the input matrix **Y(t)** and its approximation

$$\mathbf{W} \cdot \mathbf{F(t)} \tag{2.7}$$

the activation signals vector *F(t)* and the synergy matrix *W* can be written in a manner that the i-th element has both positive and negative component. For example, for the activation signals vector there will be:

$$
\begin{aligned}
f_i^+(t) &= f_i(t) \quad \textit{when} \quad f_i(t) \geq 0 \\
f_i^-(t) &= -f_i(t) \quad \textit{when} \quad f_i(t) < 0
\end{aligned}
\tag{2.8}
$$

Using this strategy with every element of the two vectors, the relation (2.7) can be written as

$$Y(t) = [W_1^+, W_1^-, W_2^+, W_2^-, ... W_D^+, W_D^-] \cdot [f_1^+(t), f_1^-(t), f_2^+(t), f_2^-(t), ..., f_D^+(t), f_D^-(t)]^T \tag{2.9}$$

where D is the number of DOFs. Thus the DOF-wise approach models a joint with two activation signals, which correspond to the different directions of each DOF. Summing up, in order to control a number D of DOFs, *N = 2D* activation signals will be required [22][21].

Now, from the equation (2.9) it is possible to show the benefit of this approach: considering the scenario in which only one DOF is activated (in general the i-th), the previous relation become simply

$$Y(t) = [W_i^+, W_i^-] \cdot [f_i^+(t), f_i^-(t)]^T \tag{2.10}$$

As presented in [21], this *"divide and conquer"* approach allows to split the whole signals mixture in a defined number of simple mixtures, related to each active DOF. As said before, every sub-mixture is an instantaneous BSS linear problem that can be

solved applying a non-negative factorization.

2.3   Experimental Procedures

This work of thesis focuses on the extraction of a control signal from muscular activity in order to provide a robust input signal for controlling motors of a lower limb rehabilitation exoskeleton. Four motors (two for knee joint and two for ankle joint) were available in the considered exoskeleton; for this reason, this work focused on knee and ankle flexion-extension movements. For what concerns the experimental phase, 7 able-bodied and non pathological subjects with age between 25 and 30 years participated in the experiment. More specifically, 2 subjects were involved during the pilot phase while the others performed the complete experiment. All people involved were males. This choice is due to the different fat distribution between genders. Indeed, as explained in [24], for a given body mass index (BMI) women have an higher fat layer compared with men, estimable at 10 percent roughly.

The protocol consisted of two steps. The purpose of the first one was to estimate a synergy matrix W from the EMG signals recorded during knee and ankle flexion extension performed separately. This process have been replicated for a number of selected channels subsets from the original electrode configuration in order to realize subsequent inferences. The second step was intended to verify the possibility to extract the activation signals from EMG signals detected during combined knee and ankle flexion extension using the estimated matrices obtained in the first step. In order to evaluate the performances of the system, extracted activation signals were compared with the true knee and ankle joint angle recorded from two electrogoniometers. In any case, all subjects were seated comfortably for the duration of the test. For what concerns the first experiment, ankle movements have been performed with the subject seated on a chair and foot on the ground, whereas he was seated with suspended foot to realize knee movements and for the duration of the second experiment. Moreover, in order to make easier and repeatable the task execution, a trapezoidal cue (similar for knee and ankle joint) was displayed on a computer screen positioned in front of the subject, as shown in Figure 2.3.
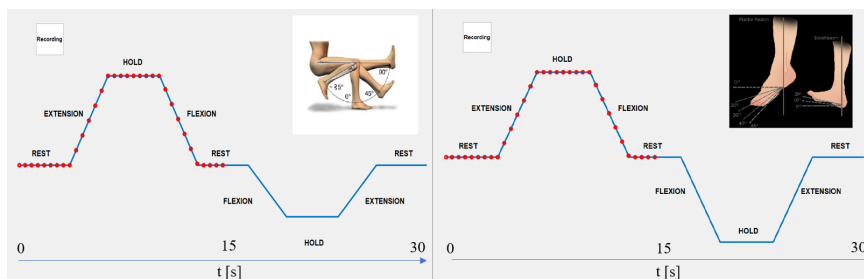
FIGURE 2.3: *Displayed trapezoidal trajectories during Exp.1 for Knee (left-side) and Ankle (right-side) movements. Labels applied on the cue indicate which phase of the movement the subject has to perform. Red markers only help the patient to keep a constant velocity.*

2.3.1 First Experiment

During the Step1 (Exp.1), the subject was asked to perform two tasks: 1) the flexion extension of the knee and 2) the plantar/dorsal flexion of the ankle separately. Each task included ten repetitions. For each task the subject was instructed to follow the trapezoidal cue reported in Figure 2.3. Each extension and flexion phase lasted 3 s while the rests lasted 5 s. The whole sequence lasted 30 seconds. In order to give at the subject a velocity feedback for a correct task execution, a sequence of red circle shaped markers was displayed on the trapezoidal cue. For clarity, the dynamic sequence shown on the cue was not related to the patient muscolar activation. Instead, it was only useful to give an information about the phase of the movement to perform. The same protocol was employed separately for both knee and ankle joint, insulating for each joint the interested DOF as required from DOF-wise approach. In addiction, the physiological range of motion of each joint were identified from literature[28]. For the ankle, the subject seated on a chair (reference position), the range identified in literature indicates 80° (30° for dorsiflexion and 50° for plantar flexion). For the knee, with the subject seated, the range was set in 125° (90° for extension and 35° for flexion). It is useful to specify that these range of motion only give a general information. Each subject moved with his own range of motion.
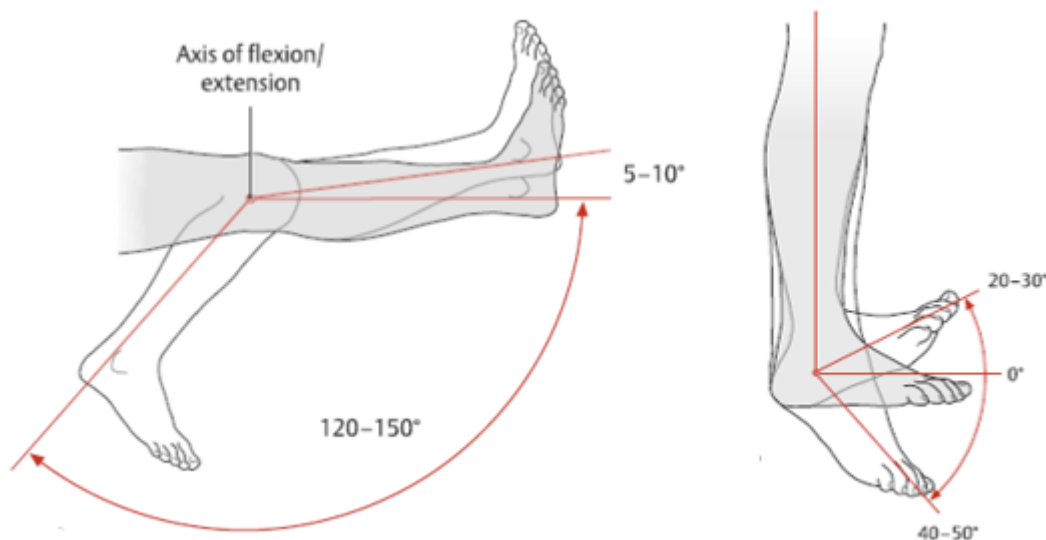
FIGURE 2.4: *Range of Motion for Knee flex-extension and Ankle dorsi and plantar flexion[28].*

High-density surface EMG signals were recorded from the most important agonist and antagonists knee and ankle muscles of the right leg of each subject. Four semi-disposable adhesive grids of 32 electrodes were placed on *tibialis anterior*, *gastrocnemius medialis*, *gastrocnemius lateralis* and *rectus femoris*. In addiction, three semi-disposable adhesive grids of 64 electrodes were placed on *vastus medialis*, *vastus lateralis* and *biceps femoris* (see Figure 2.8). All matrices were arranged in eight rows and four columns (case of 32 electrodes) or eight rows and eight columns (case of

64 electrodes) with 10 mm interelectrode distance (OT Bioelettronica & Lisin, Turin, Italy). An overview of the employed matrices is shown in Figure 2.5.

(a)   (b)
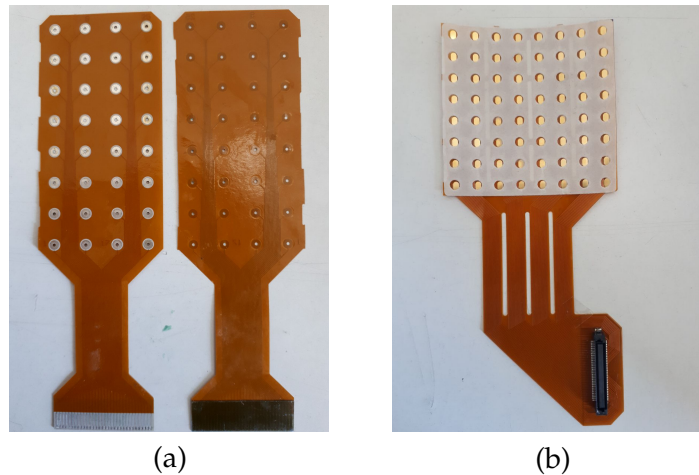
FIGURE 2.5: *Electrodes grids employed: 32 electrodes (arranged in 8x4 grid, IED=10mm)* **(a)**, *64 electrodes (arranged in 8x8 grid, IED=10mm)* **(b)**.

A patient reference electrode was positioned on the right ankle. The skin was prepared using abrasive paste prior to electrode placement.
Monopolar surface EMG signals were acquired (Quattrocento, OT Bioelettronica, Turin, Italy) with sample frequency of 2048 Hz and a 16-bit A/D converter. Signals were observed during the recording through a customized graphic user interface implemented on MATLAB®platform.

2.3.2 Second Experiment

The second experiment (Exp.2) was focused on the simulation of a complete movement activating both knee and ankle joint. In this phase the subject has been seated with the foot suspended. The protocol included ten repetitions of 30 seconds where the subject followed the same trapezoidal cue used in Exp.1 but this time the exercise was articulated in the following way: each subject performed the same exercise related to knee joint and he activated the ankle for a dorsi-flexion when knee was completely extended or flexed, while he performed a plantar-flexion when knee was in the central rest phase. High-density surface EMG signals were recorded with the same matrices used in Exp.1. In addiction, an elastic band bounded on both sides (under the knee and on the top of the right feet) was used to simulate a resisting force during ankle flexion-extension (see Figure 2.6). This was useful to keep a similar ankle muscular activation with the subject seated in a different position.

The aim of the Exp.2 was to test the performances of the proposed method, comparing the extracted control signals with an angle signal. In order to record an angular signal from both knee and ankle joint, two electrogoniometers were employed (SG110 and SG150, Biometrics Ltd). Both goniometers were placed during the Exp.1 with the subject standing, as shown in Figure 2.7. Angular variations have been acquired
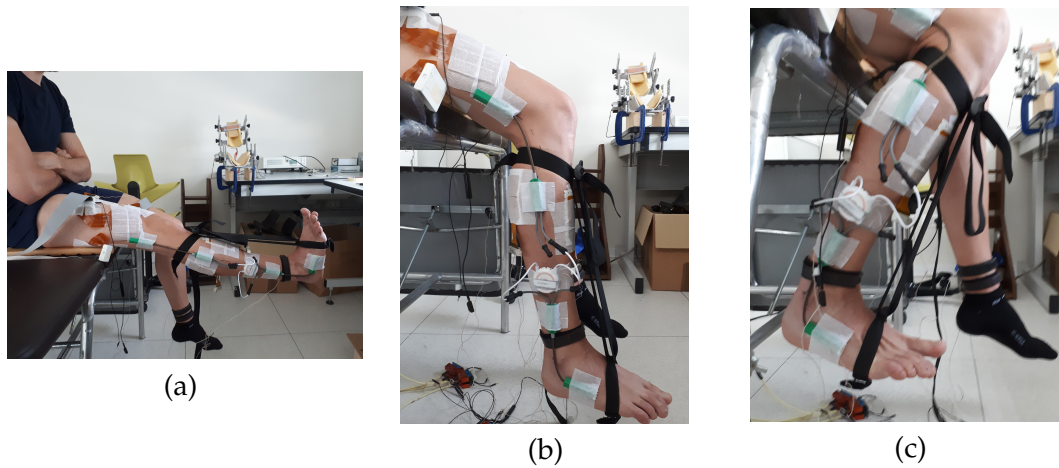
FIGURE 2.6: *Figure shows the principal phase of Exp.2:* **(a)** *Combination of Knee extension and Ankle dorsiflexion;* **(b)** *Knee during resting phase and Ankle plantar flexion;* **(c)** *Combination of Knee flexion and Ankle dorsiflexion.*

with a general purpose probe (DuePro, OTBioelettronica, Turin, Italy) linked to the electrogoniometers. Thus, data were transmitted via bluetooth to the probe station and sent to the EMG signals amplifier (the same of Exp.1) using two BNC-BNC cables. The whole system has been realized in order to synchronize the EMG and angle signals acquisition.
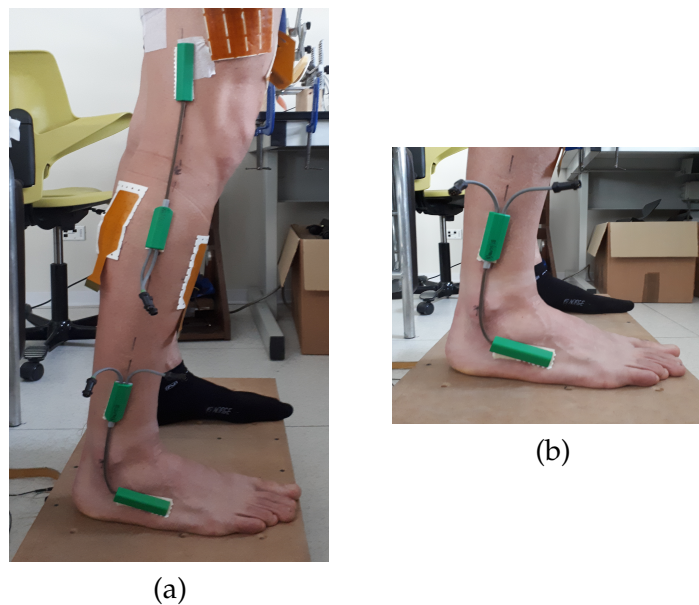
FIGURE 2.7: *Detail of electrogoniometers placement.* **(a)** *Overall positioning for Knee (SG150, Biometrics Ltd) and Ankle (SG110, Biometrics Ltd).* **(b)** *Electrogoniometer placement on Ankle joint.*

2.4 Data Processing

All recorded signals have been processed offline after the recording phase. In total, 96 and 224 monopolar EMG signals were recorded from ankle and knee joint, respectively. For all signals of each trial, the power line interference was removed with a notch filter. After that, signals were digitally band-pass filtered (Butterworth digital filter, fourth-order, pass-band 20-400 Hz) and the single differentials (SD) signals were evaluated considering one or two inter-electrode distance, namely hereafter 1 IED and 2 IED. After that, SD signals were visually inspected in order to remove channels corresponding to residual artifacts or missing contact (bad-channels). Once the bad channel was selected for a trial, it was removed for all of them.

Furthermore, from the SD signals (both IED) the root mean square (RMS) feature of EMG signals was calculated using non-overlapped 250 ms length windows. Hence, the signals were down-sampled to 4Hz. The choice to calculate the RMS feature was suggested from literature. In fact, as proved in [25], the joint angle can be predicted with good results using the RMS feature. In addiction, all evaluated RMS signals have been averaged between all trials in order to obtain a single averaged RMS dataset.

Thereafter, to realize some inferences for each joint the recorded signals were pooled together linking the electrodes of all matrices counter-clock wise.

This produced two general matrices with the following configurations:

Knee Joint Matrix

- Vastus Lateralis Matrix (cols from 1 to 8);

- Rectus Femoris Matrix (cols from 9 to 12);

- Vastus Medialis Matrix (cols from 13 to 20);

- Biceps Femoris Matrix (cols from 21 to 28).

Ankle Joint Matrix

- Tibialis Lateralis Matrix (cols from 1 to 4);

- Gastrocnemius Medialis Matrix (cols from 5 to 8);

- Gastrocnemius Lateralis Matrix (cols from 9 to 12).

(A) (B) (C) (D)
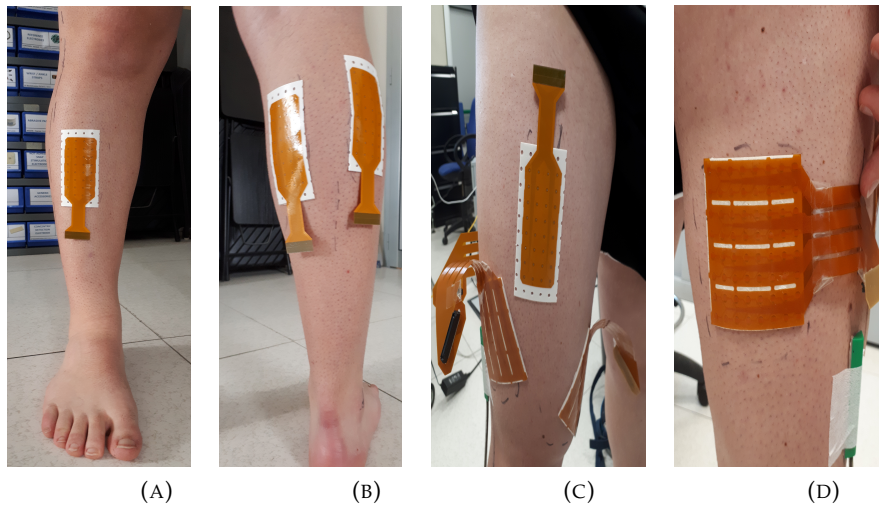
FIGURE 2.8: *Matrices positioning on interested muscles, right leg.(A) Ankle front view. 32 electrodes matrix on tibialis anterior;(B) Ankle back view. 32 electrodes matrices placed on gastrocnemius medialis (left side) and lateralis (right side);(C) Knee front view. 32 electrodes matrix on rectus femoris and a two 64 electrodes matrices placed on vastus lateralis (left side) and medialis (right side);(D) Knee back view. 64 electrodes matrix on biceps femoris.*

At this point, from these configurations (196 electrodes for knee joint and 84 for ankle joint with 1 IED, 84 and 36 electrodes with 2 IED respectively), 8 channels subsets with 1 IED and 5 with 2 IED were extracted for both knee and ankle joint from the complete configurations. To do this, a uniform selection (UNI) method, similar to a previous approach that select equally spaced electrodes [26] was used. Hereafter, the attribute *Complete* will be used to denote the configuration that include all channels of the high-density grid. Instead, the attribute *Reference* followed by the number of selected electrodes will indicate a general sub-configuration. Furthermore, in attempt to prove the robustness of this method for shift issues, shifted configuration have been evaluated for a portion of Reference configurations. Regarding the muscle fibers direction, both transverse (shortened *T*) and longitudinal (shortened *L*) displacements have been considered. Thus a transverse shift will correspond to select the electrode on the left-side from the channel considered, a longitudinal shift will select the electrode below the channel considered.

For example, a reference configuration composed of 28 electrodes and transversally shift will be namely as *Reference28T*. All selected channels subsets are shown in Table 2.1 and Table 2.2.

Knee Joint, 1 IED	Channels	Ankle Joint, 1 IED	Channels
Complete	196	*Complete*	84
Reference56	56	*Reference24*	24
Reference56T	56	*Reference24T*	24
Reference28	28	*Reference12*	12
Reference28T	28	*Reference12T*	12
Reference28L	28	*Reference12L*	12
Reference14	14	*Reference6*	6
Reference14T	14	*Reference6T*	6
Reference14L	14	*Reference6L*	6

TABLE 2.1: *Summary of the electrodes configurations selected for Knee and Ankle joint with IED=10mm. Capital letters T and L indicate a shift in direction transverse or longitudinal to the muscle fiber, with respect to the selected reference configuration.*

Knee Joint, 2 IED	Channels	Ankle Joint, 2 IED	Channels
Complete	84	*Complete*	36
Reference28	28	*Reference12*	12
Reference28T	28	*Reference12T*	12
Reference14	14	*Reference6*	6
Reference14T	14	*Reference6T*	6
Reference14L	14	*Reference6L*	6

TABLE 2.2: *Summary of the electrodes configurations selected for Knee and Ankle joint with IED=20mm. Capital letters T and L indicate a shift in direction transverse or longitudinal to the muscle fiber, with respect to the selected reference configuration.*

Moreover, for absolute clarity, a few channels subsets configurations are shown in Figure 2.9. All selected electrodes subsets can be appreciated in Appendix A.
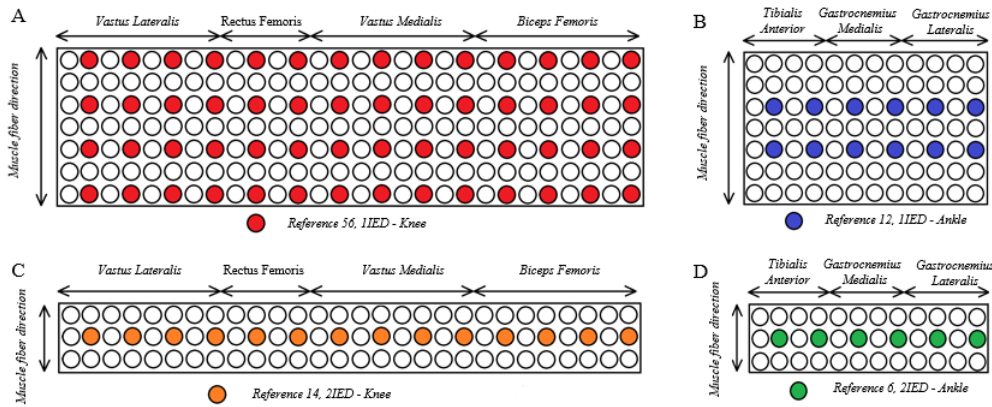
FIGURE 2.9: *Examples of reconstructed matrices for Knee and Ankle joints. Only colored electrodes were selected* **A)** *Knee Joint - Reference 56, IED=10mm,* **B)** *Ankle Joint - Reference 12, IED=10mm,* **C)** *Knee Joint - Reference 14, IED=20mm,* **D)** *Ankle Joint - Reference 6, IED=20mm.*

For the Exp.1, RMS signals of all configurations were factorized into the product of a channel weighting matrix W and the activation signals matrix F(t). Muscular activations have been processed one joint (and thus one DOF) at a time, as suggested from DOF-wise approach. In order to decompose each input matrix, a NMF algorithm [18] with dimensionality of the activation function equal to 2 was applied. The method employs at the beginning a multi-random initialization phase, as widely explained in Chapter 2.2.1. The number of initialization procedures was 10. Afterwards, the factorization based on ALS algorithm (Chapter 2.2.2) occurred.

For the knee joint, the algorithm was also applied with dimensionality of the activation function in the range 1-3 in order to verify the correctness of DOF-wise approach. In all cases, to minimize the phenomena of local minima, the factorization was run 10 times with different initial values for W and F(t) matrices and the launch with the lowest cost function was selected. As discussed in Chapter 2.1, the NMF outcomes suffer of indeterminacy especially in order. Thus, it was necessary to reorder both activation signals and channel weighting vectors, so that the muscular activation of extensors appeared before that of flexors. At this point, reconstructed signals were calculated multiplying the estimated W and F(t) matrices.

The quality of reconstruction was quantified by the multivariate coefficient of determination R^2, calculated similarly to [27]. Usually this indicator is between 0 and 1, where the lower limit means signals completely different while the upper one indicates a complete similarity. It is expressed as:

$$R^2 = 1 - \frac{RSS}{TSS} = 1 - \frac{\sum_{i=1}^{n}(y_i - \hat{f}_i)^2}{\sum_{i=1}^{n}(y_i - \bar{y})^2} \qquad (2.11)$$

where *RSS* represents the residual sum of squares and *TSS* the total sum of squares. More precisely, y_i is the i-th recorded sample, $\hat{f}_i$ is the i-th reconstructed sample and

$\bar{y}$ is the mean of the whole observation. In this work of thesis, the R^2 indicator was calculated between each channel of input matrix and of reconstructed matrix. In addiction, an averaged value between channels was assessed in order to compare different channels subsets.

Furthermore, channel weighting vectors obtained from the factorization of different subsets of electrodes were compared with the common channels of the complete configuration applying a normalized dot product (NDP)[22]. This was useful to verify the similarity between weights with a channel reduction or with a channel shift. For what concerns the estimated activation signals, the peak of a normalized cross-correlation function (NCC) between the reference configurations and the complete one has been calculated, with the aim of investigate if the number of electrodes influences the shape of the primitives extracted.

Finally, for each channel subset configuration the multi-DOF estimated synergy matrix was created by joining two channel weighting vectors extracted from signals of ankle movements and two from knee movements. The synergy matrix W has a number of rows equal to the electrodes of the selected configuration and four columns to represent the extracted synergies.

With regard to Exp.2, the input matrix for complete configuration included 320 monopolar EMG signals. It was organized in order to have inside ankle signals at first and then knee signals. All signals were processed in the same way of Exp.1 but the bad channels to remove were the same selected after visual analysis in Exp.1 data processing. In addiction, in this phase the calculated RMS signals were not averaged since each of 10 recorded trials of EMG signals was correlated with its own recorded angular signal. At this point, the activation signals matrix *F(t)* can be calculated simply as

$$\mathbf{F(t)} \quad = \quad W^+ \cdot \mathbf{Y(t)} \tag{2.12}$$

where *Y(t)* is the EMG input matrix and W^+ is the Moore-Penrose pseudoinverse of weighting channel vectors matrix *W* [22], assembled in Exp.1.

The advantage of the method employed is evident. In fact, supervised methods need to perform a training phase where both EMG signals and a control signal are recorded. These control signals can be for example force or position, as shown in [21] and [26]. The recorded data are then used to train an algorithm and create an association between input and output. The proposed method, similar to [22], collects only EMG data and then, by the application of a NMF algorithm, is able to extract directly the activation signals. In addiction, it is not entirely unsupervised but semi-supervised. This is due to the fact that it is necessary to be aware of which DOF is active at the beginning.

The activation signals matrix calculated in (2.12) has the following structure:

$$F(t) = \begin{bmatrix} f_1^+(t) \\ f_1^-(t) \\ f_2^+(t) \\ f_2^-(t) \end{bmatrix} \qquad (2.13)$$

where the first and second rows represent the ankle control signals during extension (or dorsiflexion) and flexion (or plantar flexion), while the last two rows are about the knee control signals in the same phases. Thus the matrix has 4 rows and 120 columns, due to the calculated RMS samples. Each component of (2.12) is normalized to its maximum value. From the four control signals related to each movement phase for two DOFs, the final control signals were calculated as:

$$\begin{aligned} f_1(t) &= f_1^+(t) - f_1^-(t) \\ f_2(t) &= f_2^+(t) - f_2^-(t) \end{aligned} \qquad (2.14)$$

In addiction, the extracted activations signals have to be multiplied by some scaling factors. These coefficients were determined because the final control signals matrix $F(t) = [f_1(t); f_2(t)]$ has to match the range of joint angles of each DOF performed[29]. For this reason, during the Exp.2, the subject performed also two single joint movements in order to calibrate the electrogoniometers. Angle signals from knee and ankle joint were low-pass filtered with a Butterworth digital filter, fourth-order with 10 Hz cut frequency and then down-sample to 4 Hz (the same of EMG).

In order to quantify the goodness of the extracted control signals from different subsets channel configuration and from different joint (knee or ankle) compared to the angular signal recorded during the complete movement, the R^2 indicator (2.11) was evaluated for each trial.

After the phase of control signals extraction and comparison with the data recorded from the electrogoniometers, a statistical test was necessary to investigate which factors influence the trend of R^2 performance indicator. For this reason, a three-way analysis of variance (ANOVA) test was applied to all R^2 values pooled together for ankle and knee. The selected factors for the statistical test were number of subjects (for each subject 10 repetitions for each configuration were considered), channels configurations and joints (ankle or knee). The ANOVA test was repeated for both datasets with 1IED and 2IED. For all tests, statistical signficance was set at *p < 0.05*.

Chapter 3

Results

In this chapter all outcomes of this work of thesis are showed.

3.1 First Experiment

The aim of the Exp 1 was to perform separately knee and ankle joint movements in order to estimate a multi-DOF synergy matrix for subsequent phase. To verify the correctness of this method, a few analysis regarding both weighting vectors and primitives extracted were realized.

3.1.1 Dimensionality Analysis

In order to justify the DOF-wise approach in the experimental setup, data recorded from knee joint have been factorized obtaining the whole number of synergies extractable. For a number N of interested muscles in knee joint equal to 4, the maximum number of synergies extracted corresponds to N-1. For this reason, the factorization was repeated a few times with dimensionality of activation function from 1 to 3. This study was applied only on knee joint because of the lower number of interested muscles in the ankle joint; in fact in this case N=3 and the maximum number of extracted synergies is 2, as performed from the DOF-wise approach. Data of both 1IED and 2IED were factorized for all subjects. Figure 3.1 (left side) provides a useful information for what concerns the variance of the EMG pattern with 1IED (through the R^2 parameter) in function of the factorization dimension, corresponding to the number of synergies extracted. The graph shows the variance trend for each reference configuration. In general, it is evident that only one weighting vector is not able to explain the EMG pattern. Indeed, moving from one to two synergies, the performances increase of a 25% roughly. From two basis vectors (DOF-wise approach) to three the variance trend shows a change in slope, due to the fact that the R^2 values increases not more than 2%. In order to compare the situation with a different dimension, Figure 3.1 on the right side focuses on the last part of the global trend. The use of DOF-wise approach (2 synergies) yielded a mean R^2 (between 10 runs) of 97,04% for the *Complete Configuration* and 97,45% $\pm$ 0.5% for the *Reference Configurations Group*. Thus, two vectors suffice to explain >95% of the variance. Using three synergies for

the data factorization, the mean R^2 reaches 98,2% and 98.5% $\pm$ 0.2% for the *Complete Configuration* and *Reference Configurations Group*, respectively.
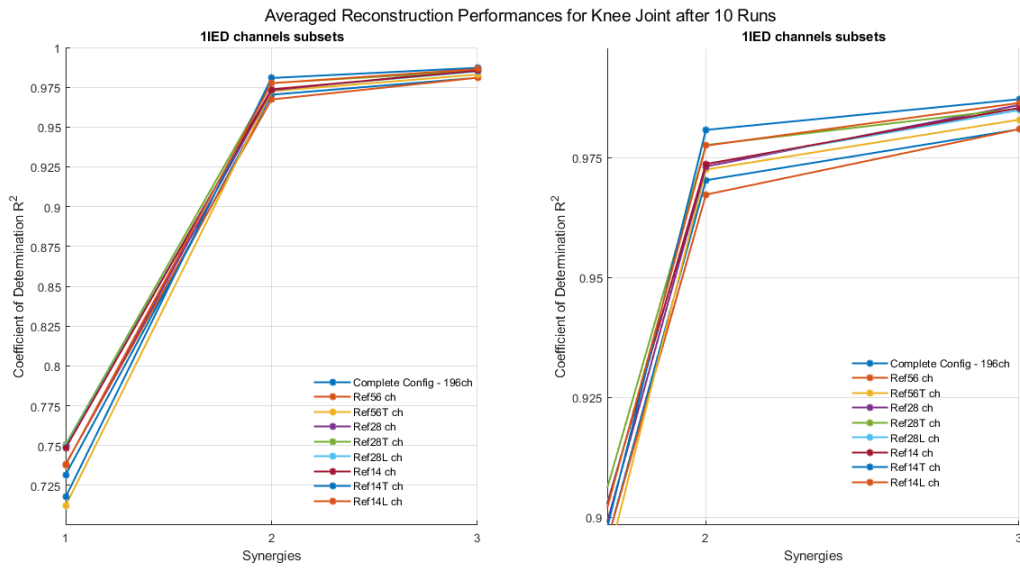
FIGURE 3.1: *Trend of the averaged explained variance of the EMG pattern for 1IED (for all channels subset) as a function of the factorization dimension for Knee Joint, Subject 2. The graph on the left side shows a global trend, while the one on the right focuses on the change of slope, between 2 and 3 synergies.*

For what concerns EMG Knee signals evaluated with 2IED, the analysis led to the same conclusion, as showed in Figure 3.2. Indeed, with two synergies (DOF-wise approach) the *Complete Configuration* presents a mean R^2 (between 10 runs) of 97,77%. This value is almost identical to that one of the average of 5 *Reference Configurations*, with R^2 of 97,96% $\pm$ 0.2%. Increasing the factorization dimension from 2 to 3, the *Complete Configuration* shows a mean R^2 of 98,46% and 98,52% $\pm$ 0.2% for the *Reference Configurations Group*.

Summing up, for the knee joint the NMF algorithm was employed with different factorization dimension and the variance of the EMG pattern explained with the DOF-wise approach was very similar if compared with the result obtained with a traditional NMF. The same situation held true for all selected channels subsets, for both 1IED and 2IED.

3.1.2 Factorization Performance

The NMF algorithm was applied separately to both knee and ankle EMG dataset for all patients. This is due to the DOF-wise approach. Indeed, in order to estimate a complete synergy matrix *W* for each selected channels subset, it is necessary to extract the sub-optimal weighting vectors (or sinergies) for knee and ankle joint. For this reason, after the factorization with the parameters explained in Chapter 2.4, for each channels configuration (for both 1IED and 2IED) the reconstruction performances were evaluated. It is worth recalling that a general reconstructed signal has been
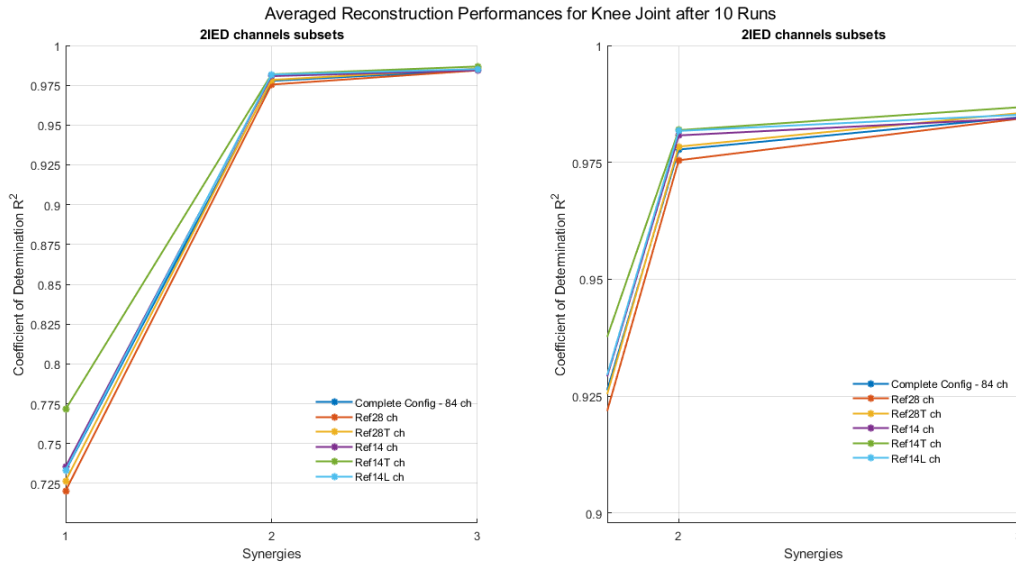
FIGURE 3.2: *Trend of the averaged explained variance of the EMG pattern for 2IED (for all channels subset) as a function of the factorization dimension for Knee Joint, Subject 2. The graph on the left side shows a global trend, while the one on the right focuses on the change of slope, between 2 and 3 synergies.*

calculated as the product between the synergy matrix and the activation signals vectors extracted with the data decomposition. For this purpose, the coefficient of determination R^2 was evaluated keeping in mind that a reasonable reconstruction percentage is about 90%.

The following figures, 3.3 and 3.5, show the goodness of the NMF algorithm for knee joint dataset (Subject 2). Both represent in the left side the reconstruction trend of the signals included within each configuration as a function of selected (the effective number of residual channels after the bad channel removal is reported on the x-axis) electrodes. Therefore, for each sub-configuration the R^2 trend indicates the quality of reconstruction moving from electrodes placed on Vastus Lateralis (leftmost side on the graph) to those on Biceps Femoris (the righmost one), according to the electrodes organization explained in Chapter 2.4 and showed, in example, in Figure 2.9. Regarding to the right side of the Figures, a bar plot graph with averaged R^2 value across channels of each analyzed configuration is showed. This allows to identify globally the goodness of the proposed method and to evaluate the variability of the R^2 for each configuration. With reference to Figure 3.3, it is evident that the reconstruction performances oscillate around 97,5%. Despite this outcome *Complete Configuration*, *Reference56* and *Reference56T* show a wider variability. Indeed, observing the trend of the R^2 for these configuration, some channels of Rectus Femoris show a lower reconstruction value. In order to appreciate the difference reconstructed electrodes signals, a comparison between the worst and the best channel of the Complete Configuration is showed in Figure 3.4.
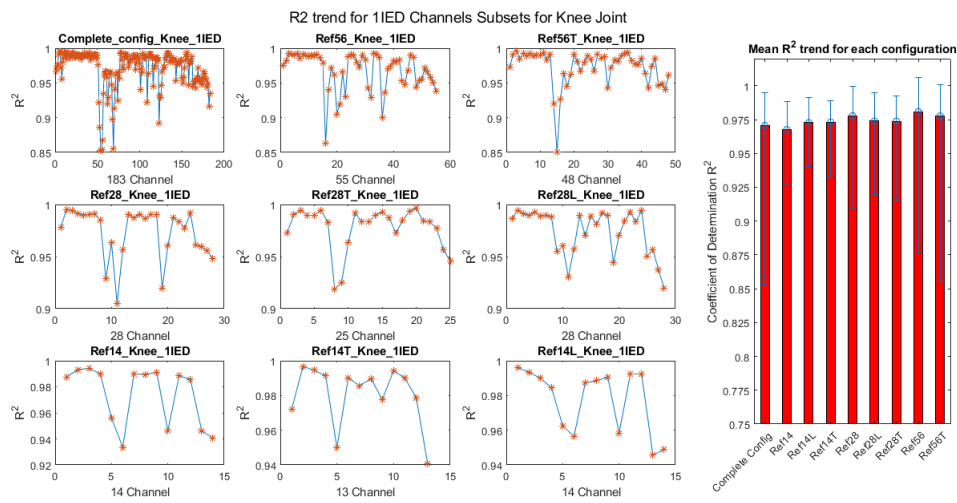
FIGURE 3.3: *Figure shows the goodness of the signal reconstruction (percentage of R^2) after the non-negative factorization(Subject 2)-Knee Joint,1IED. On the left side are represented the reconstruction trends of each channels subset across residual channels (expressed on x-axis). On the right side a bar plot with averaged reconstruction values for each configuration is showed.*
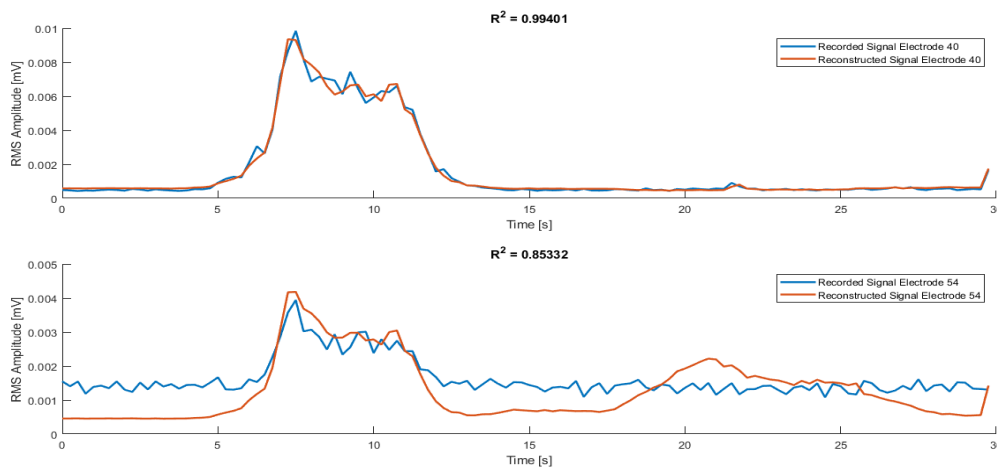
FIGURE 3.4: *Comparison between different results from NMF. Top: reconstruction with R^2=99.4% related to Electrode 40 of Complete Knee Configuration - 1IED (Rectus Femoris). Bottom: reconstruction with R^2=85.35% related to Electrode 54 of Complete Knee Configuration - 1IED (Rectus Femoris).*

For what concerns the reconstruction of knee joint with 2IED (Figure 3.5), the mean R^2 value across six channels subsets is 97.5% roughly. Unlike the dataset calculated with 1IED, in this case there is a smaller variability. In fact, looking at each configuration, the coefficient of determination does not drop below a 90%.
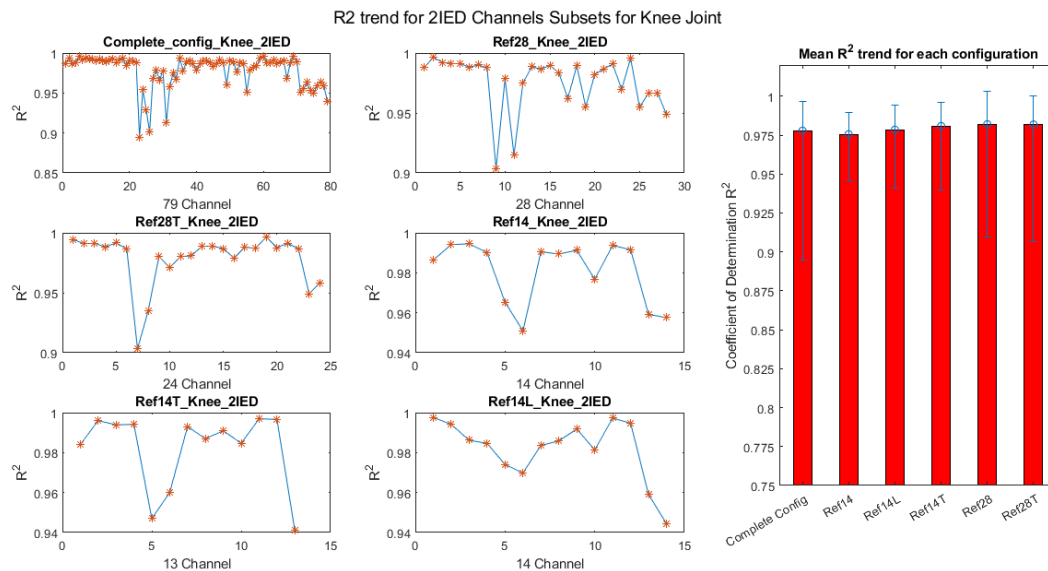
FIGURE 3.5: *Figure shows the goodness of the signal reconstruction (percentage of R^2) after the non-negative factorization(Subject 2)-Knee Joint,2IED. On the left side are represented the reconstruction trends of each channels subset across residual channel (expressed on x-axis). On the right side a bar plot with averaged reconstruction values for each configuration is showed.*

Observing the case of ankle joint dataset, globally the reconstruction performances does not change. In addiction, a slight growth for what concern the mean R^2) across channels subsets can be observed. Figure 3.6 and Figure 3.7 show the goodness of NMF algorithm for ankle joint. In this case, within each R^2 trend, the information is related to Tibialis Anterior (leftmost side on the graph) and Gastrocnemius Lateralis (the righmost one), according to the electrodes organization explained in Chapter 2.4 and showed, in example, in Figure 2.9. For both 1IED and 2IED ankle signals dataset, the overall mean performance is about 98,5%. More specifically, for a wide number of selected channels subsets the values of coefficient of determination slowly decrease in the middle section of the graph, corresponding to the electrodes placed on gastrocnemius medialis.
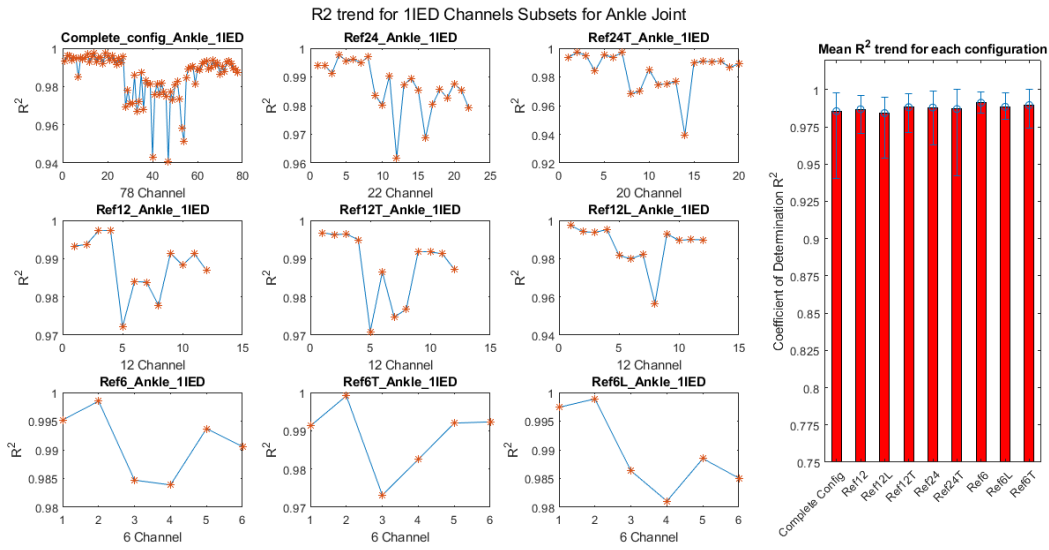
FIGURE 3.6: *Figure shows the goodness of the signal reconstruction (percentage of R^2) after the non-negative factorization(Subject 2)-Ankle joint,1IED. On the left side are represented the reconstruction trends of each channels subset across residual channel (expressed on x-axis). On the right side a bar plot with averaged reconstruction values for each configuration is showed.*
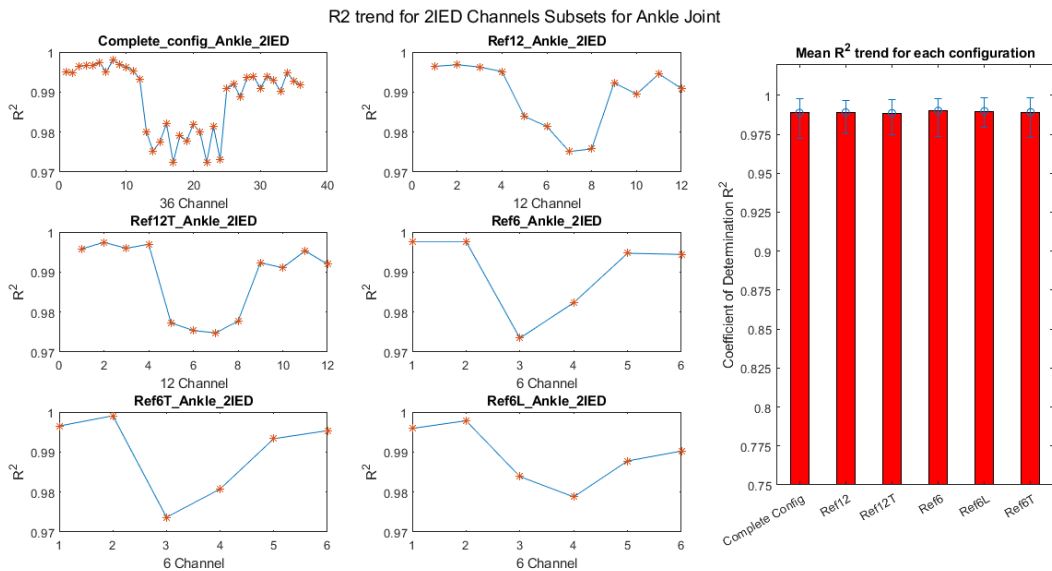
FIGURE 3.7: *Figure shows the goodness of the signal reconstruction (percentage of R^2) after the non-negative factorization(Subject 2)-Ankle joint,2IED. On the left side are represented the reconstruction trends of each channels subset across residual channel (expressed on x-axis). On the right side a bar plot with averaged reconstruction values for each configuration is showed.*

3.1.3   Weighting Vectors Comparison

In this section, an analysis of extracted synergies (or weighting/basis vectors) is proposed. The NMF algorithm applied with a DOF-wise approach calculated 2 synergies for each considered joint, one for the extensors muscles and one for the flexors. As explained in Chapter 2.1, BSS problem suffers of ambiguity in order and the extracted synergies can be reversed. For this reason, it was necessary reorder them in a coherent way in order to keep the extensors synergy before the flexors one in time.

The first analysis was to assess the weights amplitude across interested muscles using color maps. This was useful to confirm or disprove if the calculated synergies are consistent with the muscles (it was expected to see a major activation of extensors muscles for the extensors synergy, rather than of flexors). Figure 3.8 shows an example of weights amplitude distribution for what concerns the knee joint with 1IED. The most representative channels subsets in terms of number of electrodes are presented. The figure is organized in the following way: each row includes, for the same configuration, two maps: one for the extensors synergy (left side) and one for the flexors synergy (right side). All color maps have a number of elements corresponding to the electrodes of each channel subsets. Every weights of two maps in a row are normalized to the maximum value between extensors and flexors synergy. In addiction, colorless elements with a cross marker indicates the bad channels removed during processing phase. On the x-axis an information about muscles is provided (with coherence with what explained in Chapter 2.4), whereas on y-axis the muscle fiber direction (from proximal at the top to distal at the bottom) is indicated.
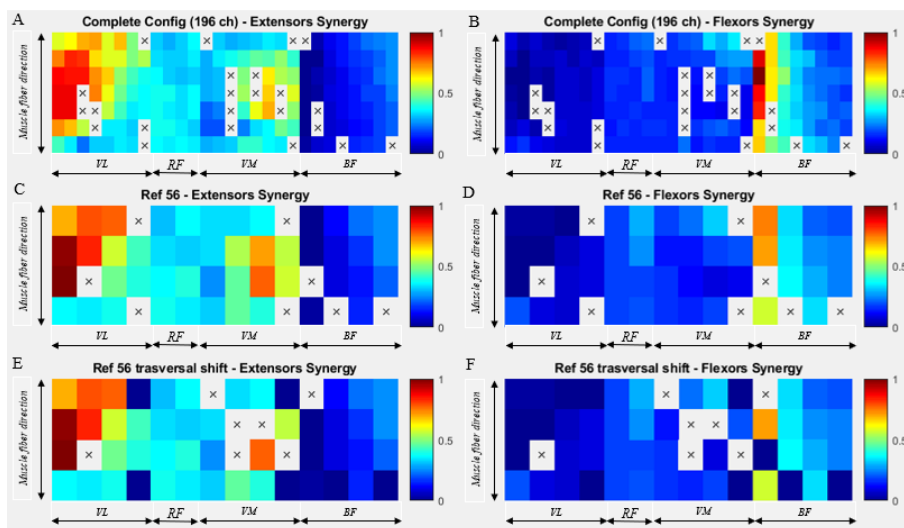
FIGURE 3.8: *Colormaps of extracted weighting vectors from NMF for a representative subject, Knee Joint 1IED. Each row shows in the left side column the weights map related to the synergy of extensors muscles and in the right side column that one of the synergy of flexors muscles. Each map in a row is normalized to the maximum values between the weighting vectors for a specific configuration. Colorless elements with cross marker indicate a bad channel removed.*

Observing Figure 3.8 for the *Complete Configuration* (colormaps A,B) it is evident the separation from extensors and flexors muscles. In the map A, the most activated region is that on the middle of Vastus Lateralis. The weights amplitude decreases moving proximally and medially. In addiction, the nearest zone to the knee shows less activation if compared with the rest of the muscle. Also Vastus Medialis presents a major activation in the middle section, whereas Rectus Femoris shows weights with lower amplitude. In the map B, all extensors muscles keep a low activation, and this is consistent with the synergy considered. For what concerns the flexor, the most activated region consists is a slice in the medial zone that covers the muscle in vertical. This part appears more activated in comparison with the rest of Biceps Femoris and this has explanation in the matrix placement. In fact, that activation is related to the Semitendinosus muscle, partially covered because of the size of the matrix employed. By looking at the others colormaps in Figure 3.8, it is clear that down-sampling the number of electrodes or shifting them transversally, the global behavior is the same. Also the weights amplitude distribution for 2IED confirms the same situation. Figure 3.9 compares the *Complete Configuration* and *Reference28*. It is evident that, even if the signals dataset has been calculated with twice the IED, the weighting vectors amplitude held the same distribution respect the case with 1IED.
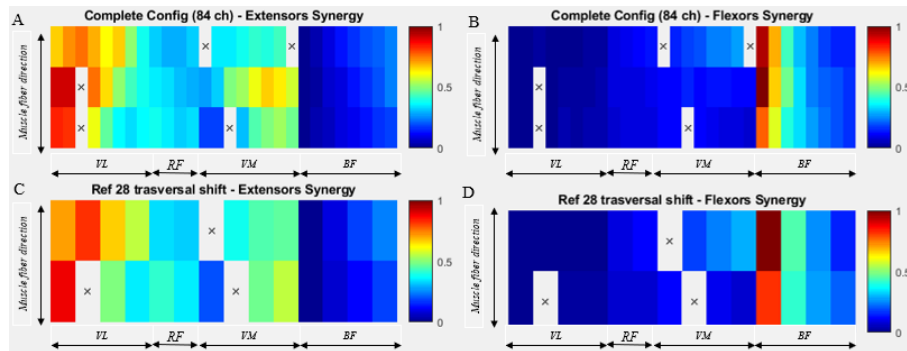
FIGURE 3.9: *Colormaps of extracted weighting vectors from NMF for a representative subject, Knee Joint 2IED. Each row shows in the left side column the weights map related to the synergy of extensors muscles and in the right side column that one of the synergy of flexors muscles. Each map in a row is normalized to the maximum values between the weighting vectors for a specific configuration. Colorless elements with cross marker indicate a bad channel removed.*

For what concerns the ankle joint, there a few differences in terms of activation as compared with knee joint. Figure 3.10 and Figure 3.11 show the colormaps for 1IED and 2IED, respectively. In the colormaps with 1IED, the only extensor (Tibialis Anterior) in the map A presents a major amplitude medially. This happens for the channels subsets inside the maps C and E as well. Regarding the lateral region instead, the *Complete Configuration* shows a lower weighting vectors amplitude in the most proximal electrodes if compared with *Reference24* or *Reference24T*. Looking at the flexors synergy, in general Gastrocnemius lateralis has weights with the highest

amplitude. More specifically, *Reference24* (map D) indicates a uniform distribution; on the opposite the *Complete Configuration* (map B) shows a non-uniformity. Here again, the dataset with 2IED confirms the same observed behavior of 1IED, as clearly visible in Figure 3.11.
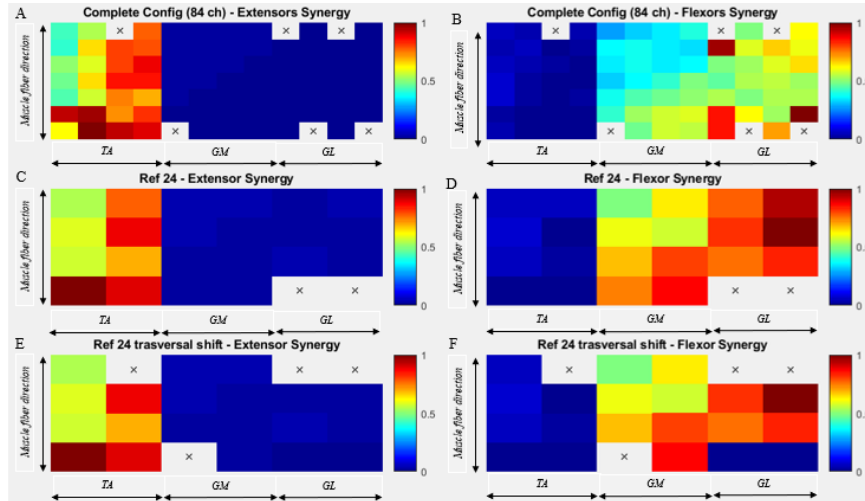
FIGURE 3.10: *Colormaps of extracted weighting vectors from NMF for a representative subject, Ankle Joint 1IED. Each row shows in the left side column the weights map related to the synergy of extensors muscles and in the right side column that one of the synergy of flexors muscles. Each map in a row is normalized to the maximum values between the weighting vectors for a specific configuration. Colorless elements with cross marker indicate a bad channel removed.*
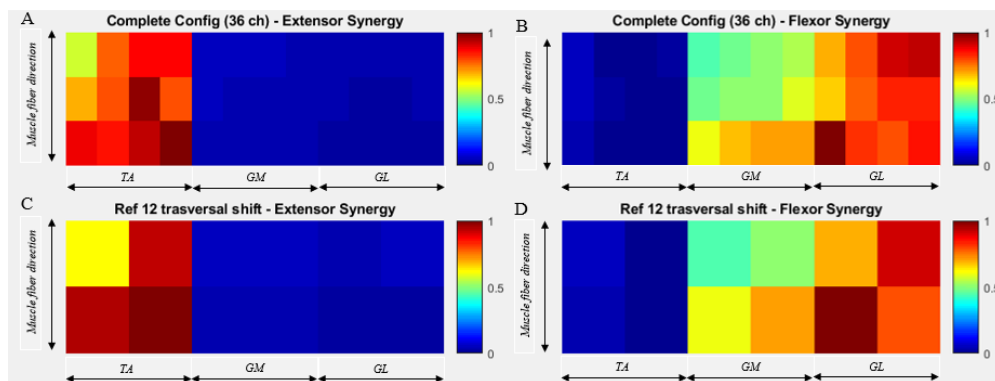
FIGURE 3.11: *Colormaps of extracted weighting vectors from NMF for a representative subject, Ankle Joint 2IED. Each row shows in the left side column the weights map related to the synergy of extensors muscles and in the right side column that one of the synergy of flexors muscles. Each map in a row is normalized to the maximum values between the weighting vectors for a specific configuration. Colorless elements with cross marker indicate a bad channel removed.*

Thus, for both studied joint it has been demonstrated that a data factorization based on the DOF-wise approach (2 synergies for joint) allowed to verify a correct separation between extension and flexion movement phase.

Furthermore, in order to quantify the total contribution of each synergy inside a given muscle, the sum of all common weights for all of them has been calculated. Thus, every muscle is defined by two values; one related to the presence of the first synergy and the other related to the second one. To realize a comparison, each couple of values has been normalized to the maximum. The following Figures show for all channels subsets (both joints) a pair of bar plot related to each muscle. In addition, normalization values for each bar plot couple are indicated in Table 3.1, 3.2, 3.3, 3.4. Figures 3.12 and 3.13 are referred to knee joint for 1IED and 2IED respectively. The first one indicates globally a correct behavior in a wide number of configuration; this means that the extensors show low values for what concerns the flexor sinergy, and vice-versa. Although Vastus Lateralis, Medialis and Biceps Femoris present correct values, Rectus Femoris highlights an important contribution also in flexor synergy. This could be motivated with the fact that, during the exercise, the subject co-activated the muscles. In any case this does not happen in 2IED configuration, as showed in Figure 3.13. Here the presence of rectus femoris in the flexors synergy is restricted.
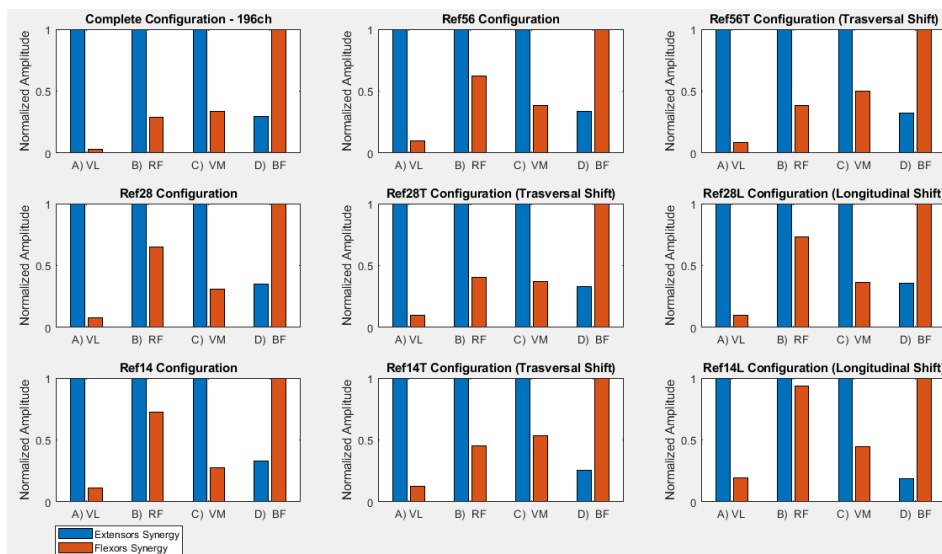
FIGURE 3.12: *Comparison between the different contribution of the extracted synergies across muscles for all channels subsets of Knee joint, 1IED. Each couple of bars has been normalized to the maximum value.*
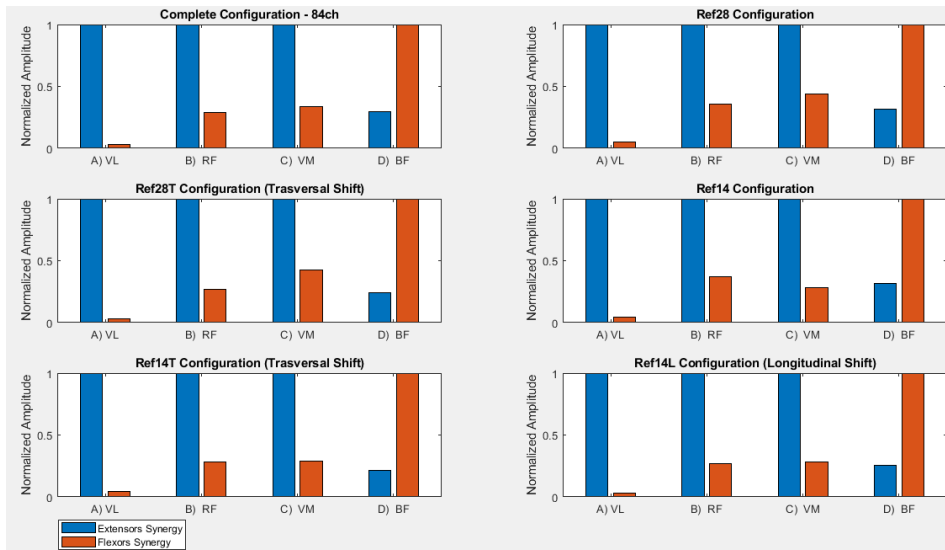
FIGURE 3.13: *Comparison between the different contribution of the extracted synergies across muscles for all channels subsets of Knee joint, 2IED. Each couple of bars has been normalized to the maximum value.*

With regard to the ankle joint, Figure 3.14 and Figure 3.15 highlight a sub-optimal behavior if compared with the knee. In this case it is noticeable that the Tibialis Anterior has a contribution from flexors synergy approximatively equal to zero, whereas the Gastrocnemius Medialis shows in almost all configuration a limited contribution from extensors synergy.
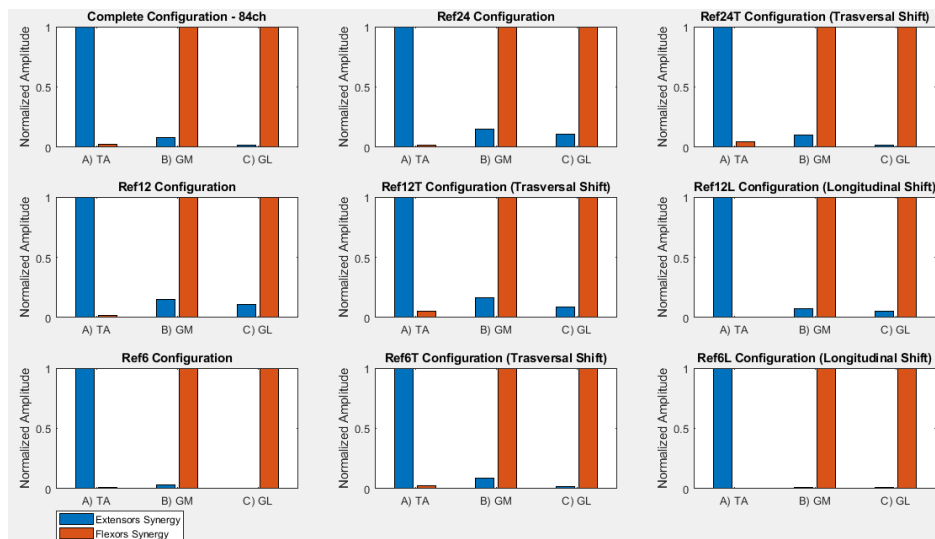
FIGURE 3.14: *Comparison between the different contribution of the extracted synergies across muscles for all channels subsets of Ankle joint, 1IED. Each couple of bars has been normalized to the maximum value.*
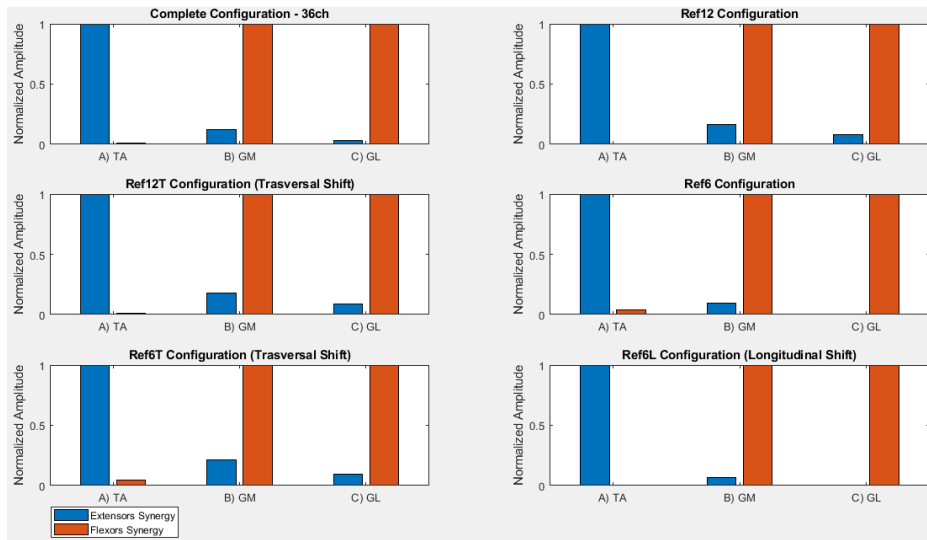
FIGURE 3.15: *Comparison between the different contribution of the extracted synergies across muscles for all channels subsets of Ankle joint, 2IED. Each couple of bars has been normalized to the maximum value.*

Knee Joint, 1 IED	VL	RF	VM	BF
Complete	2.0327	0.2626	1.4196	1.3177
Reference56	0.5614	0.0922	0.4015	0.3627
Reference56T	0.5619	0.0584	0.3895	0.3906
Reference28	0.3207	0.0432	0.2124	0.1839
Reference28T	0.2543	0.0336	0.2153	0.1855
Reference28L	0.3295	0.0465	0.2202	0.1965
Reference14	0.1472	0.0222	0.107	0.0927
Reference14T	0.1706	0.011	0.1105	0.1009
Reference14L	0.1824	0.0225	0.1208	0.0878

TABLE 3.1: *Normalization values of synergies vectors across muscles depicted in Figure 3.12, Knee Joint 1IED.*

Knee Joint, 2 IED	VL	RF	VM	BF
Complete	1.5547	0.231	1.1096	0.993
Reference28	0.5649	0.0806	0.3416	0.3293
Reference28T	0.4221	0.0646	0.3784	0.3355
Reference14	0.2697	0.0408	0.1867	0.1752
Reference14T	0.2927	0.0441	0.119	0.1551
Reference14L	0.3298	0.0444	0.2107	0.1715

TABLE 3.2: *Normalization values of synergies vectors across muscles depicted in Figure 3.13, Knee Joint 2IED.*

Ankle Joint, 1 IED	TA	GM	GL
Complete	2.0327	0.2626	1.4196
Reference56	0.5614	0.0922	0.4015
Reference56T	0.5619	0.0584	0.3895
Reference28	0.3207	0.0432	0.2124
Reference28T	0.2543	0.0336	0.2153
Reference28L	0.3295	0.0465	0.2202
Reference14	0.1472	0.0222	0.107
Reference14T	0.1706	0.011	0.1105
Reference14L	0.1824	0.0225	0.1208

TABLE 3.3: *Normalization values of synergies vectors across muscles depicted in Figure 3.14, Ankle Joint 1IED.*

Ankle Joint, 2 IED	TA	GM	GL
Complete	1.5547	0.231	1.1096
Reference28	0.5649	0.0806	0.3416
Reference28T	0.4221	0.0646	0.3784
Reference14	0.2697	0.0408	0.1867
Reference14T	0.2927	0.0441	0.119
Reference14L	0.3298	0.0444	0.2107

TABLE 3.4: *Normalization values of synergies vectors across muscles depicted in Figure 3.15, Ankle Joint 2IED.*

In addition, a inter-configuration analysis was developed as measure of similarity for what concerns the weighting vectors extracted. This process aims to investigate if the basic assumption of linear instantaneous signals mixture can be confirmed. Indeed, as explained in Chapter 1.6, high similarity between weights of different channels subsets indicates that the combinations of activation signals at the electrodes positions is approximatively linear instantaneous[22].

For this reason, common channels between the *Complete Configuration* and each *Reference Configuration* were extracted. At this point, after a normalization to the maximum (calculated between the Complete Configuration and the Reference one to compare), the NDP was applied. The process was repeated for every configuration of all IED and joint. Logically, common bad channels were not considered for the computation. The following Figures show the outcomes obtained for a representative subject (the investigation was evaluated on datasets of all subjects). In general, each figure includes two columns with different graphs; left side column depicts configurations for the extensors synergy, right side column instead is about flexors. Weights from two categories have been compared using bars with different colors. In addiction, bars position is still related to the electrode location (if a limited number of bad channels has been selected). In fact, moving from the leftmost zone to the rightmost one, depicted weights are related respectively to *Vastus Lateralis*, *Rectus Femoris*, *Vastus Medialis*, *Biceps Femoris* for knee joint and to *Tibialis Anterior*, *Gastrocnemius Medialis*,

Gastrocnemius Lateralis for ankle joint. With this assumption, it is supposed that for knee joint column with extensors synergy shows low weights amplitude in the last part of the graph (contribution of flexor muscle), while this should be happen from the beginning until three-fourths of the graph for flexors synergy. Instead ankle joint will show the highest weights amplitude in the first part (*Tibialis Anterior*) of extensors synergy column and the same should be happen from middle section to the end of flexors synergy column.

In Figure 3.16 and 3.17 it is possible to observe all channels subsets for what concerns knee joint for 1IED of a representative subject. In general, trend of weights amplitude are consistent with the previous concept. In this regard, it is noticeable that amplitudes related to the extensors muscles in the flexors synergy column are not so restricted as expected. This can be motivated with a little muscular co-activation during knee flexion. Nevertheless, the weights similarity is high as proved by NDP values depicted on each graph.
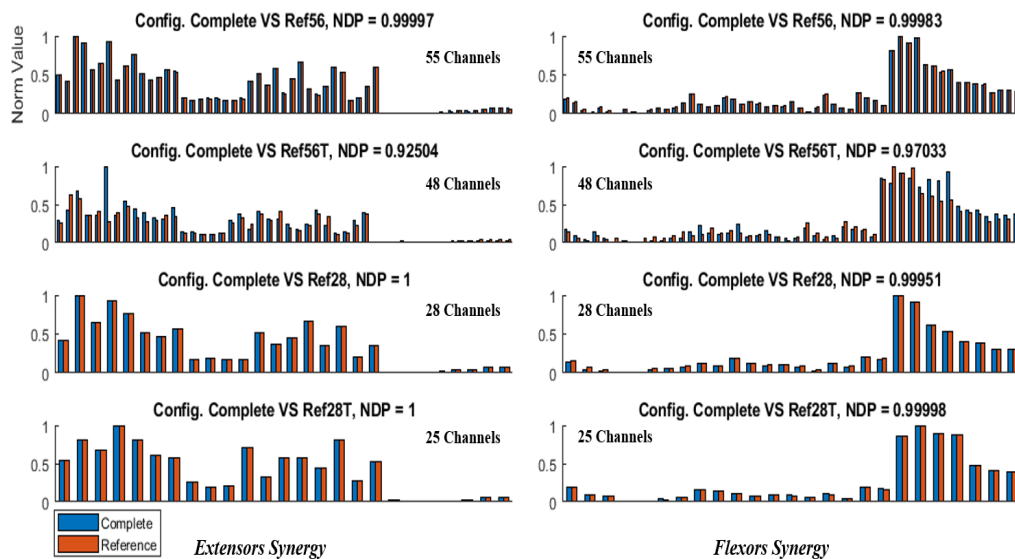
FIGURE 3.16: *Weights comparison of common channels between Complete and Reference configurations for Knee Joint, 1IED (Reference Configurations 1-4). Similarity was assessed through Normalized Dot Product (NDP).*
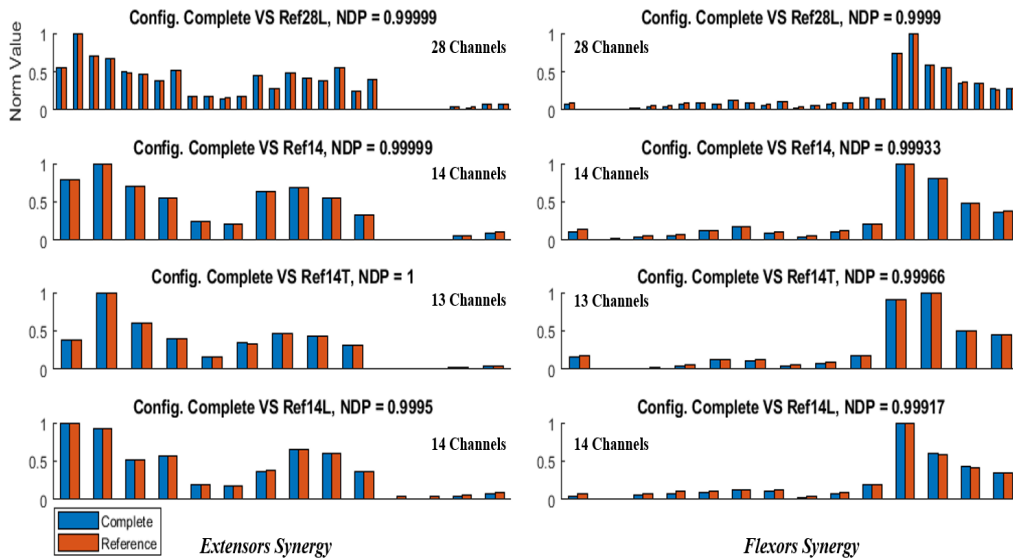
FIGURE 3.17: *Weights comparison of common channels between Complete and Reference configurations for Knee Joint, 1IED (Reference Configurations 5-8). Similarity was assessed through Normalized Dot Product (NDP).*

Channels subsets of 2IED knee joint dataset showed in Figure 3.18 confirm what has been said for 1IED basis vectors. Moreover, in this case the amplitudes in flexors synergy column appear more limited for extensors muscles compared to previous situation.
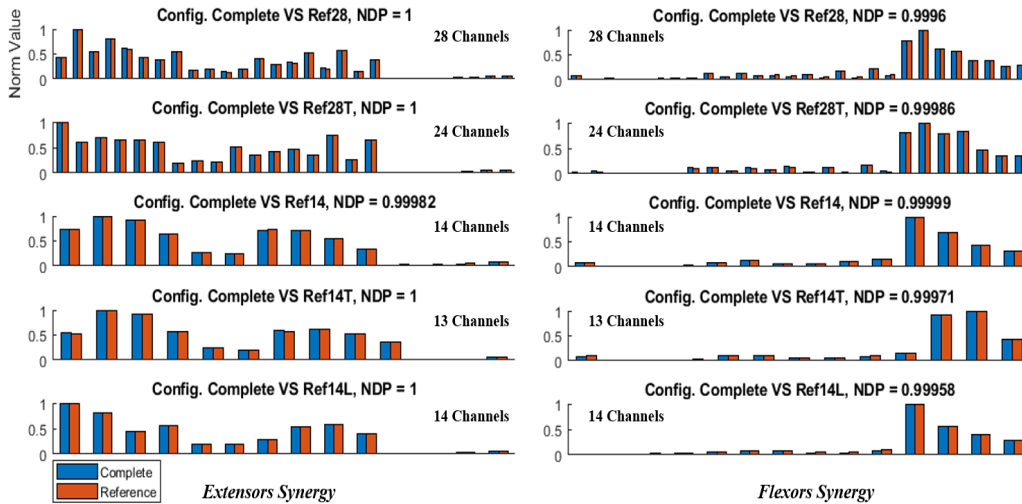
FIGURE 3.18: *Weights comparison of common channels between Complete and Reference configurations for Knee Joint, 2IED. Similarity was assessed through Normalized Dot Product (NDP).*

Looking at Figure 3.19 and 3.20 the similarity analysis regarding ankle joint with 1IED is showed. In this case, even if the NDP values are globally extremely high, the comparison with *Reference24T* shows for the both synergies NDP values out of global distribution. By focusing on this channels subset, it is noted a huge difference for what concerns a few couples of values in the region of *Tibialis Anterior* and both *Gastrocnemius*. This can be due to some residual bad channels.
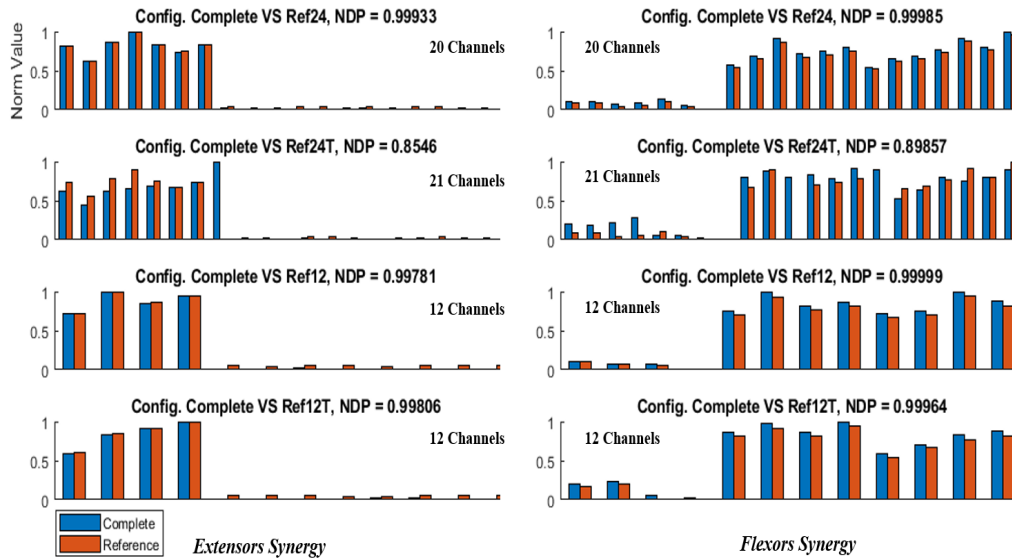
FIGURE 3.19: *Weights comparison of common channels between Complete and Reference configurations for Ankle Joint, 1IED (Reference Configurations 1-4). Similarity was assessed through Normalized Dot Product (NDP).*
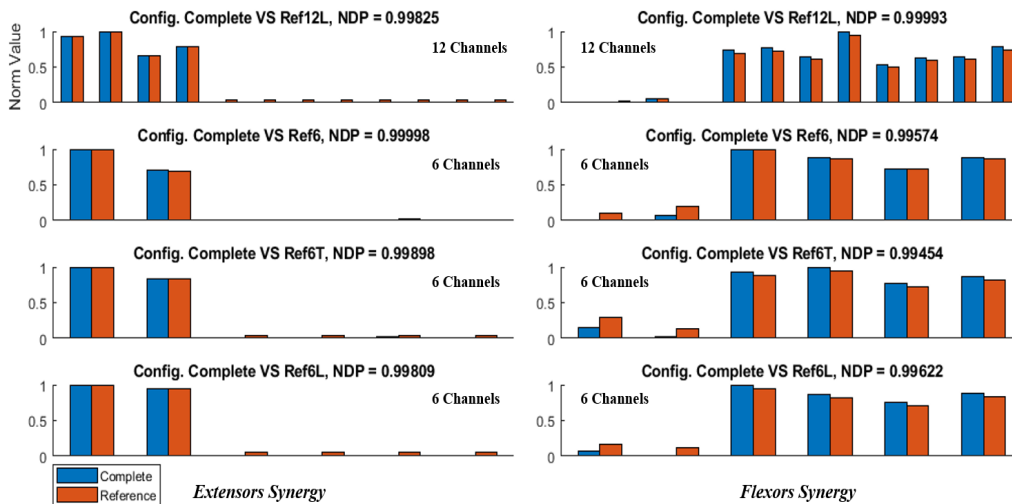
FIGURE 3.20: *Weights comparison of common channels between Complete and Reference configurations for Ankle Joint, 1IED (Reference Configurations 5-8). Similarity was assessed through Normalized Dot Product (NDP).*
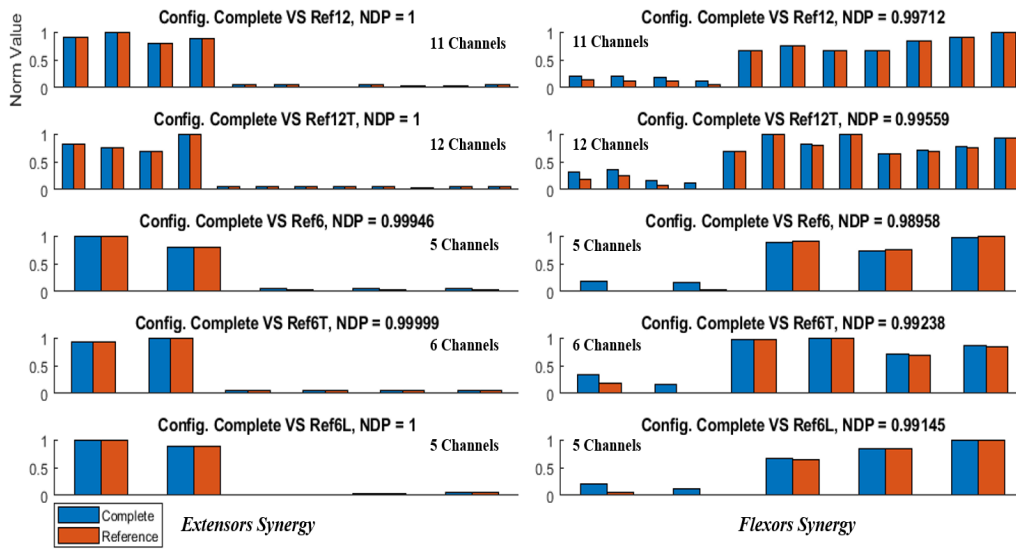
FIGURE 3.21: *Weights comparison of common channels between Complete and Reference configurations for Ankle Joint, 2IED. Similarity was assessed through Normalized Dot Product (NDP).*

Regarding to the coherence of weights trend amplitude, the extensors synergy highlights that the contribution of flexors is quiet null, whereas there is a limited presence of extensors in the first part of flexors synergy. This considerations interest the weights vectors of 2IED Ankle Joint, as visible in Figure 3.21.
Summing up, the analysis of similarity showed for both studied joints NDP values extremely high. This confirms the basic hypothesis expressed in this work of thesis. In addiction, Table 3.5 summaries the averaged NDP values across channels subsets, differentiating between extensors and flexors synergy.

Joint	NDP Extensors Synergy	NDP Flexors Synergy
Knee - 1IED	0.9916	0.9960
Knee - 2IED	1	0.9997
Ankle - 1IED	0.9806	0.9856
Ankle - 2IED	0.999	0.9932

TABLE 3.5: *Average NDP values for Knee and Ankle configurations across all subjects.*

3.1.4 Activation Signals Comparison

The outcome of NMF algorithm consists in the product between synergy matrix and activation signals vectors, as said previously. This section focuses on the analysis of extracted primitives, in order to verify that their properties are not related to channels subsets selected. Figure 3.22 and Figure 3.23 show non-negative factorization results for the *Complete Configuration* of knee and ankle joint, respectively. Each of them presents as first column the normalized weighting vectors. This representation is slightly different compared to the previous one, but however is useful to identify the weights amplitude trend of each synergy across channels and to highlight in which position the extensors synergy decreases in amplitude and vice versa. The number of effective considered elements after bad channels removal is indicated on x-axis. Second column shows instead the activation signals vectors as a function of samples (or time by dividing for the sampling frequency of 4 Hz, as explained in Chapter 2.4). It is noticeable that in this graph the extensors synergy is depicted temporally before the flexors one; this is consistent with the temporal execution of the movement. For what concerns the rows, they indicate 1IED and 2IED configuration, respectively.
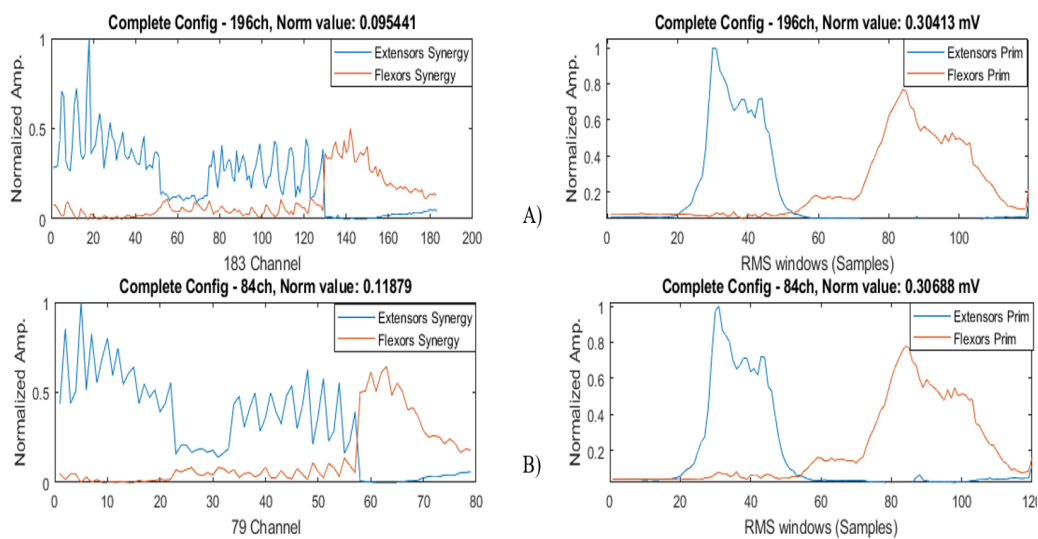
FIGURE 3.22: *NMF Outcomes for Knee Joint for a representative subject. Left column shows synergies vectors across channels, right column the primitives as a function of samples. First row (A) is related to 1IED, second (B) to 2IED.*

Looking at Figures 3.22, it is evident that weights amplitude of extensors is higher than flexors for both inter-electrode distances. More specifically, the lateral region of *Vastus Lateralis* shows the greatest amplitude while flexors muscles reach values just over 0.5. This difference is evidences also in the primitives column. In fact, activation signal of flexors is always lower than extensors. For what concerns the primitives shape, all activation signals vectors are very similar by comparing different IED. In addiction, flexors primitives is slightly visible also within extensors primitive region and this is consistent with the flexors weights amplitude in the first part of left column.

Outcomes for ankle joint showed in Figure 3.23 highlight that, contrary to knee joint, weights amplitudes trend present a sharp difference between extensors and flexors. Moreover, weight values for flexors (Gastrocnemius Muscles) are lower if compared with knee flexors (Biceps Femoris). Also in this case, the shape of extracted primitives is very similar for both IED and the presence of flexors primitive within extensors region is restricted compared with knee.
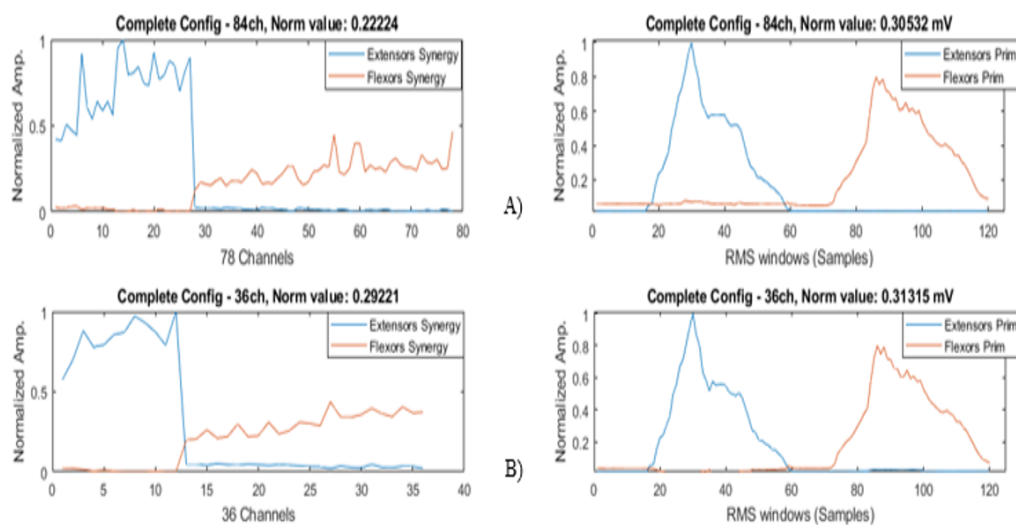
FIGURE 3.23: *NMF Outcomes for Ankle Joint for a representative subject. Left column shows synergies vectors across channels, right column the primitives as a function of samples. First row (A) is related to 1IED, second (B) to 2IED.*

Regarding the extracted channel subsets, in order to evaluate the similarity between primitives, following figures show the activation signals extracted for every sub-configuration. It is evident that primitives shape does not depend from the number of electrodes used.
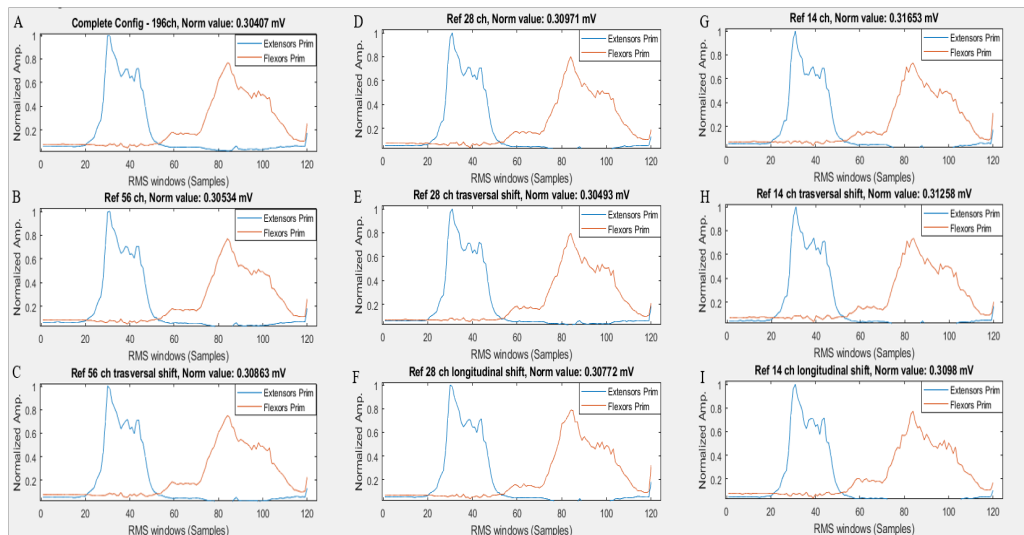
FIGURE 3.24: *Overview of extracted primitives for every channels subsets of a representative subject, Knee Joint 1IED.*
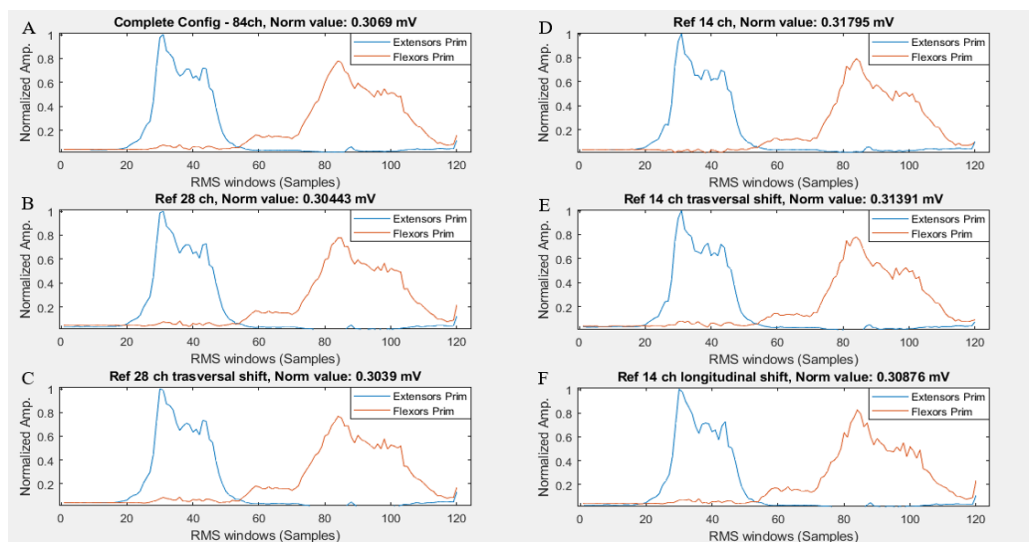
FIGURE 3.25: *Overview of extracted primitives for every channels subsets of a representative subject, Knee Joint 2IED.*
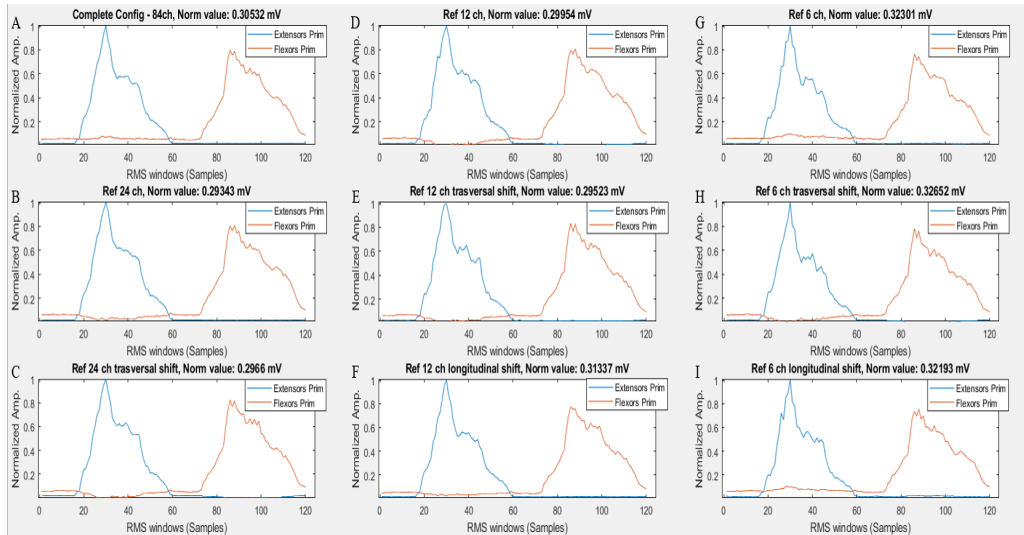
FIGURE 3.26: *Overview of extracted primitives for every channels subsets of a representative subject, Ankle Joint 1IED.*
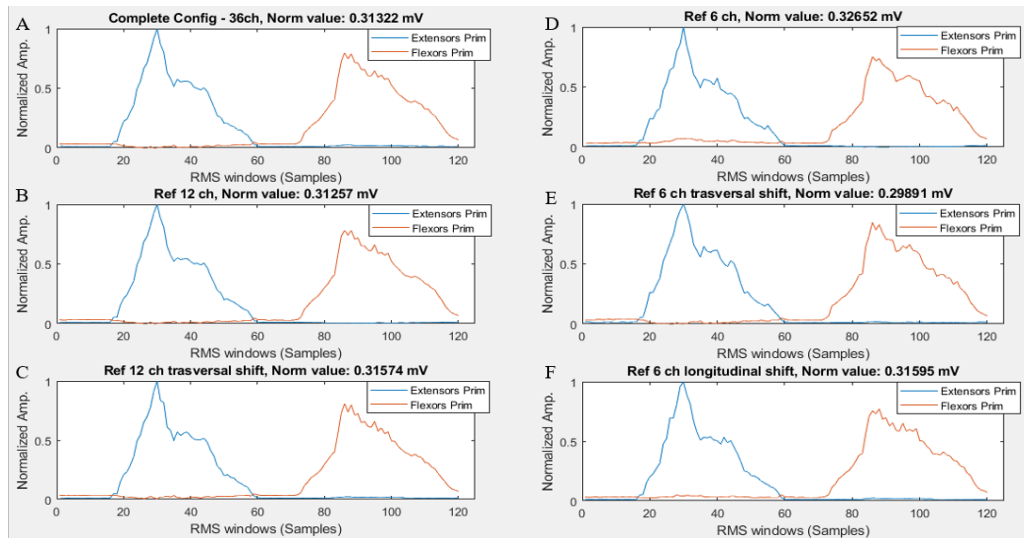
FIGURE 3.27: *Overview of extracted primitives for every channels subsets of a representative subject, Ankle Joint 2IED.*

Moreover, it was necessary to quantify the effective similarity of primitives between different configuration. For this reason, the *Complete Configuration* of each dataset was compared with all channels subsets by using a normalized cross correlation (NCC), as said in 2.4. The similarity indicator considered was the maximum value of each correlation. Following figures show each evaluated comparison for a representative subject; in general, left side column of every figure is related to extensors primitive while on the right side the flexors primitive is depicted.
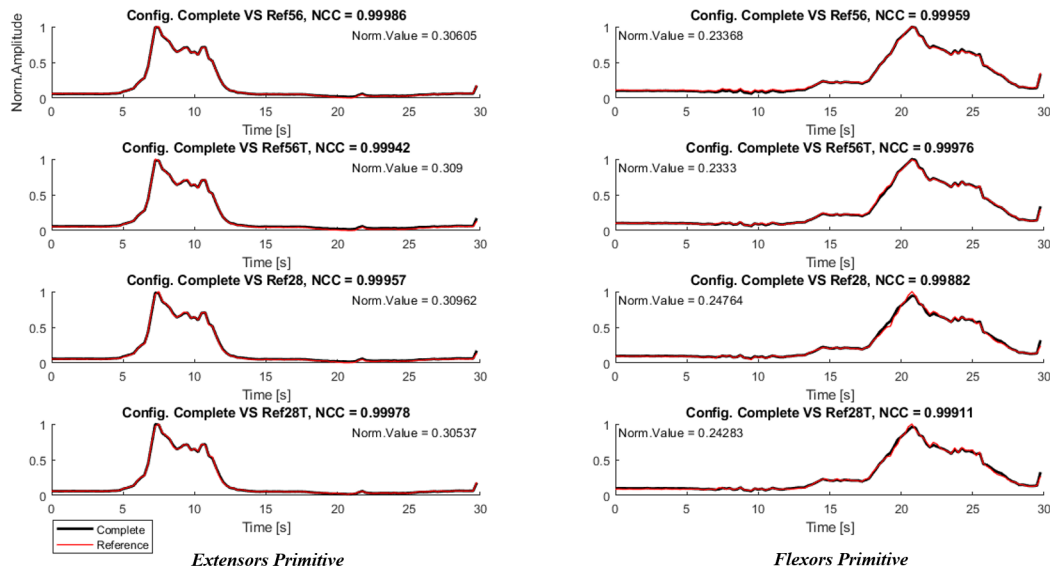
FIGURE 3.28: *Analysis of similarity between activation signals of Complete configuration and those of Reference configuration for a representative subject, Knee Joint 1IED (Subsets 1-4). Maximum value of Normalized Cross Correlation is depicted for each graph.*
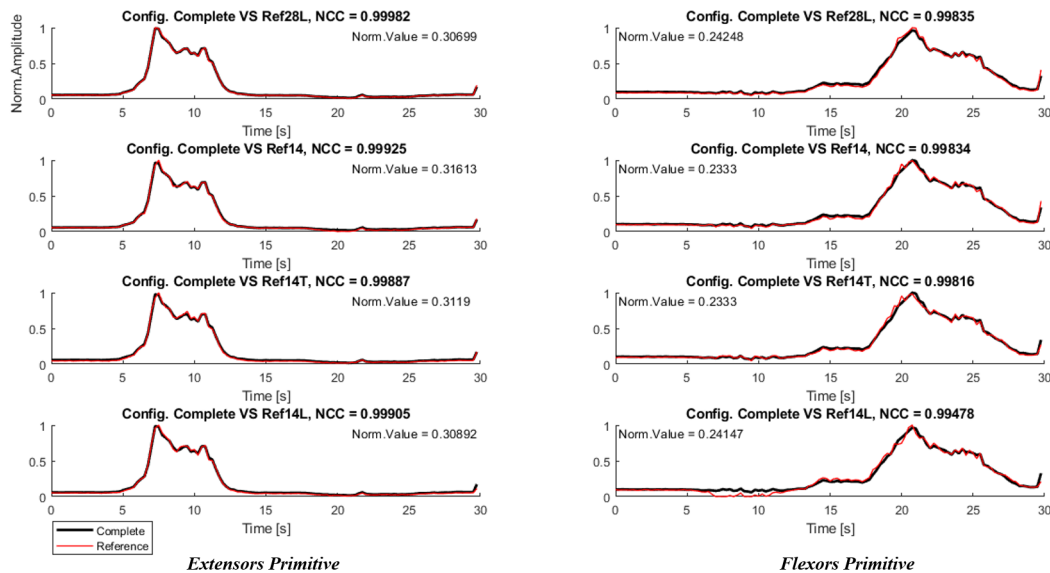
FIGURE 3.29: *Analysis of similarity between activation signals of Complete configuration and those of Reference configuration for a representative subject, Knee Joint 1IED (Subsets 5-8). Maximum value of Normalized Cross Correlation is depicted for each graph.*
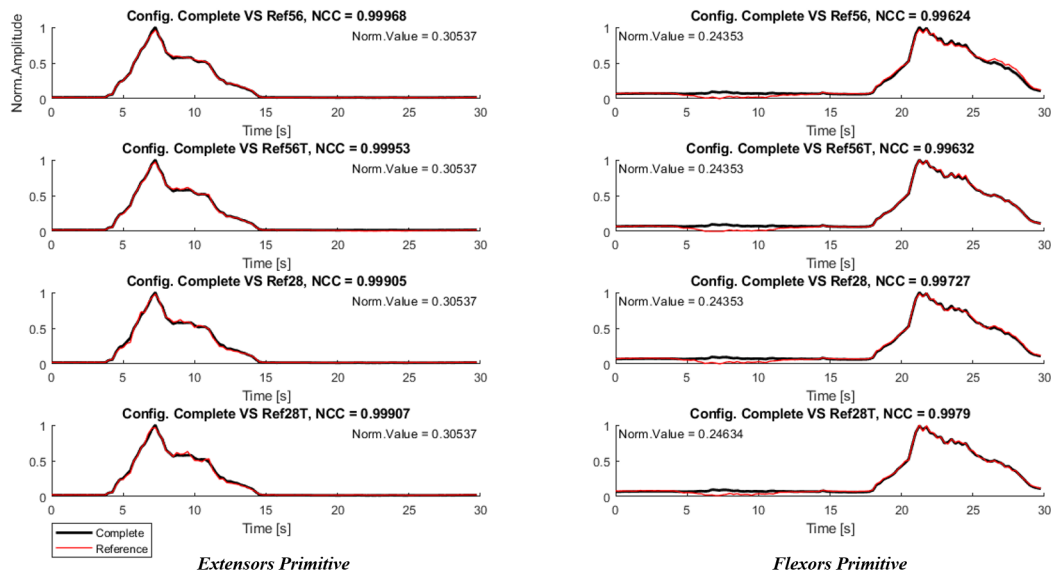
FIGURE 3.30: *Analysis of similarity between activation signals of Complete configuration and those of Reference configuration for a representative subject, Ankle Joint 1IED (Subsets 1-4). Maximum value of Normalized Cross Correlation is depicted for each graph.*
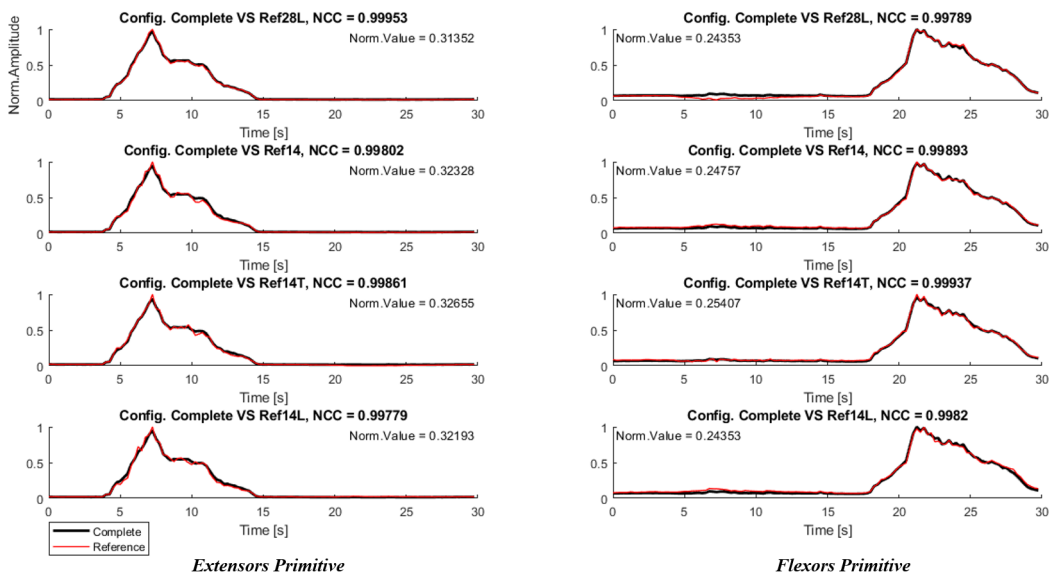
FIGURE 3.31: *Analysis of similarity between activation signals of Complete configuration and those of Reference configuration for a representative subject, Ankle Joint 1IED (Subsets 5-8). Maximum value of Normalized Cross Correlation is depicted for each graph.*
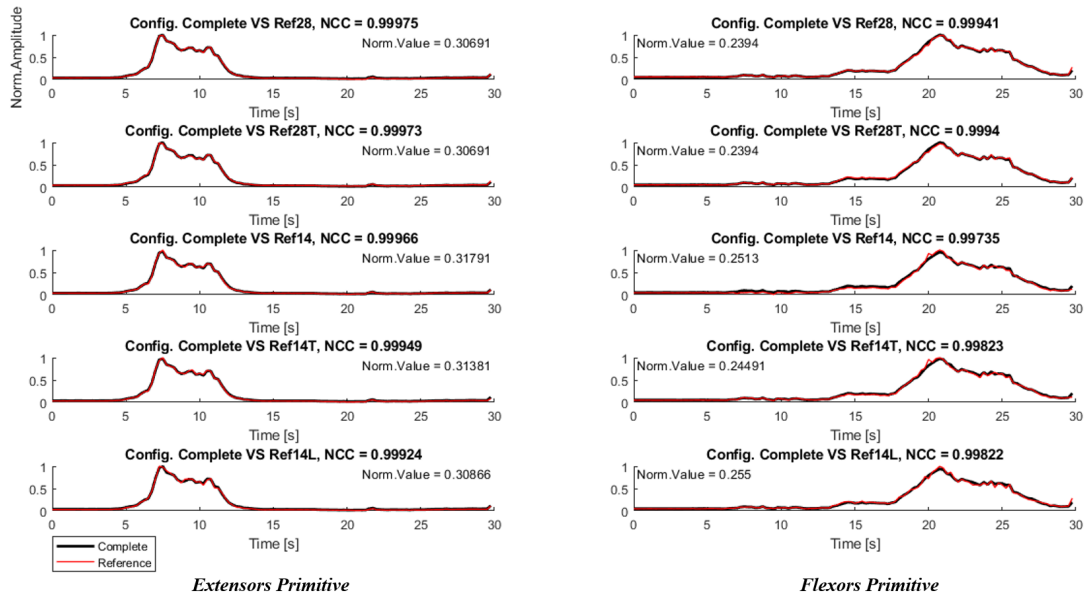
FIGURE 3.32: *Analysis of similarity between activation signals of Complete configuration and those of Reference configuration for a representative subject, Knee Joint 2IED. Maximum value of Normalized Cross Correlation is depicted for each graph.*
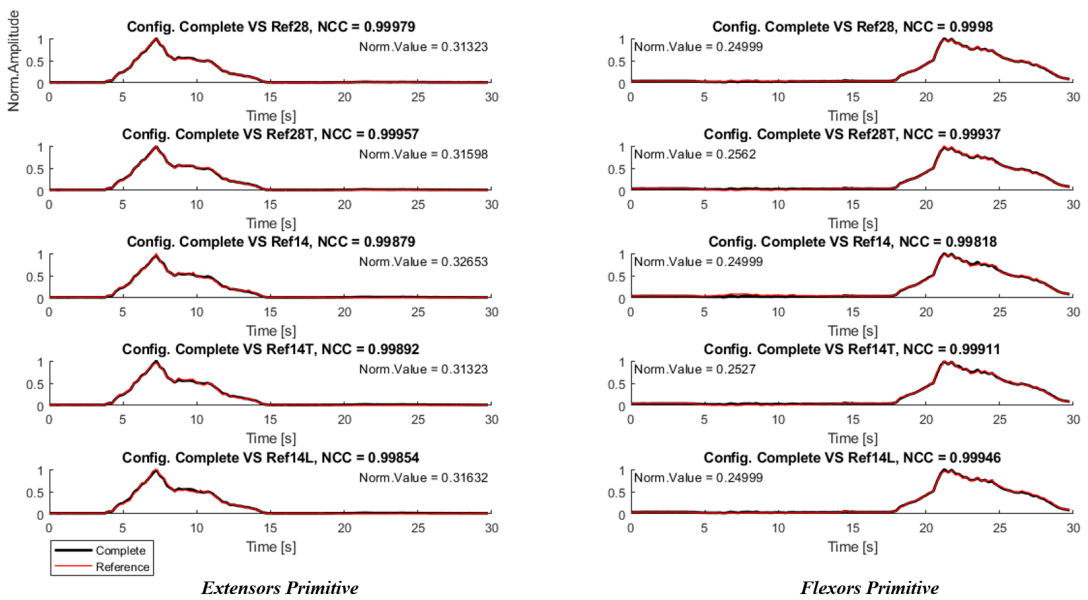
FIGURE 3.33: *Analysis of similarity between activation signals of Complete configuration and those of Reference configuration for a representative subject, Ankle Joint 2IED. Maximum value of Normalized Cross Correlation is depicted for each graph.*

It is evident that the number of channel is not relevant for the primitives shape. In fact, for every channels subsets, the similarity analysis with the Complete Configuration led to NCC values very high. This consideration, coupled with the fact that also shifted configuration were included in the investigation, allows to confirm again that the activity recorded on muscles surface can be approximated as linear combination of activation signals. In addiction, it proves that the extracted primitives are robust if used as control signal.

3.2 Second Experiment

The aim of Exp 2 was instead to couple two different joint in a complete movement in order to extract a control signal using the weights matrix estimated in the Exp 1. In addiction, the goodness of result was assessed comparing a post-processed control signal with angle signals, recorded during Exp 2.

3.2.1 Control Extraction

Signals recorded during Exp 2 are organized in ankle data followed by knee data. Before every analysis, they have been processed from raw data to RMS. Figure 3.34 shows an example of complete exercise where it is possible to appreciate the activations of all involved muscles in time.
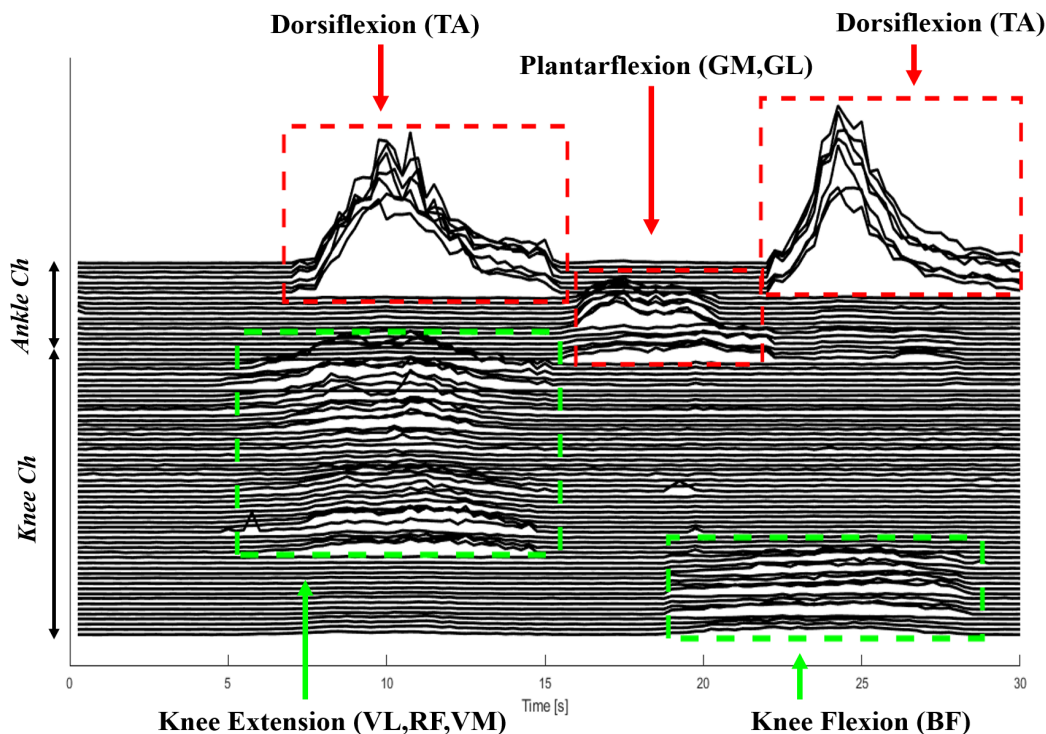
FIGURE 3.34: *Figure shows RMS signals with 1IED (subset with 24 channels for ankle and 56 for knee) as a function of time (Exercise 2, Subject 4). Signals are organized with ankle EMG on the top, knee EMG from middle to bottom region. Green boxes indicate the activation of knee muscles, while red boxes refer to ankle muscles.*

In fact, as explained in Chapter 2.3.2, knee extension and maintenance phase is coupled with an ankle dorsiflexion as highlighted by red and green dotted lines boxes on left side. Then, knee returns to rest phase (indeed it is not visible a relevant activation) and ankle performs a plantarflexion. Finally knee executes a flexion and, during maintenance phase, ankle conducts a dorsiflexion again as depicted inside the colored boxes on right side. At this point both joint comes back to rest position.

The extraction of control signals occurs employing the equation 2.12 expressed in Chapter 2.4. Thus, from every RMS matrices are extracted four signals related to ankle and knee joint. In example, Figure 3.35 shows the control signals of *Complete Configuration* (1IED), evaluated from 10 trials realized by a representative subject. Within each graph, first and second rows corresponds to control signals of ankle joint. They are related to extensors and flexors, respectively. The last two rows instead refers to knee joint. Observing each graph, it is noticeable that the control signals trend reflects the behavior discussed in Figure 3.34. This supports the employed method based on the product for the Penrose-Moore pseudo-inverse of the estimated synergies matrix. In addiction, signals trend is globally the same to indicate a good execution of the multi-DOF movement.
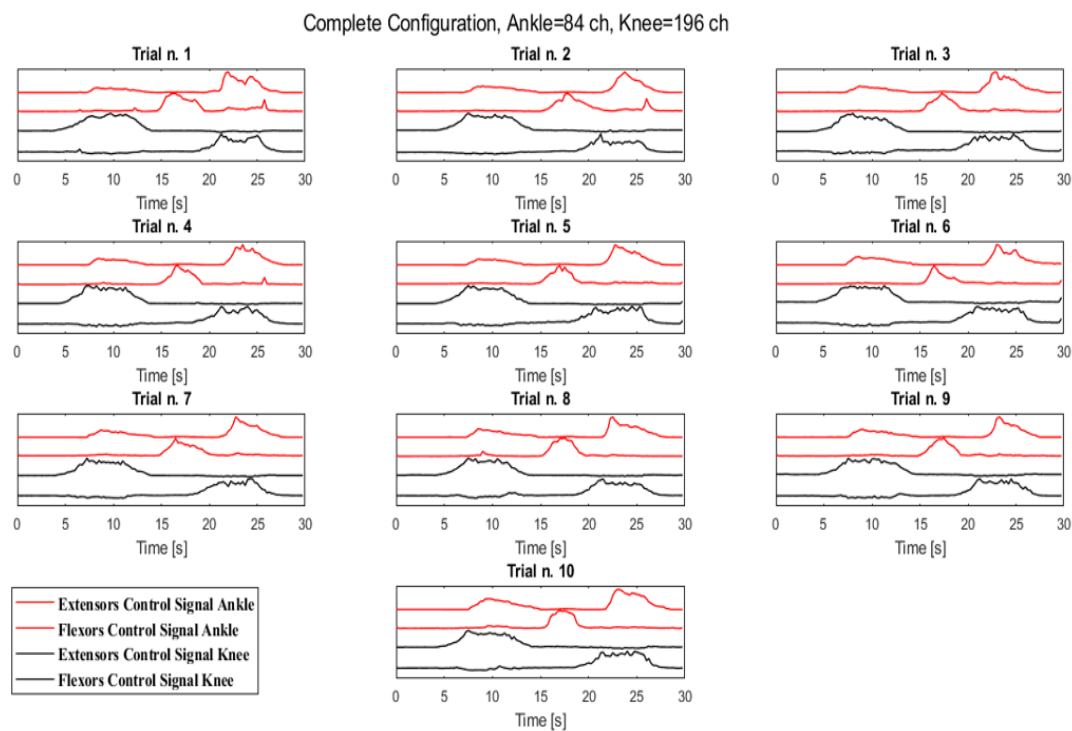
FIGURE 3.35: *Figure shows the calculated control signals for an exercise including 10 trials with Complete electrodes Configuration - 1IED, Subject 3. Each graph includes control signals for ankle (first two, extensors and flexors) and knee joint (last two, extensor and flexors).*

For completeness, an example of *Complete Configuration* with 2IED of a different subject from previous one is depicted in Figure 3.36. It is evident that trend and temporal coherence remained unchanged.

FIGURE 3.36: *Figure shows the calculated control signals for an exercise including 10 trials with Complete electrodes Configuration - 2IED, Subject 4. Each graph includes control signals for ankle (first two, extensors and flexors) and knee joint (last two, extensor and flexors).*

As said previously, the calculation with relation 2.12 led to four control signals. However, in order to pilot a multi-DOF exoskeleton, it is necessary to provide separately a signal to control each joint. For this reason, control signals of each joint have been combined to obtain only two signals. With the purpose of verify a robust control with all selected channels subset, next figures compare the outcomes achieved with *Complete Configuration* (the largest) and *Reference Configuration* composed of 6 electrodes for ankle and 14 for knee (the smallest one).

In particular, each figure depicts on left side the construction of ankle control signal and, on the other side, the one of knee. Every joint control signal is obtained as difference between calculated raw signals (for each joint extensors and flexors control). Each couple of control signals presents a large number of peaks and a not-smooth trend. Thus, in order to enhance it and increase the goodness of each joint control signal, a moving average filter was applied. Effects of filtering are easily visible: black line indicates the signal before filtering, red one the same but filtered.

Complete Configuration – Ankle 84 ch, Knee 196 ch

FIGURE 3.37: *Example of joint control signals construction from signals calculated with relation 2.12 for Complete Configuration - 1IED, Patient 3. Black lines indicate signal before a moving-average filter, red lines post-filtering.*

Reference Configuration – Ankle 6 ch, Knee 14 ch
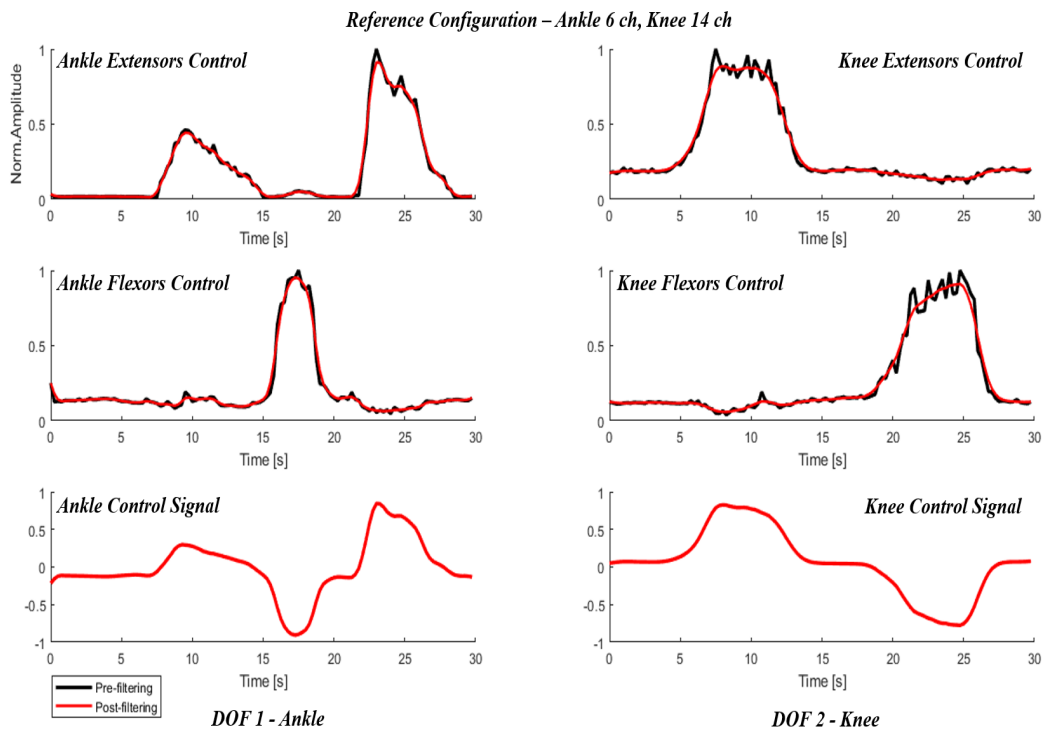
FIGURE 3.38: *Example of joint control signals construction from signals calculated with relation 2.12 for the smallest Reference Configuration - 1IED, Patient 3. Black lines indicate signal before a moving-average filter, red lines post-filtering.*

Figure 3.37 and 3.39 show similar results, both with regards to the extensors and flexors controls and shape of final joint signal control. This represents an achievement that strengthens the fact that a robust control can be reached also using a very limited number of electrodes. In addiction, an analysis of similarity was conducted through a normalized cross correlation (NCC) between filtered joint control signals of Complete and Reference configuration. For what concerns ankle joint, similarity was assessed in 99,74% while knee reached 99,46%.

The same considerations has been repeated considering the control signals calculated for 2IED.
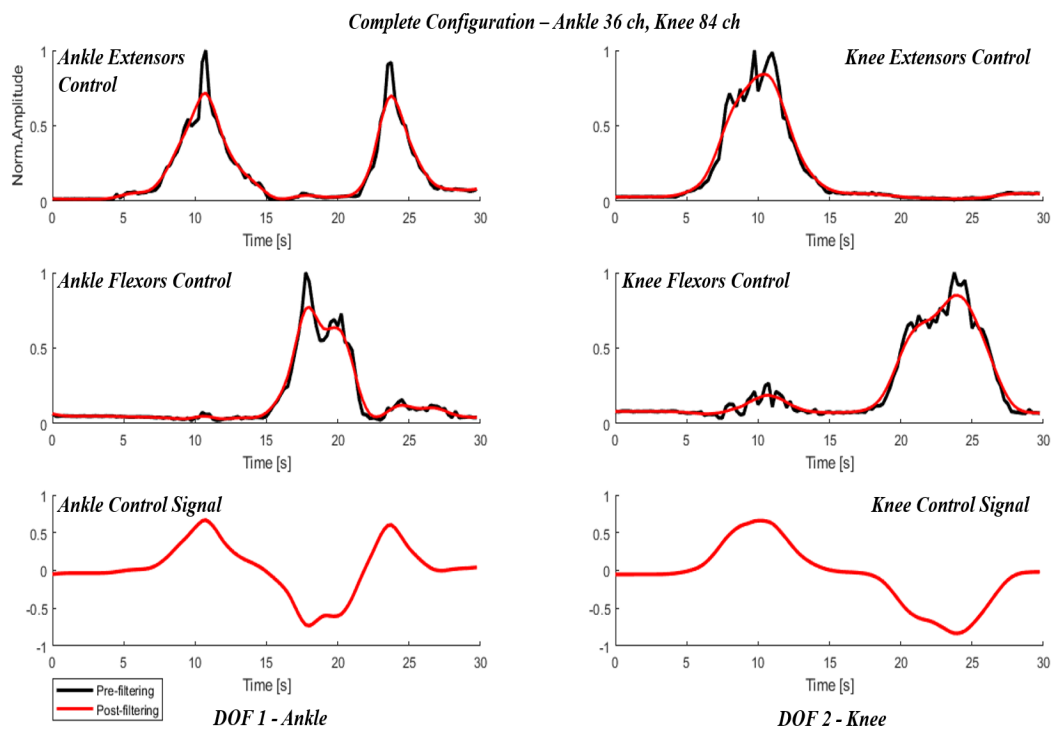
FIGURE 3.39: *Example of joint control signals construction from signals calculated with relation 2.12 for Complete Configuration - 2IED, Patient 4. Black lines indicate signal before a moving-average filter, red lines post-filtering.*

In this case, signals from a different subject have been considered in order to highlight any difference regarding the shape of calculated control signals, due to the different execution from patient to patient. Also this time, *Complete Configuration* and the smallest *Reference Configuration* are compared in Figure 3.39 and 3.40, respectively. Observing both figures, there are a few differences from previous case. Now the ankle extensors control reaches similar value in both dorsiflexion. In addiction, knee extensors and flexors controls appear very similar to 1IED case but, for either subjects, knee flexors control shows a limited activation in the temporal extensor region as said in result for Exp 1. Moreover, the comparison between the considered configurations led to the same conclusions: normalized cross correlation for ankle joint control signal was assessed in 99,66% while knee joint was 99,29%.
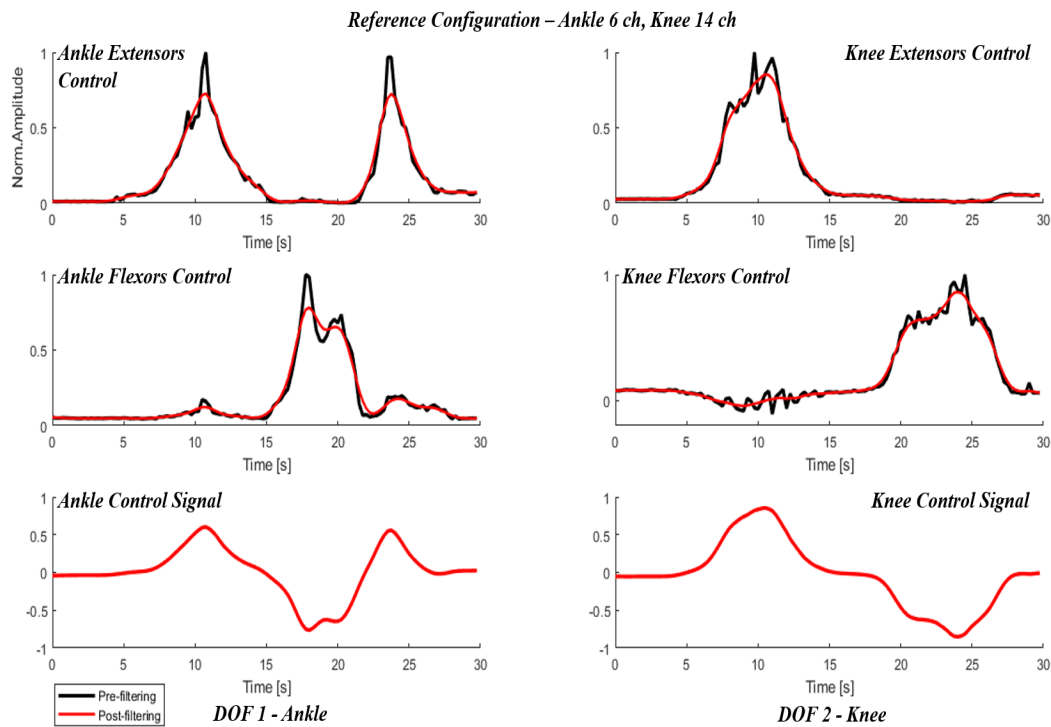
FIGURE 3.40: *Example of joint control signals construction from signals calculated with relation 2.12 for the smallest Reference Configuration - 2IED, Patient 4. Black lines indicate signal before a moving-average filter, red lines post-filtering.*

3.2.2 Recorded Angle Signals

Angle signals have been recorded through electrogoniometers. A calibration with single joint movements has been realized before the experiment starts, as explained in Chapter 2.4. At this point, EMG recording were accompanied by angle signals during each trial. Thus, 10 signals related to complete movement for both ankle and knee joint were recorded.

In example, Figure 3.41 and Figure 3.42 show all repetitions of angles recorded for a representative subject. Looking at ankle joint, patient respects the same path in almost every trials. It is noticeable that just before first dorsiflexion, angle signal of almost all subject indicates a small and fast plantarflexion. This is probably due to the movement complexity; indeed within this interval patient simultaneously performs an extension of knee. The transition leads to an ankle descending and this is consistent because ankle dorsiflexion must take place only with knee extended. Moreover, comparing this specific region of Figure 3.41 and 3.42, a match between hold phase of knee extended and ankle dorsiflexion can be appreciated. In addiction, another point of consideration is the different amplitude in terms of angle from first and second dorsiflexion. This is simply due to the movement development. Just before the second dorsiflexion, ankle of subject is completely flexed. Thus, moving towards the opposite condition, he can't able to control perfectly the range of motion and the second dorsiflexion does not correspond with the one.
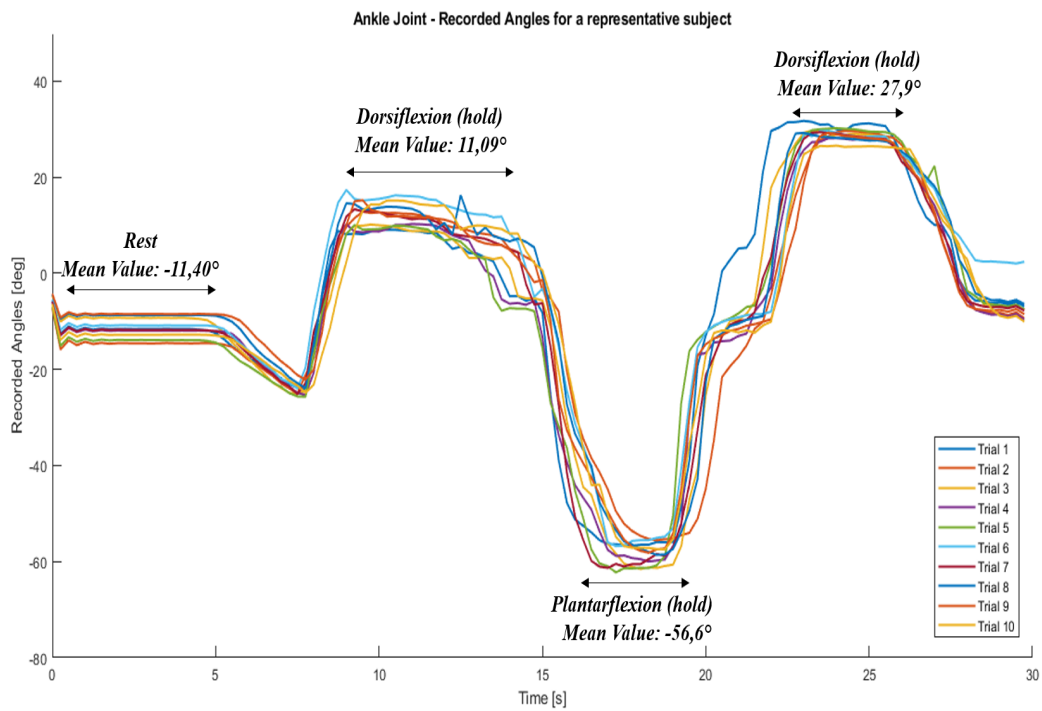
FIGURE 3.41: *Figure shows all recorded angle signals for ankle joint during Experiment 2. Averaged values of principal phases of the movement are indicated with the graph.*
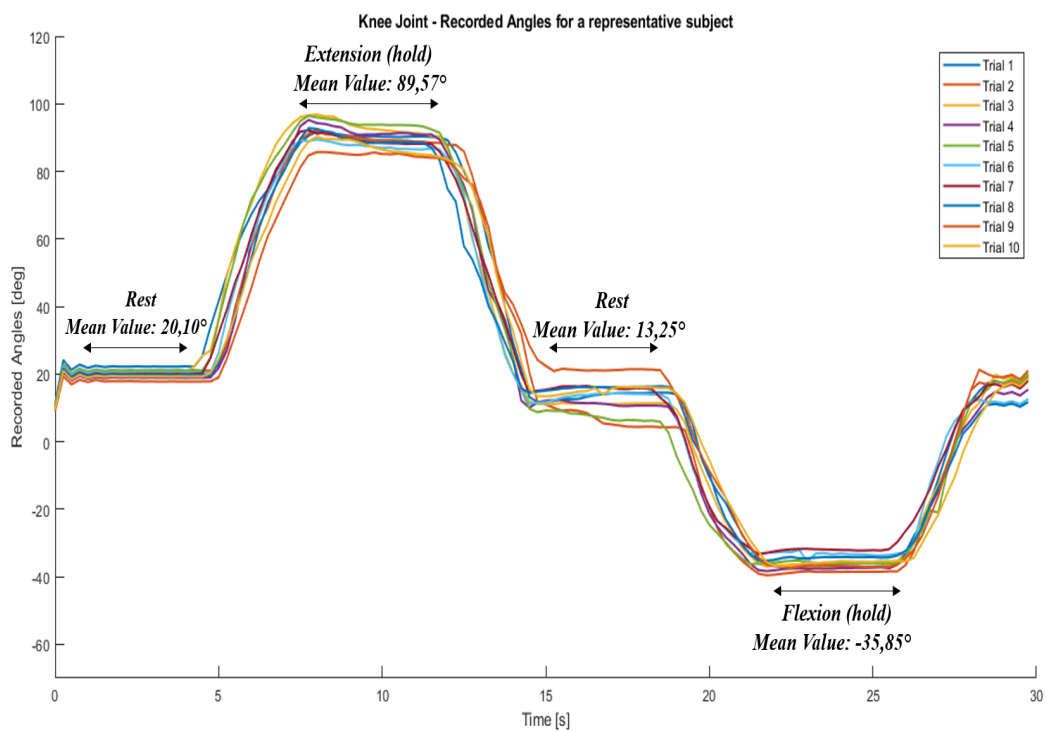
FIGURE 3.42: *Figure shows all recorded angle signals for knee joint during Experiment 2. Averaged values of principal phases of the movement are indicated with the graph.*

For each holding or rest phase, the mean value across every repetitions was calculated. For what concerns knee joint, the global trend is slightly more homogeneous compared to ankle. This is due to the fact that knee joint movement is dominant and it is easier to perform.

Finally, a common aspect is that both joint show an offset at the beginning. This is coherent with the calibration of electrogoniometers that presented the same gap. In addiction, initial inclination of both joint has been measured with a traditional goniometer.

3.2.3   Reconstruction Performances

The fundamental aim of Exp.2 was to validate the proposed method useful to perform a control signal for a lower limb exoskeleton. In this regard, an analysis to goodness of the extracted control was necessary. For this reason, calculated control signal for each joint was compared with the angle recorded from each electrogoniomer. The comparison was realized for every repetition of each channels subset by calculating the R^2 indicator as measure of similarity.

Angle signals are expressed in degrees while the extracted controls are EMG, weighed by a synergy matrix. For this reason before the comparison, control signals were multiplied by some scaling factors in order to obtain a result expressed in degrees. In addiction, employed scaling factors were chosen in order to match angle and control signals. Further, rescaled control signals sometimes showed a rugged trend with peaks and imperfections. Thus they were filtered by using a moving average filter in order to achieve a smoother trend.

Following figures show the outcomes obtained from signals comparison. In general, within each graph have been depicted the calculated control signal from equation 2.12 and 2.14, the filtered control signal to smooth the control trend (it has been superimposed) and the angle signal from electrogoniometers related to ankle or knee joint. The coefficient of determination has been assessed comparing the angle signal and filtered control signal. For each joint, two different investigations were developed: performances evaluation for a given trial across every channels subsets and R^2 trend across repetitions for the largest electrodes configuration. The first one was useful to joint goodness and stress the robustness of this method, the other tho verify if a change in performance can be related to number of repetitions.

Regarding the first analysis for 1IED, Figure 3.43 shows all configuration of a specific trial for ankle joint of a representative subject. Inside each graph, red line indicates the recorded angle signal, the green one and the black dotted line instead depict the control signal before and after filtering, respectively. Looking at the R^2 values across every channels subsets, it is noticeable that no one configuration polarizes the performance value. In fact, all R^2 are very similar each other. Nevertheless, the global performance does not exceed 80%.
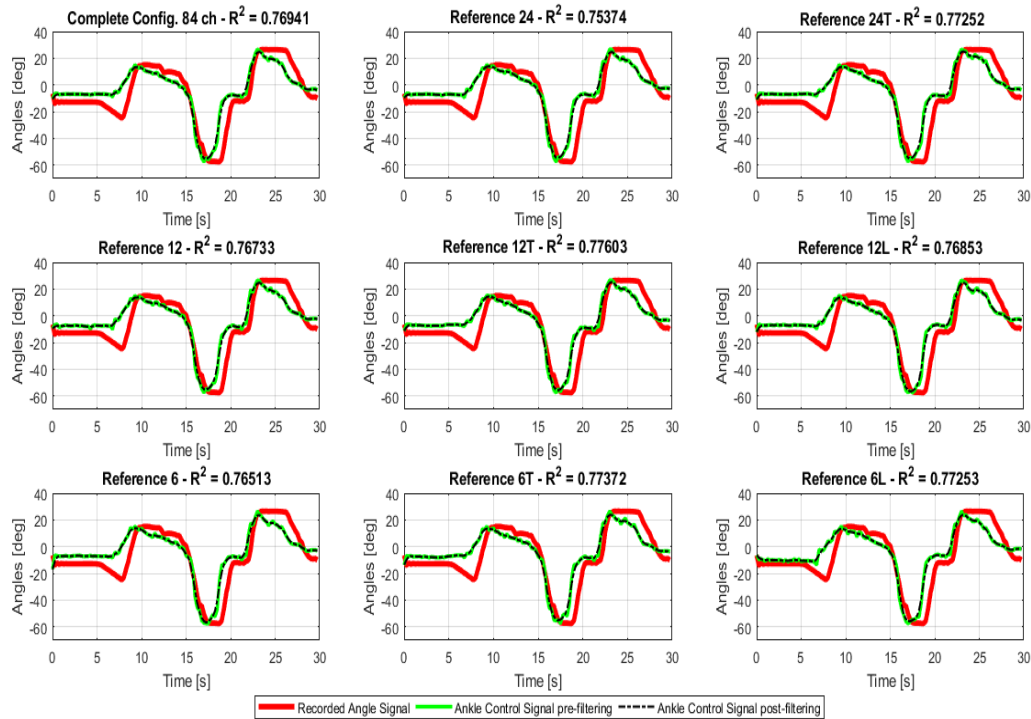
FIGURE 3.43: *Comparison of performance regarding the ankle control signal goodness across all channels subsets for a specific common repetition with 1IED, Patient 3.*

This can be visually explained; it is evident that the control signal follows the angle trajectory in the middle region of movement, whereas it are not able to map the short plantarflexion at the beginning. This could be due to a restricted muscular activation.

In contrast to the ankle, knee joint performance across channels subsets are definitely higher. Observing Figure 3.44 it is possible to appreciate that R^2 values achieve 95% in almost every configuration. In general, knee control signal in this case is able to follow the angle cue in each phase of the movement. The only remarkable consideration is about the extension maintenance phase: for a wide number of channels subset, control signal overshoots the angle trajectory in amplitude. In addiction, the signal before filtering highlights a sawtooth pattern in that plateau. This could be due to the isometric contraction. Moreover, *Reference56* and *Reference14* lose the contact with recorded angle trajectory during the final plateau, probably for a wrong activation.
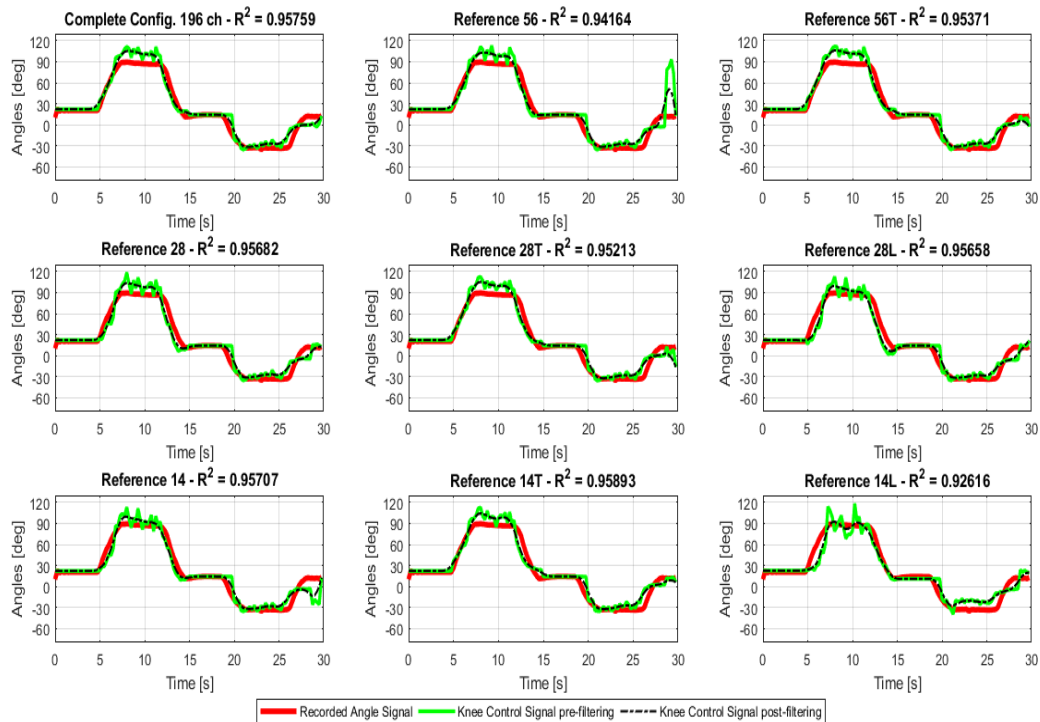
FIGURE 3.44: *Comparison of performance regarding the knee control signal goodness across all channels subsets for a specific common repetition with 1IED, Patient 3.*

For what concerns the second investigation, Figure 3.45 and Figure 3.46 depict a whole set of repetitions with respective coefficients of determination for the *Complete Configuration* of ankle and knee joint.

Ankle movements show a variable performance from 68% to 78%. It is noticeable that sometimes also the plantarflexion phase does not fit exactly the angle signal, even if the global trend is always respected. In addiction, occasionally wrong activation lead to overshoot and undershoot phenomena but the filtering effect is able to compensate them. On the opposite knee joint in Figure 3.46 keeps very high R^2 values, even if trial 1 presents the lowest matching with 88%. The presence of this out-layer can be explained with a twice overshoot amplitude, compared with other trials.

The same analysis has been performed also with extracted control signals of dataset with 2IED. For completeness, all results are reported from Figure 3.47 to Figure 3.50. It is evident that the considerations related to dataset with 1IED persist also doubling the inter-electrode distance. Thus, ankle control signal across configurations keeps the performance value below 80% while knee values reach in almost all cases 95%. The difference of R^2 values between the considered joint is also related to the complexity and range of movement. In fact, the control of knee during the exercise is surely easier than those of ankle. Moreover, knee explores a range of movement wider than ankle dorsi and plantarflexion; this allows to equalize each transition and to avoid change in direction as happen in the first part of ankle control signal.
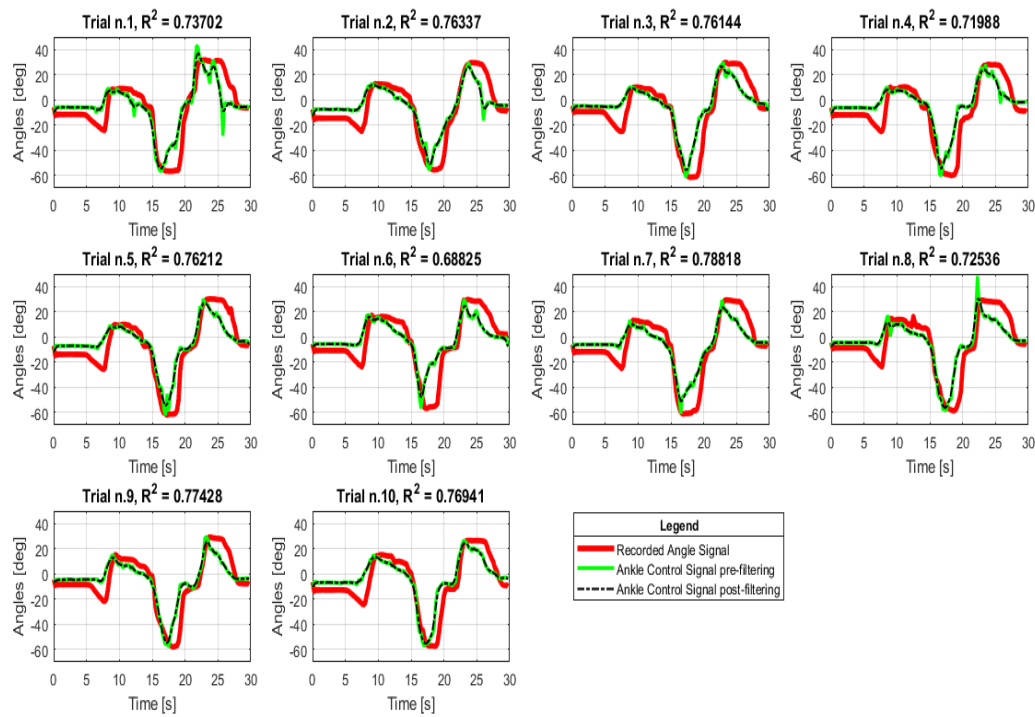
FIGURE 3.45: *Comparison of performance regarding the ankle control signal across a whole set of repetitions, 1IED - Patient 3.*
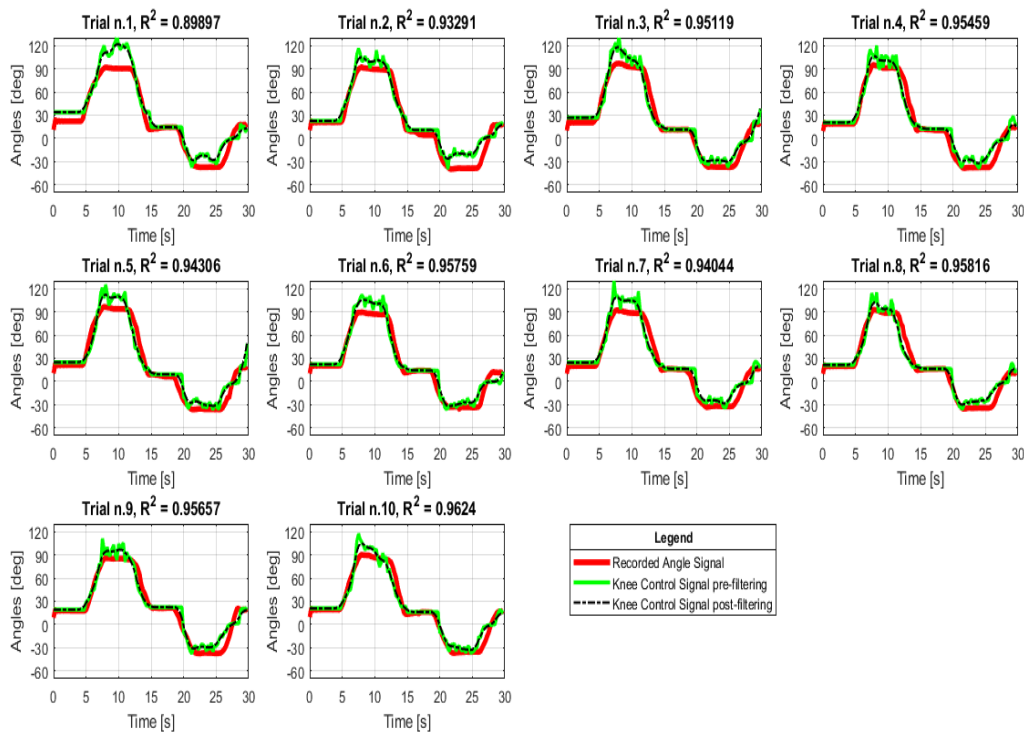
FIGURE 3.46: *Comparison of performance regarding the knee control signal across a whole set of repetitions, 1IED - Patient 3.*
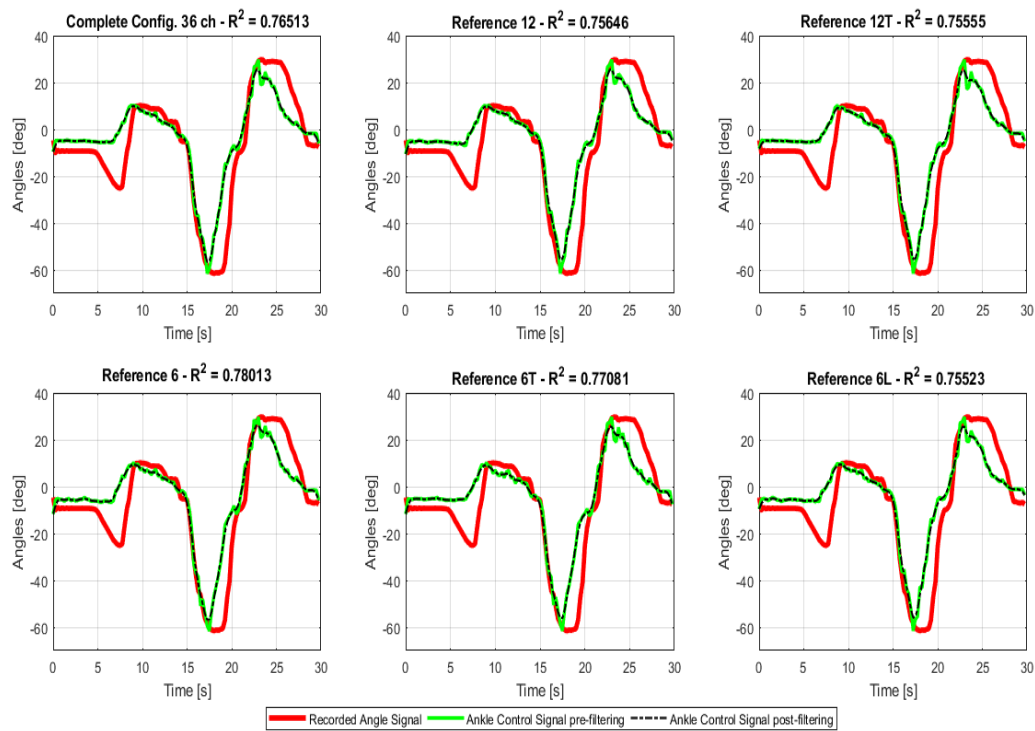
FIGURE 3.47: *Comparison of performance regarding the ankle control signal goodness across all channels subsets for a specific common repetition with 2IED, Patient 4.*
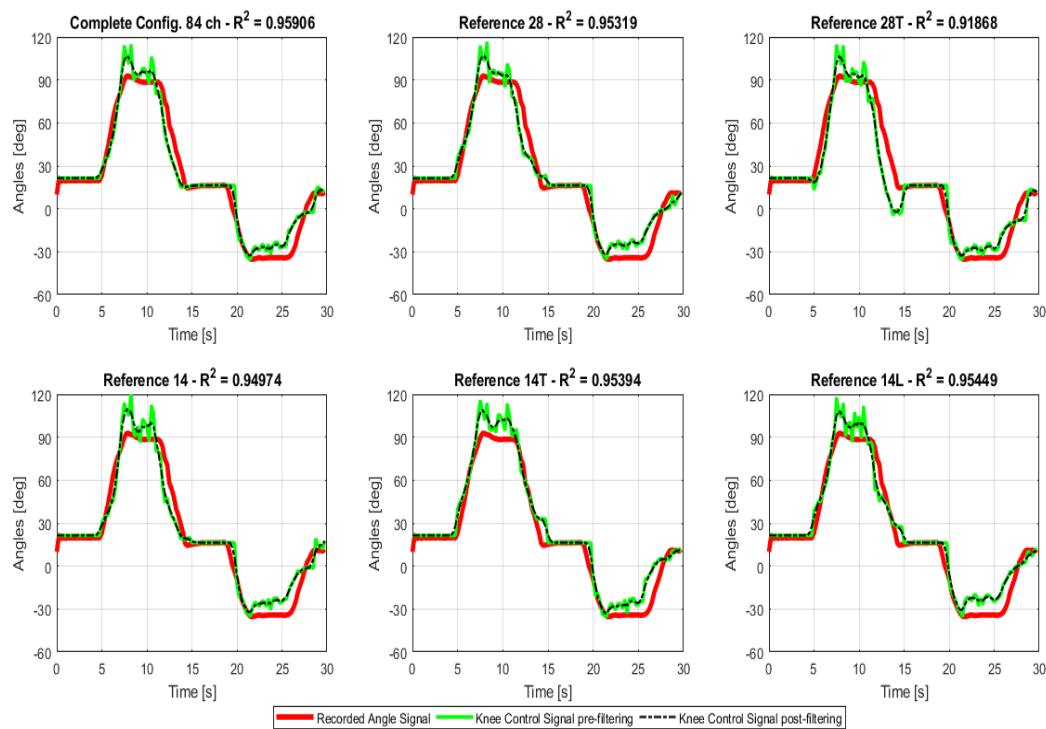
FIGURE 3.48: *Comparison of performance regarding the knee control signal goodness across all channels subsets for a specific common repetition with 2IED, Patient 4.*
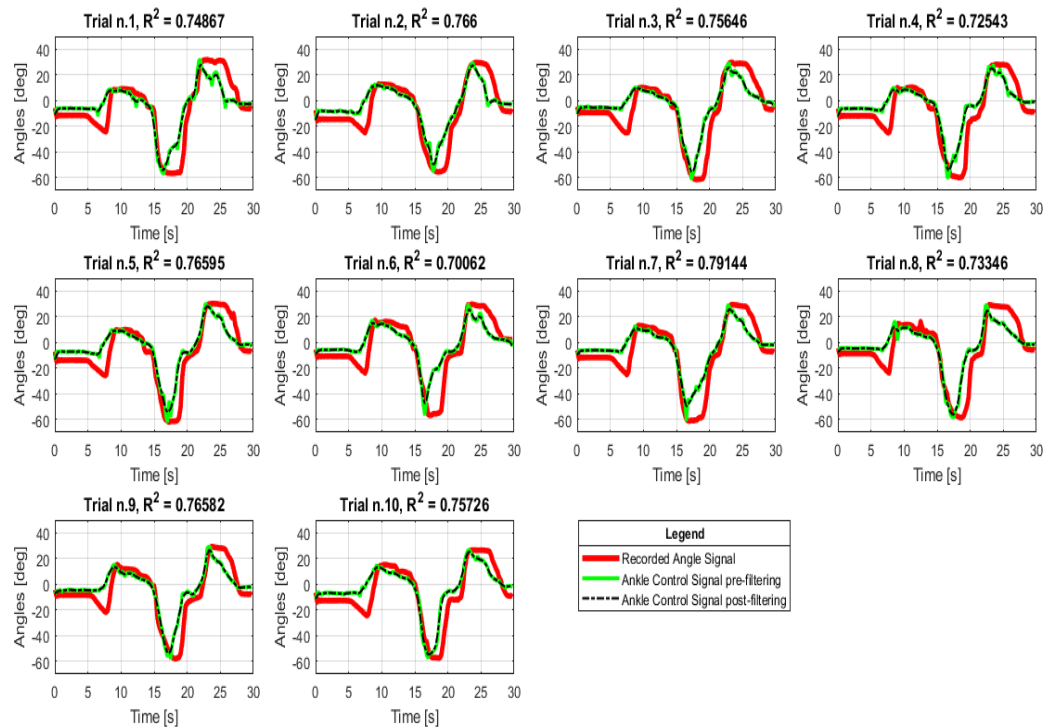
FIGURE 3.49: *Comparison of performance regarding the ankle control signal across a whole set of repetitions, 2IED - Patient 4.*
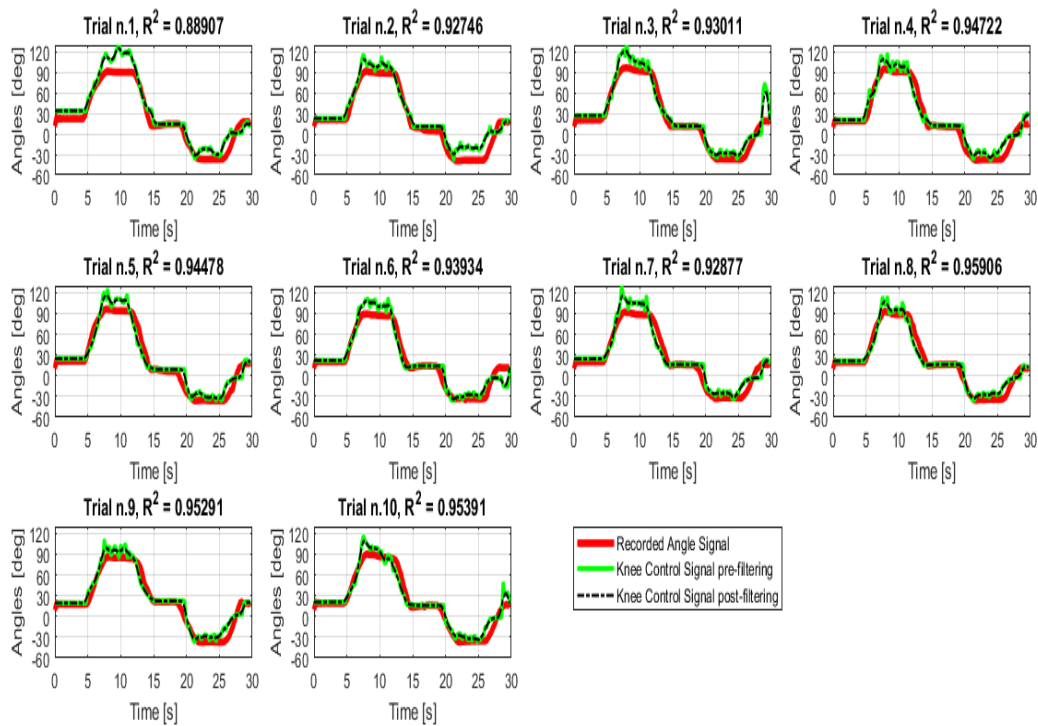
FIGURE 3.50: *Comparison of performance regarding the knee control signal across a whole set of repetitions, 2IED - Patient 4.*

Summing up, results showed that the control signals extracted from a multi-DOF movements match the angle recorded from both joint during the exercise in a suboptimal way. For each joint the average performance value has been calculated across every subjects. Outcomes provided mean R^2 of 75% for ankle and 95% for knee in case of 1IED, whereas 2IED dataset led to 73% for ankle and 93% for knee.

3.3 Statistical Test

The analysis of performance of this work of thesis involved a significant number of factors. In fact, R^2 values have been calculated by considering a given subject, configuration, interested joint and also specific repetition. All this variables participated to define a range of values for the coefficient of determination. A three-way analysis of variance (ANOVA) test was performed. Selected factors for the statistical test were number of subjects (5), selected channels subsets (from the *Complete Configuration* to the smallest *Reference* one) and joint (Knee or Ankle). This test aims to identify which factors influence the R^2 behavior. The analysis was repeated for both dataset with 1IED and 2IED. In addiction, statistical significance for all test was set at *p < 0.05*. Results are reported in Tables 3.6 and 3.7. Both test led to the same conclusions. R^2 values are not influenced by the electrodes configuration used. Conversely, performance values are dependent by subjects and joint.

Factors	p-value
Subjects	*p < 0.05*
Channels Subsets	0.9701
Joint	*p < 0.05*

TABLE 3.6: *ANOVA test results for 1IED dataset. Input data are R^2 values, while factors are Subjects (5), Channels Subsets (9) and Joint (2).*

Factors	p-value
Subjects	*p < 0.05*
Channels Subsets	0.8314
Joint	*p < 0.05*

TABLE 3.7: *ANOVA test results for 2IED dataset. Input data are R^2 values, while factors are Subjects (5), Channels Subsets (6) and Joint (2).*

Chapter 4

Conclusion and Future Work

This work of thesis aimed to provide a robust control signal for a lower-limb exoskeleton by using high-density surface EMG and performing a dimensionality reduction of the electrodes number. The control extraction represented the final part of this project. In fact, at first it was necessary to verify the main assumption underlying the employed model. Thus, changing the boundary conditions from that has been demonstrated in [22], it was necessary to verify the hypothesis that a muscle signal mixtures included into EMG signals recorded on muscular surface can be approximated as linear instantaneous. In this way, it is possible extract the activation signals directly from recorded surface EMG.

For this reason, this research focused on two main aspects. The first one was to investigate the similarity of results obtained with different electrodes configurations, the second one to validate the method quantifying the control signal goodness.

This strategy influenced the experimental setup that has been split in two experiments. During Exp.1, each subject performed simple movements of knee and ankle joint separately. Exp.2 instead couples the two joint. In this phase, each patient carried out a complete exercise articulating both joint.

Data recorded during Exp.1 were factorized through Non-Negative Matrix Factorization (NMF) algorithm. It has been used in order to decompose a EMG signals matrix in two matrices, one for synergies and one for primitives signals. The product of resulting matrices approximates the input dataset. The factorization was repeated for all selected channels subsets, reducing the number of electrodes from 196 to 14 for knee and 84 to 6 for ankle. In addiction, input matrices were constructed also doubling the inter-electrode distance during the processing phase.

Experiment 1 led to important results; first of all, the factorization algorithm used allowed to achieve performance of signals reconstruction greater than 90%. This indicates that NMF, as in other field, is a suitable method for data mining. Moreover, an investigations on weighting vectors amplitude was conducted. In this regard, an high similarity between weights of different channels subsets has been found. The same results have been achieved by verifying the correlation between primitives extracted from configurations with a wide or limited number of channels. This confirmed the

main hypothesis formulated in this work of thesis: EMG signals recorded on muscular surface include signal mixtures that are approximately linear instantaneous. With this condition, the activation signals extracted are not influenced from the electrodes number or placement.

The second experiment instead allowed to extract the control signal for each joint starting from the synergies matrix, one for each channels configuration, estimated during Exp.1. At this point, with the purpose to quantify the goodness of the control, a comparison between estimated control signals and angle signals recorded from two electrogoniometers during all trials was performed. Naturally, calculated controls were converted in angles by using some scaling factors before the comparison.

Analysis of performance showed that the control extracted for knee joint, for both 1IED and 2IED, matched the recorded angle with accuracy of 95% while ankle control signal reached a little less than 80%, defending the fact that ankle movements were harder to reconstruct.

Thus, this thesis proposed a useful method for lower-limb that overcomes the necessity of collect both EMG and kinematics (supervised method) as control strategy. It is not completely unsupervised but semi-supervised, because during the Exp.1 related with the synergies matrix estimation it is necessary to know which DOF (in this case which joint) is active during the signals recording. Beyond that, the employed method allowed to extract the control signal of each joint simply multiplying the EMG input signals and the inverse of the estimated synergies matrix. In addiction, the employed algorithm showed a really restricted computational time in the range of a few minutes.

The whole research highlighted also some critical aspects that need to be improved with further development. First of all, the experimental setup was conducted by using cumbersome instrumentation. A large number of cables and connectors is not certainly appropriate in a clinical perspective, so it is necessary to move toward wearable technologies. This necessity is supported by the main result of this research, which is the fact that activation signals can be extracted with a limited number of electrodes.

In addiction, the experiments were conducted on able-bodied and non pathological subjects. The adopted DOF-wise approach requests to distinguish a given degree of freedom for each considered joint. This was easily performed from every patients. Nevertheless, this action can be difficult for a pathological subject. In fact, he is not necessarily able to execute an ankle dorsi or plantarflexion rather than a pronation/supination. In this case DOF-wise approach could lead to wrong synergy matrix and, consequently, to a poor control. In this direction, recently *Farina et al.* proposed to modify the existent model including sparseness constraints to the matrix of activation signals [30]. The concept of sparseness refers to the representation of

data vectors by using only a restricted number of units that are out of a large population. Numerically, this means that there are a few representative elements with non-zero values whereas everyone take values close to zero. Thus, in a normalized scale, a vector with the highest sparseness will show only a non-zero element. As the opposite, all equal elements lead to a null sparseness [31]. This correction limits the solutions space; indeed the solution related to a single DOFs is the sparser one within the infinite solutions.

As showed in [30], the reformulation of adopted model could simplify the calibration phase (performed in this thesis as Exp.1) and each patient would not be obliged to distinguish the activation of a single DOFs rather than an other.

In conclusion, the important confirmation resulted from this work of thesis for what concerns the reliability of sEMG signals as control for a lower-limb exoskeleton and future researches that aim to improve the existent models, certainly will enhance the use a exoskeleton for rehabilitation purposes and many other applications.

Appendix A

Channels Subsets Representation

A.1 1IED Configurations - Knee and Ankle Joint
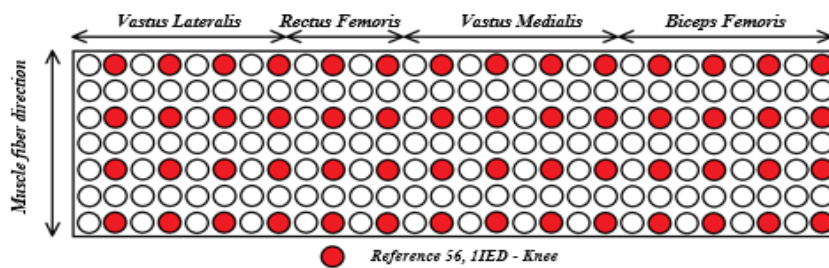
FIGURE A.1: *Reference 56 channels, Knee Joint 1IED*
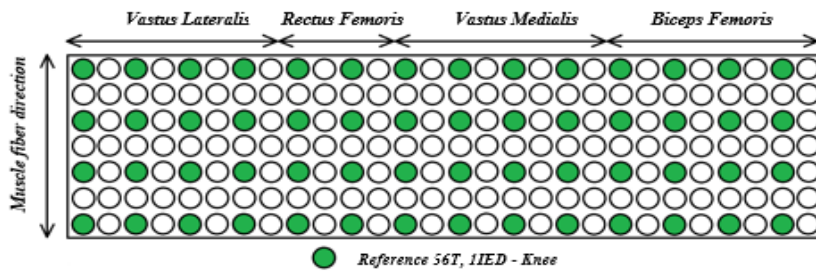
FIGURE A.2: *Reference 56 channels with trasversal shift, Knee Joint 1IED*
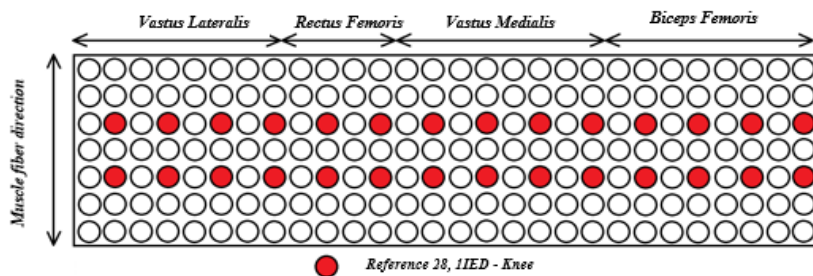
FIGURE A.3: *Reference 28 channels, Knee Joint 1IED*
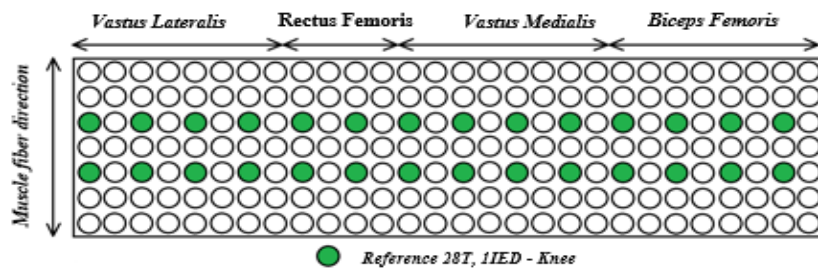
FIGURE A.4: *Reference 28 channels with trasversal shift, Knee Joint 1IED*
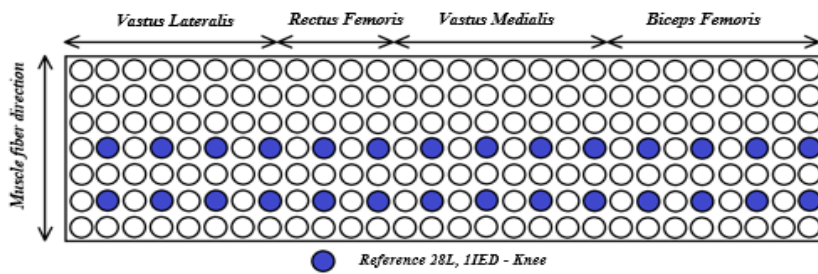
FIGURE A.5: *Reference 28 channels with longitudinal shift, Knee Joint 1IED*
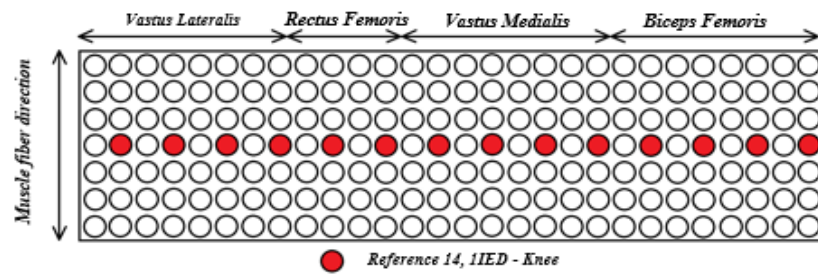
FIGURE A.6: *Reference 14 channels , Knee Joint 1IED*
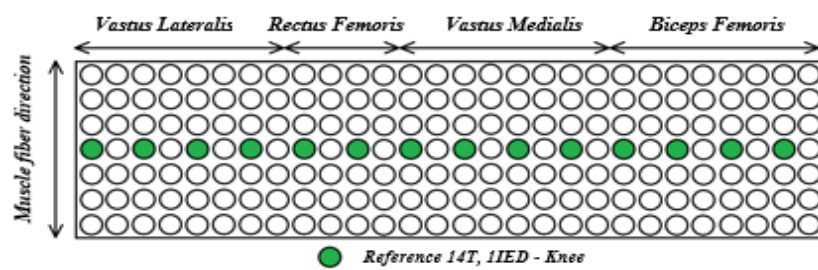
FIGURE A.7: *Reference 14 channels with trasversal shift , Knee Joint 1IED*
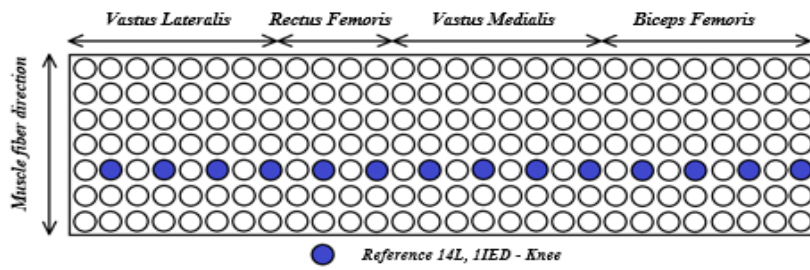
FIGURE A.8: *Reference 14 channels with longitudinal shift, Knee Joint 1IED*
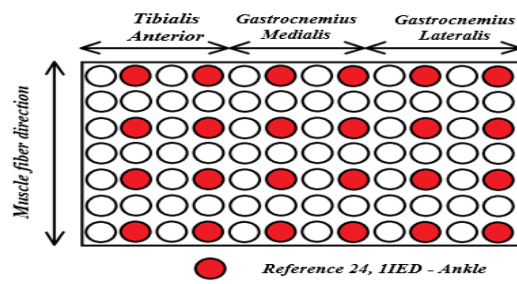
FIGURE A.9: *Reference 24 channels, Ankle Joint 1IED*
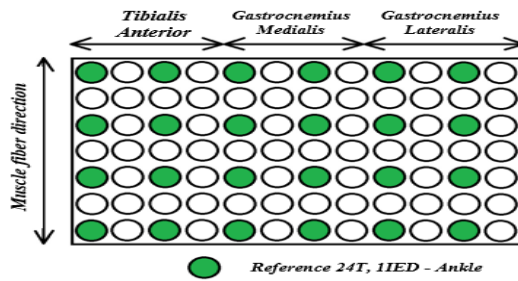
FIGURE A.10: *Reference 24 channels with trasversal shift , Ankle Joint 1IED*
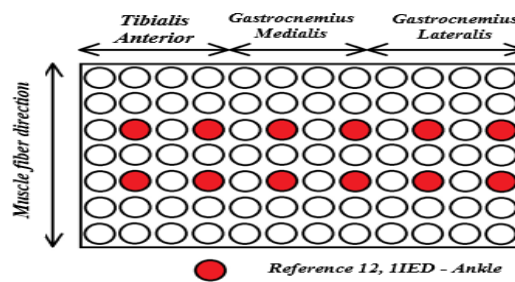
FIGURE A.11: *Reference 12 channels, Ankle Joint 1IED*
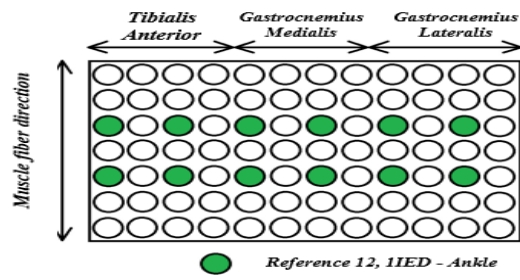
FIGURE A.12: *Reference 12 channels with transversal shift, Ankle Joint 1IED*
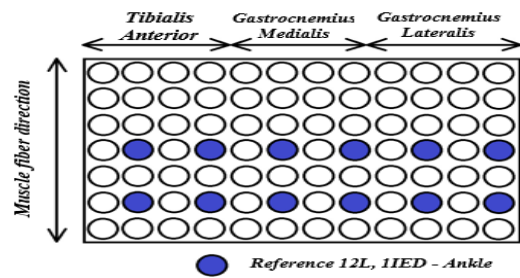
FIGURE A.13: *Reference 12 channels with longitudinal shift, Ankle Joint 1IED*
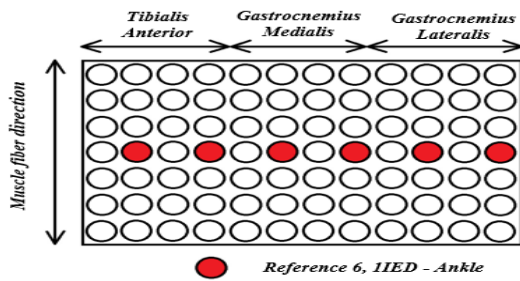
FIGURE A.14: *Reference 6 channels, Ankle Joint 1IED*
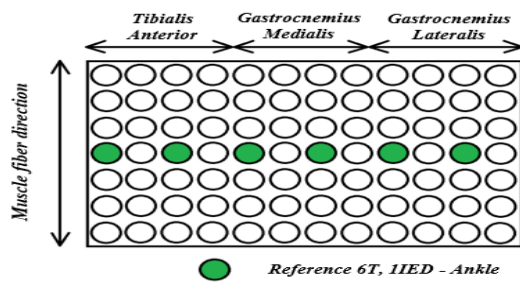
FIGURE A.15: *Reference 6 channels with transversal shift, Ankle Joint 1IED*
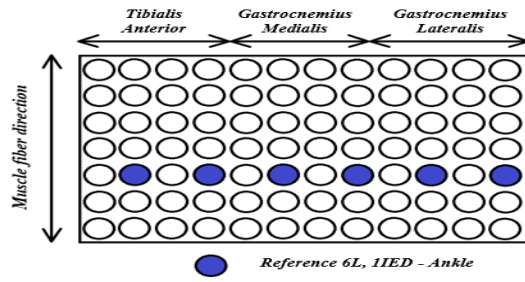
FIGURE A.16: *Reference 6 channels with longitudinal shift, Ankle Joint 1IED*

A.2 2IED Configurations - Knee and Ankle Joint
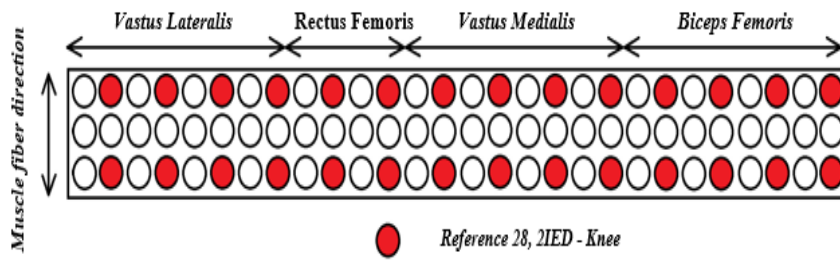
FIGURE A.17: *Reference 28 channels, Knee Joint 2IED*
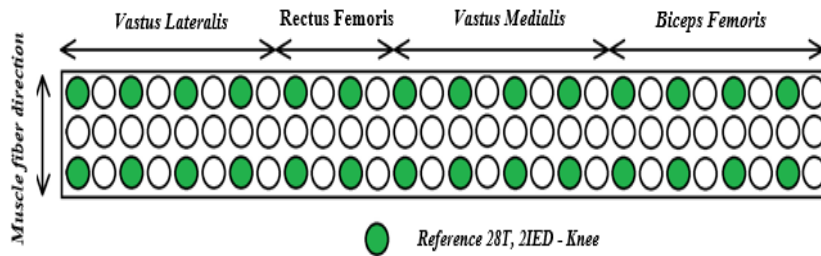
FIGURE A.18: *Reference 28 channels with trasversal shift, Knee Joint 2IED*
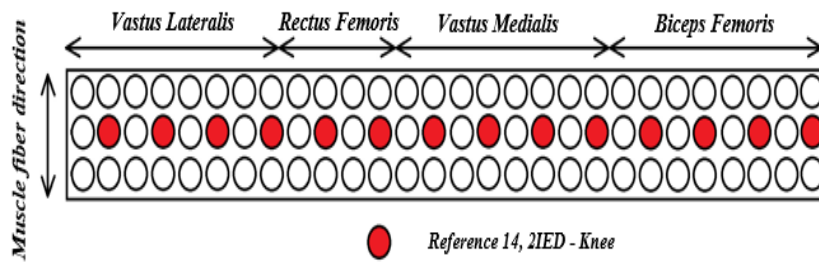
FIGURE A.19: *Reference 14 channels, Knee Joint 2IED*
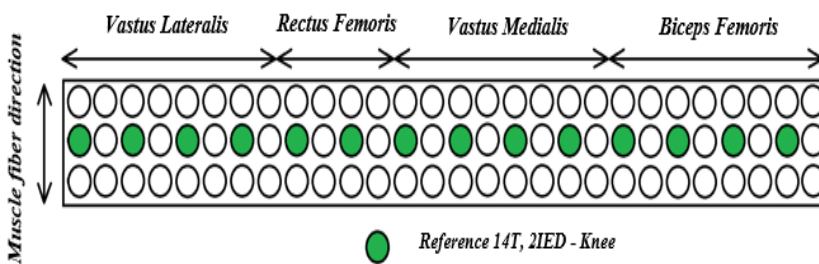
FIGURE A.20: *Reference 14 channels with transversal shift, Knee Joint 2IED*
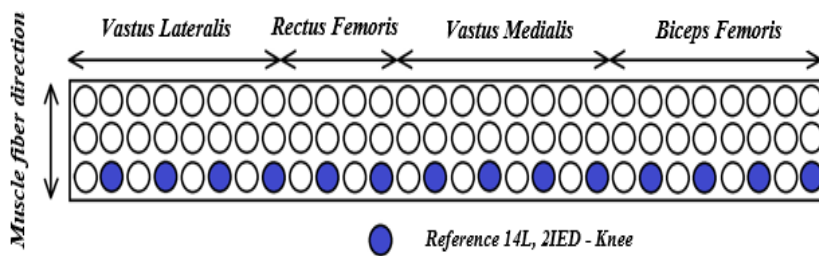
FIGURE A.21: *Reference 14 channels with longitudinal shift, Knee Joint 2IED*
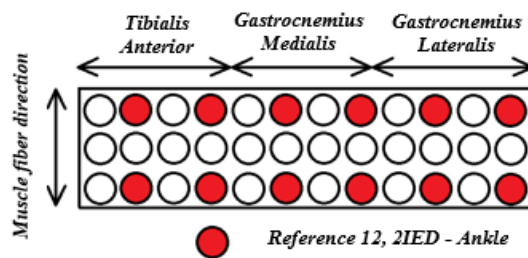
FIGURE A.22: *Reference 12 channels, Ankle Joint 2IED*
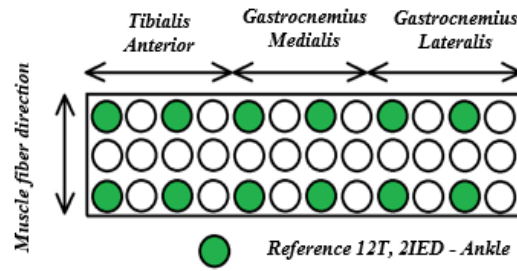
FIGURE A.23: *Reference 12 channels with transversal shift, Ankle Joint 2IED*
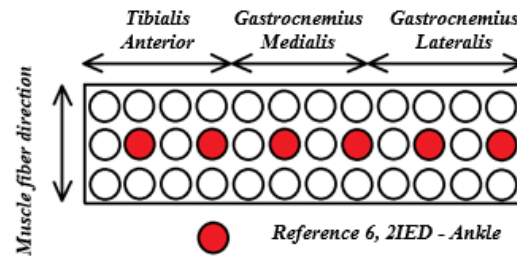
FIGURE A.24: *Reference 6 channel, Ankle Joint 2IED*
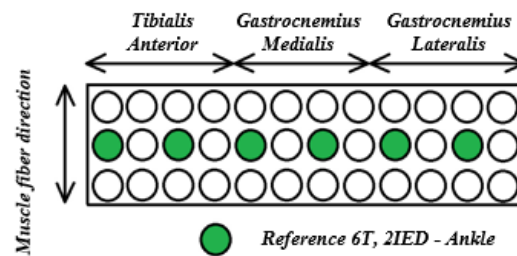
FIGURE A.25: *Reference 6 channels with transversal shift, Ankle Joint 2IED*
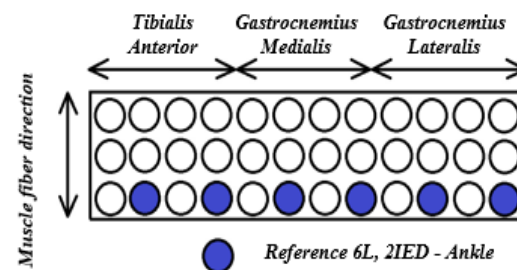
FIGURE A.26: *Reference 6 channels with longitudinal shift, Ankle Joint 2IED*

Bibliography

[1] Weiguang Huo et al., *Lower Limb Wearable Robots for Assistance and Rehabilitation: A State of the Art*, IEEE Systems Journal, vol.10, No.3, 2016.

[2] Wei Meng et al., *Recent development of mechanisms and control strategies for robot-assisted lower limb rehabilitation*, Mechatronics, vol.31 pp. 132–145, 2015.

[3] D. Bourbonnais and S. V. Noven, *Weakness in patients with hemiparesis*, Am. J. Occupational Therapy, vol. 43, No. 5, pp. 313–319, 1989. Am. J. Occupational Therapy, vol. 43, no. 5, pp. 313–319, May 1989.

[4] Marchal-Crespo, Reinkensmeyer, *Review of control strategies for robotic movement training after neurologic injury*, J Neuroeng Rehabil, 2009.

[5] Bortole, Venkatakrishnan *The H2 robotic exoskeleton for gait rehabilitation after stroke: early findings from a clinical study*, Journal of Neuroengineering and rehabilitation, 2006.

[6] Johnson, Onuma *Stroke: a global response is needed*, Bull World Health Organ, 2016.

[7] Roberto Merletti, Philip Parker, *Electromyography - Physiology, Engineering, and Noninvasive Applications*, Wiley Edition, 2004.

[8] Roberto Merletti, Dario Farina, *Surface Electromyography Physiology, Engineering, and Applications*, Wiley, 2016.

[9] Silvia Muceli et al.,*Identifying Representative Synergy Matrices for Describing Muscular Activation Patterns During Multidirectional Reaching in the Horizontal Plane*, Journal of Neurophysiology, No.103, pp.1532-1542, 2010.

[10] F.H.Martini, M.J.Timmons et al., *Human Anatomy*, Pearson, 2009.

[11] M.Schuenke et al., *Atlas of Anatomy - General Anatomy and Musculoskeletal System*, Thieme, 2010.

[12] Christian Fleischer *Controlling Exoskeletons with EMG signals and a Biomechanical Body*, Technische Universitat Berlin, 2007.

[13] Adam Zoss, H. Kazerooni, Andrew Chu, *On the Mechanical Design of the Berkeley Lower Extremity Exoskeleton (BLEEX)*, IEEE/RSJ International Conference on Intelligent Robots and Systems, pp.3465-3472, 2005.

[14] Hiroaki Kawamoto, Yoshiyuki Sankai, *Power Assist System HAL-3 for Gait Disorder Person*, Computers Helping People with Special Needs, pp. 196-203, 2002.

[15] Claude Lagoda, Juan C. Moreno, Jose Luis Pons, *Human-robot interfaces in exoskeletons for gait training after stroke: State of the Art and challenges*, Applied Bionics and Biomechanics, vol. 9, pp. 193-203, 2012.

[16] Guillarme Durandau et al., *EMG-driven of human-machine interaction in individuals waering the H2 exoskeleton*, International Federation of Automatic Control, 2016.

[17] Andrzej Cichocki et al., *Nonnegative Matrix and Tensor Factorizations Applications to Exploratory Multi-way Data Analysis an Blind Source Separation*, Wiley Edition, 2009.

[18] Michael W. Berrya et al., *Algorithms and applications for approximate nonnegative matrix factorization*, Computational Statistics & Data Analysis, No.52, pp. 155-173, 2009.

[19] Daniel D.Lee, Sebastien Seung, *"Algorithms for Non negative Matrix Factorization"*, Adv.Nueral Inform. Process. System, No.13, pp.556-562, 2009.

[20] M.C. Tresch, P. Saltiel, E. Bizzi, *The construction of movement by the spinal cord*, Nature Neuroscience, vol. 2, pp. 162-167, 1999.

[21] Ning Jiang, Kevin B. Englehart, Philip A. Parker, *Extractiong Simultaneous and Proportional Neural Control Information for Multiple DOF Prostheses From the Surface Electromyographic Signal*, IEEE Transaction on Biomedical Engineering, vol. 56, No.4, 2009.

[22] Silvia Muceli, Ning Jiang, Dario Farina, *Extracting Signals Robust to Electrode Number and Shift for Online Simultaneous and Proportional Myoelectric Control by Factorization Algorithms*, IEEE Transaction on neural systems and rehabilitation engineering, vol. 22, No. 3, 2014.

[23] D. Farina et al., *Blind Separation of Linear Instantaneous Mixtures of Nonstationary Surface Myoelectric Signals*, IEEE Transactions on Biomedical Engineering, vol.51, No.9, 2004.

[24] Kalypso Karastergiou et al., *Sex differences in human adipose tissues – the biology of pear shape*, Biology of Sex Differences, 2012.

[25] Hahne J.M et al., *Simultaneous and proportional control of 2D wrist movements with myoelectric signals*, IEEE Int. Workshop on Mach. Learn. Sig. Process (MLSP), pp 1-6, 2012.

[26] Silvia Muceli, Dario Farina, *Simultaneous and Proportional Estimation of Hand Kinematics From EMG During Mirrored Movements at Multiple Degrees-of-Freedom*,IEEE Transaction on neural systems and rehabilitation engineering, vol. 20, No. 3, 2012.

[27] Marco Gazzoni et al., *Quantifying Forearm Muscle Activity during Wrist and Finger Movements by Means of Multi-Channel Electromyography*, Plos One, vol. 9, 2014.

[28] Michael Schuenke et al., *Atlas of Anatomy - General Anatomy and Musculoskeletal System*, Thieme, 2010.

[29] Ning Jiang et al., *Intuitive, Online, Simultaneous, and Proportional Myoelectric Control Over Two Degrees-of-Freedom in Upper Limb Amputees*, IEEE Transaction on neural systems and rehabilitation engineering, vol. 22, No. 3, 2014.

[30] Chuang Lin et al., *Robust extraction of basis functions for simultaneous and proportional myoelectric control via sparse non-negative matrix factorization*, Journal of Neural Engineering, vol.15, 2018.

[31] Patrik O. Hoyer, *Non-negative Matrix Factorization with Sparseness Constraints*, Journal of Machine Learning Research, No.5, pp. 1457–1469, 2004.